Interaction of UVA (320-380 nm) radiation with human skin cells

Watkin, Richard David

Award date:
2000

Awarding institution:
University of Bath

Interaction of UVA (320-380 nm) Radiation with Human Skin Cells

Submitted by Richard David Watkin
for the degree of Ph.D.
Of the University of Bath
2000

Richard David Watkin

ProQuest LLC
789 East Eisenhower Parkway
P.O. Box 1346
Ann Arbor, MI 48106-1346

Acknowledgements

I would like to express particular gratitude to Prof. Rex Tyrrell for not only providing me with the opportunity to carry out research, but for his support, encouragement, and advice throughout the project.

I would also like to thank Dr Patrice Morliere and Dr Anthony Smith for their advice on the aconitase assay, and others who have helped me during my research, both friends and colleagues. I am particularly grateful to Clare and Damian who have continually provided me with invaluable assistance and support.

Dedication

To Mum, Dad, Damian
and Clare

Abstract

The generation of reactive oxygen species (ROS) by UVA radiation (320-380 nm) is responsible for damage to intracellular biological macromolecules, cytotoxicity and many other effects. Both the endogenous chromophore protoporphyrin IX (PPIX) and 'free' iron are potentially important sources of ROS after UVA irradiation in human cells. The aim of this study was to determine the importance of PPIX in the inactivation of human cells after UVA irradiation, and to determine what effect UVA irradiation had on intracellular 'free' iron levels.

By modulating levels of the intracellular chromophore PPIX in human cells by exogenous administration of the haem precursor δ-aminolevulinic acid (ALA) and irradiating these cells with graded doses of UVA, it was determined that the basal content of PPIX in TK6 human lymphoblastoid cells is insufficient to make a significant contribution to the UVA-mediated inactivation of these cells. The basal content of PPIX was however found to make a significant contribution to UVA-mediated inactivation of the primary human fibroblast cell line, FEK4, which implicates PPIX as a critical UVA chromophore in this cell line.

We document in this study the development of a flow cytometry-based fluorescence assay system that is capable of determining membrane damage and changes in intracellular 'free' iron levels. By using this assay and the cytoplasmic aconitase assay, we have confirmed that UVA irradiation of human skin cells results in an increase in intracellular 'free' iron levels. We also demonstrate that while administration of ALA to FEK4 cells does lower the intracellular 'free' iron levels, this type of treatment strongly exacerbates the increase in 'free' iron levels observed after UVA irradiation.

The effects of ALA treatment and UVA irradiation on ferritin levels in FEK4 cells was also determined in this study using a polyclonal (anti-ferritin) antibody enzyme-linked immunosorbent assay. We demonstrate in this study that UVA irradiation of cells, and to a much greater extent, UVA irradiation of cells treated with ALA, results in the

degradation of ferritin. This provides strong evidence for ferritin being a major source of the increase in intracellular 'free' iron levels observed after such treatments.

It is hoped that data obtained from this study will contribute to an advancement in the understanding of the intracellular effects of UVA irradiation and that this may help in the protection against, and prevention of, processes such as UVA-induced photocarcinogenesis and photoageing.

Contents

Abbreviations

ALA	δ-aminolevulinic acid
ALA-PDT	δ-aminolevulinic acid-photodynamic therapy
ABTS	di-ammonium 2,2'-azinobis (3-ethylbenzothiazoline-6-sulphonate)
BSA	bovine serum albumin
CA	calcein
CA-AM	calcein-acetoxymethyl ester
CHS	contact hypersensitivity
Cu-Zn-SOD	copper-zinc-superoxide dismutase
DMSO	dimethyl sulphoxide
D_2O	deuterium oxide
DOPA	dihydroxyphenylalanine
DPC	DNA-protein cross-link
ELISA	enzyme-linked immunosorbent assay
EMEM	Earle's modified minimal essential medium
EthD-1	ethidium homodimer-1
ETR	electron transfer reagent
FAPyG	formamidopyrimidine glycosylase
FAD	flavin-adenine dinucleotide
FAS	ferrous ammonium sulphate
FCS	foetal calf serum
FSC	forward scatter
Fe^{2+}	ferrous iron
Fe^{3+}	ferric iron
FMN	flavin mononucleotide
GPX	glutathione peroxidase
GSH	(reduced) glutathione
GSSG	glutathione disulphide (oxidised glutathione)
HNE	hydroxynonenal
HO	haem oxygenase
H_2O_2	hydrogen peroxide
HpD	haematoporphyrin derivative
IL-1	interleukin-1
INT	2-(4-iodophenyl)-3-(4-nitrophenyl)-5-phenyl-tetrazolium chloride
IRE	iron response element
IRP	iron-response protein
LDH	lactate dehydrogenase

LIP	labile iron pool
$LO^{\bullet}$	lipid alkoxyl radical
$LOO^{\bullet}$	lipid peroxyl radical
LOOH	lipid hydroperoxide
MDA	malondialdehyde
Mn-SOD	manganese-superoxide dismutase
MTS	3-(4,5-dimethylthiazol-2-yl)-5-(3-carboxymethoxyphenyl)-2-(4-sulphophenyl)-2H-tetrazolium, inner salt
MTT	3-(4,5-dimethylthiazol-2-yl)-2,5-diphenyltetrazolium bromide
NADH	nicotine adenine dinucleotide
NADP	nicotine adeninedinucleotide phosphate
NBD-DFO	nitrobenz-furazan-desferrioxamine
NO	nitric oxide
$^1O_2$	singlet oxygen
$O_2^{\bullet-}$	superoxide anion
$OH^{\bullet}$	hydroxyl radical
$ONOO^-$	peroxynitrite
PDT	photodynamic therapy
PMS	phenazine methosulphate
POD	peroxidase
PPIX	protoporphyrin IX
PBS	phosphate buffered saline
PUFA	polyunsaturated fatty acid
ROS	reactive oxygen species
SAME	succinyl acetone methyl ester
SDS	sodium dodecyl sulphate
SIH	salicylaldehyde isonicotinoyl hydrazone
SOD	superoxide dismutase
SSB	single strand break
SSC	side scatter
TBARS	thiobarbituric acid reactive species
TBHP	*t*-butyl hydroperoxide
Tf	transferrin
TfR	transferrin receptor
UCA	urocanic acid
UTR	untranslated terminal
UV	ultraviolet

UVA	ultraviolet-A radiation (320-380 nm)
UVB	ultraviolet-B radiation (290-320 nm)
UVC	ultraviolet-C radiation (190-290 nm)

1. Introduction

1.1 *Physiology of the Human Skin*

The skin is the largest organ of the human body and it has many functions, the most important of which is to keep internal systems intact and to protect the body from harmful external factors such as chemical agents, physical agents (e.g. ultraviolet light), and microorganisms. Amongst other functions, the skin is also important in preventing the loss of body fluids, regulating temperature, vitamin D production and immune surveillance. The skin is composed of three layers: the epidermis, the dermis and the hypodermis. The epidermis is mainly composed of keratinocytes, Langerhans cells and melanocytes. Keratinocytes produce the protein keratin, which provides a strength and flexibility to the epidermis. Langerhans cells are antigen-presenting cells, and melanocytes synthesise melanin and re-distribute it to surrounding keratinocytes by via dendritic processes. Melanins act as UV radiation absorbers and scatterers as well as free radical scavengers (Chedekel and Zeise, 1997). Melanin granules form a protective cap over the outer part of the keratinocyte nuclei in the inner layers of the epidermis. In the stratum corneum (the outermost layer of the epidermis), they are uniformly distributed to form an UV-absorbing dispersion, which reduces the amount of radiation that can penetrate the skin. The dermis is a tough and supportive connective tissue matrix that is connected to the epidermis. The thin upper part of the dermis is known as the papillary dermis because it has small fingerlike projections (papillae) containing capillaries, which nourish the epidermis. The papillary dermis is composed of loosely interwoven collagen. The coarse and horizontally running bundles of collagen are found in the thicker, lower

part of the dermis, known as the reticular dermis. Collagen fibres constitute the major structural protein of the dermis and they provide strength and resilience. Elastin fibres are also found in the dermis and provide elasticity to the skin. The ground substance of the dermis is a semi-solid matrix of glycosaminoglycans (GAG) that provides viscosity and hydration, and allows dermal structures limited movement. GAGs exist as high molecular weight polymers with a protein core, these are known as proteoglycans. Embedded in the reticular layer are many blood and lymphatic vessels, nerves and nerve endings, oil glands and hair roots. The dermis consists of a number of different cell types, particularly fibroblasts (which synthesise collagen, elastin and GAG). Other cells found in the dermis include fat (adipose) cells and immunological cell types such as dermal dendrocytes, mast cells, macrophages and lymphocytes. The deepest part of the skin is the subcutaneous layer or hypodermis. It consists of mainly fibrous, loose connective tissue such as adipose tissue. This layer is richly supplied with lymphatic vessels, blood vessels, and nerves. The coiled ducts of sweat glands, and bases of hair follicles are also found in the hypodermis.

1.2 *Electromagnetic Radiation and the Laws of Photochemistry*

Electromagnetic radiation exhibits wave-particle duality, which means it possesses characteristics of both particles and waves. It is transmitted as discrete units known as either quanta or photons. The magnitude of the energy of a photon is governed by the following relationship:

$$E = h\nu$$

Where E = energy (in J), h = Planck's constant (6.626×10^{-34} J·s), and ν = frequency (in Hz or cycles per sec). An important physical relationship that governs the properties of electromagnetic waves, is described by the following equation:

$$\nu = c/\lambda$$

where c = speed of light (3×10^{8} m/s) and λ = wavelength (m). By substituting the second equation into the first, we get the following equation that describes the energy of electromagnetic radiation at a defined wavelength:

$$E = hc/\lambda$$

From this equation it can be seen that energy and wavelength have a reciprocal relationship. As the wavelength decreases, the energy associated with it increases and vice-versa. The effect electromagnetic radiation has on a biomolecule depends on two

factors: the energy of the incident photons and the wavelength of electromagnetic radiation (rays) absorbed by a molecule. The latter constitutes the absorption spectrum of the molecule (and is determined by its molecular structure). Less energetic wavelengths, such as infrared, when absorbed by a molecule, result in both an increase in rotational energy, and an increase in the energy of vibration of the constituent atoms relative to each other (i.e. bending and stretching of bonds). As the incident wavelength becomes more energetic (e.g. UV and visible rays), electronic transitions may occur where an electron may pass from its ground state orbital to an excited energy state. Excited molecules show a greater probability of undergoing chemical reactions and it is this photon-induced chemistry that eventually gives rise to photobiological effects. At very short, energetic wavelengths, such as x-rays and γ-rays, the predominant chemical effects are bond breakage and ionisation (loss of an orbital electron from the target molecule).

The Gotthus Draper law is the primary law of photochemistry (and photobiology). This law states that light radiation must be absorbed by a molecule to induce a photochemical reaction, and in turn, photobiological reaction. It is not correct to consider that all light absorbed results in a chemical change as some of the light may be emitted as fluorescence or heat. The second law of photochemistry (the Stark-Einstein Law) states that light absorbed does not necessarily need to result in a photochemical reaction, but that if it does, only one photon is required for each molecule affected. This suggests, in general, that a photochemical change will not be induced by every photon absorbed by a molecule, but that the efficiency of producing a photochemical reaction (the quantum yield of a molecule, Φ) is of importance.

Quantum yield is defined by:

$$\Phi = \frac{\text{Number of molecules reacting chemically}}{\text{Number of photons absorbed}}$$

The greater the quantum yield of a molecule, the more efficient that molecule is at inducing a photochemical reaction after absorbing a photon.

1.2.1 *The Solar Spectrum*

The solar electromagnetic spectrum includes wavelengths that range from very short, high-energy cosmic rays (10^{-15} m), to longer, less energetic radiowaves (10^{3} m). Around 30-40% of total solar radiation, including most of the harmful wavelengths (wavelengths below 290 nm), is absorbed and filtered out by the ozone layer and molecular oxygen of the stratosphere. Wavelengths below 190 nm such as vacuum UV, gamma rays, x-rays and cosmic rays are high-energy wavelengths that are able to displace electrons from incident molecules to form ions. These wavelengths are known as ionising radiation. Wavelengths above 190 nm are unable to do this, because they lack the energy, and are known nonionising radiation.

The ultraviolet wavelengths of the solar electromagnetic spectrum stretch from 10 nm to 380 nm. The UV spectrum is divided into to different bands based on its biological effects, and also for convenience. The shortest, hence the most harmful wavelengths of

the UV spectrum are those below 290 nm and are termed vacuum UV (10–190 nm) and UVC (190–290 nm). These wavelengths (and shorter wavelengths) do not reach the earth's surface as they are absorbed and filtered out by ozone, molecular oxygen and other molecules in the stratosphere. The radiation that does penetrate through the stratosphere and thus reaches the earth's surface is summarised in Table 1.1. This is composed of approximately 10% UV, 50% visible, and 40% infrared (IR).

Table 1.1. Wavelengths of the solar spectrum that reach the earth's surface.

Type	Wavelength (nm)
UVB	290–320
UVA II	320–340
UVA I	340-380
Visible	380–760
Infrared	760–3000

The UV that reaches the earth's surface is composed of approximately 10% UVB and 90% UVA at midday. UVB intensity declines from the noontime apex, but UVA intensity usually remains relatively constant. The biological consequences of these two bands of the UV spectrum are discussed below.

1.3 *Deleterious Biological Events Induced by Solar UV Radiation*

This section discusses some of the biological consequences of exposure to either UVB (290-320 nm) or UVA radiation (320-380 nm), as these are the most harmful solar wavelengths that reach the earth's surface. UVB radiation is discussed very briefly, outlining mainly its pathological consequences. UVA radiation, on the other hand, is discussed in much greater detail because the investigation of certain molecular and cellular effects of UVA irradiation provides the basis of this project. Firstly, the generation of reactive oxygen species by UVA is discussed, followed by UVA-induced damage to particular biomolecules. The pathological consequences of UVA irradiation are also covered.

1.3.1 *Pathological Consequences of UVB Radiation (290-320 nm)*

UVB radiation is also known as erythemal UV because of its ability to induce erythema. There is evidence to suggest that UVB is responsible for the induction of non-melanoma skin cancer in man (Fitzpatrick and Sober, 1985; Brash et al., 1991). UVB induced photocarcinogenesis appears to be affected directly by genetic mutation, and indirectly by the impairment of the immune response (discussed below). UVB is absorbed by most biological macromolecules (such as lipids, proteins and nucleic acids), DNA in particular, is one of the most prominent UVB absorbing chromophores. The most frequent photoproducts formed after UVB exposure are cyclobutane-type pyrimidine dimers and (6-4) photoproducts (Freeman et al., 1986; Freeman et al., 1989; Olsen et al., 1989). UVB has been found to cause a limited number of strand breaks and there is also evidence that it can induce 8-hydroxy-2'-deoxyguanosine formation in primary murine

keratinocytes (Stewart et al., 1994). UVB is known to effect the immune system. Langerhans cells, for example, which are recognised as major antigen-presenting cells of the epidermis, have been shown using a mouse model, to have their antigen-presenting function impaired after UVB irradiation (Greene, 1979). UVB exposure has also been found to significantly deplete Langerhans cells in humans (Cooper et al., 1992). Tumours implanted into mice that had been UVB irradiated prior to implant, grew rapidly rather than being rejected, as was observed in non-irradiated mice (Kripke, 1974). This suggested that UVB exposure could result in immunosuppression. Within the past 25 years, UV-induced immunosuppression has been the subject of intense investigation (reviewed by Beissert and Granstein, 1995). Several factors have been identified as being responsible for UVB induced immunosuppression. One such factor was the development of suppressor T lymphocytes in mice after UVB irradiation, which was followed by the appearance of skin cancers. Transfer of these suppressor cells to non-irradiated recipients resulted in the inhibition of tumour rejection (Fisher and Kripke, 1982). In others studies, local and systemic immunosuppression has been demonstrated using contact hypersensitivity (CHS) in murine models after UVB exposure (reviewed by Ullrich, 1995). Urocanic acid (UCA), a molecule found in the stratum corneum, was found to absorb UV light in a similar range to DNA. Subsequent investigations on the action spectrum of UCA on the immune system revealed that UVB exerted an inhibitory effect, which occurred as a result of isomerisation of the molecule (reviewed by Norval et al., 1995, Noonan et al., 1988). It has also been observed that UVB contributes to photoaging. In experiments using hairless mice, UVB was shown to induce severe dermal elastosis (Kligman and Sayre, 1991), cause changes in collagen (an initial

increase followed by a decrease after prolonged exposure), and an increases in GAG and proteoglycans (Kligman and Kligman, 1997).

1.3.2 *UVA-Induced Oxidative Stress - Formation of ROS*

Many biological macromolecules absorb UVA, which can invariably result in the generation of reaction oxygen species (ROS), reviewed by Tyrrell (1991). For example, two studies showed (Czochralska et al., 1984; Cunningham et al., 1985) that irradiation of an aqueous solution of NADH (or NADPH) with UVA resulted in the formation of both superoxide anion ($O_2^{\bullet-}$) and hydrogen peroxide (H_2O_2). McCormick and co-workers (1976) demonstrated that irradiation of an oxygenated solution of tryptophan with wavelengths between 300 and 400 nm resulted in the photochemical oxidation of typtophan, yielding the formation of H_2O_2 and *N*-formyl kynurenin (a typtophan product). Subsequent irradiation of *N*-formyl kynurenin photoproduct with UVA irradiation was shown also to generate of H_2O_2 (Andley and Clark, 1989). H_2O_2 generation, after irradiation of either typtophan or *N*-formyl kynurenin, was postulated to occur via intermediate production of the $O_2^{\bullet-}$ (Andley and Clark, 1989). The production of these ROS in biological systems could potentially be very crucial, because in the presence of redox-active cations, such as iron, the highly reactive hydroxyl radical may be formed by Fenton and Haber Weiss chemistry (reviewed in Halliwell and Gutteridge, 1999). Various aspects of intracellular iron and its significance in relation to UVA radiation are discussed in Chapters 3-5, therefore iron is only briefly mentioned in this chapter.

Another major source of photochemical generation of ROS during UVA irradiation is that of endogenous photosensitisers. Absorption of a photon by a photosensitiser, at a defined wavelength, results in the excitation of the sensitiser to its singlet state. The excited singlet state can return to its ground state (accompanied by the emission of fluorescence) or it undergo a process known as intersystem crossing along with spin inversion, producing the longer lived, less energetic triplet state. The triplet state can react in one of three competitive mechanisms: a Type I photodynamic mechanism, which involves the interaction of the triplet state photosensitiser with another photosensitiser (involving energy transfer) or an organic substrate, producing free radical intermediates. Alternatively, a Type II mechanism may occur, which normally results in a direct energy transfer to ground state molecular oxygen. This produces either singlet oxygen ($^1O_2$), or $O_2^{\bullet-}$, and a ground state photosensitiser (less than 1% of Type II reactions result in $O_2^{\bullet-}$ formation (Foote, 1991). The third mechanism, by which a triplet state sensitiser may respond, is by relaxation back to its ground state resulting in concomitant phosphorescence emission. The mechanism that is favoured, and the products formed, are usually dependent on the environment of the reaction and the biochemical nature of the photosensitiser. For example, if the photosensitiser is bound to a substrate then a Type I mechanism might be favoured. Under aerobic conditions a Type II mechanism might be favoured. Another factor that influences the fate of the mechanism is the quantum yield and triplet lifetime of the photosensitiser. Photosensitisers with high quantum yields and longer triplet lifetimes have an increased chance of reacting with molecular oxygen, thus producing $^1O_2$. Photosensitisers that lack these properties tend to favour fluorescence and are rather inefficient as a photosensitiser (reviewed by Ryter and

Tyrrell, 1997). Molecules such as porphyrins (in particular protoporphyrin IX (PPIX) which is discussed in detail in Chapter 2), and flavins and quinones have all been postulated as being potential endogenous photosensitisers responsible for detrimental effects observed by UVA radiation.

1.3.3 *UVA-induced DNA Damage*

There are a number of different biological macromolecules that are affected as a result of exposure to UVA radiation (reviewed by Tyrrell, 1991, 1994). Despite DNA being a poor chromophore for the absorption of UVA radiation, various types of DNA damage have been observed. Damage to DNA after UVA irradiation is thought to occur primarily through the actions of sensitiser radicals and ROS. In particular, one DNA lesion that has been observed after UVA irradiation and highly documented in recent years is 7,8-dihydro-8-oxo-2'deoxyguanosine (also written as 8-oxo-dG, 8-hydroxy-2'-deoxyguanosine and 8-OHdG). UVA radiation dose-dependent increases in this lesion have been previously reported in cultured cells (Rosen et al., 1996;Kvam and Tyrrell (1997). An increase in 8-oxo-dG lesions was also observed after pre-treatment of cells with riboflavin or δ-aminolevulinic acid (ALA) followed by exposure to visible light (Pflaum et al., 1998). Singlet oxygen has been shown to mediate the formation of 8-oxo-dG resulting in strand breaks (Devasgayam et al., 1991), though the rate of induction of this lesion by UVA in mammalian cells has been reported to be 10-fold higher than single strand breaks (Pflaum et al., 1994). This lesion was first shown to be mutagenic by Kuchino and co-workers (1987) as it led to the misreading of DNA templates, both at the 8-oxo-dG site and at adjacent residues in vitro. Further studies have indicated that DNA

Fig. 1.1. Formation of 8-oxo-dG by oxidation at C8 of dG (deoxyguanine) causes structural and conformational alterations at dG that can result in mispairing of 8-oxo-dG with A (adenine), see text for details (source: Guyton and Kensler, 1993).

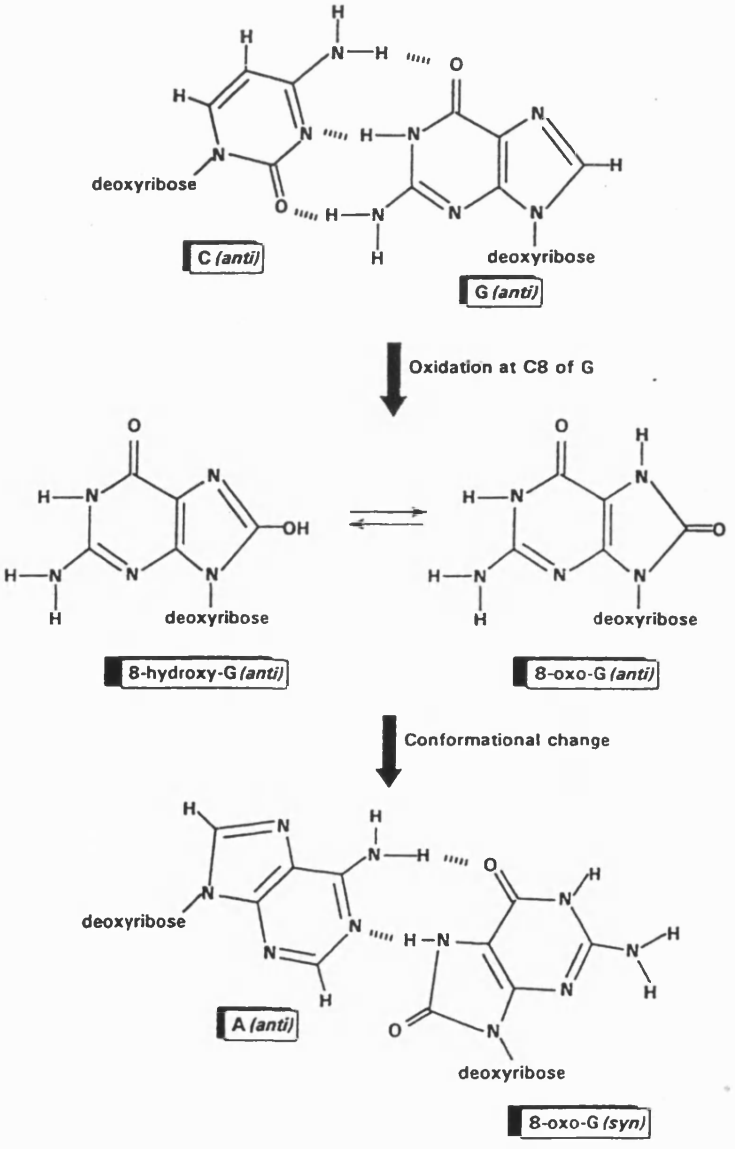

polymerases selectively incorporate dC (deoxycytosine) and dA (deoxyadenine) opposite 8-oxo-dG (Shibutanti et al., 1991). Chain extension past the dA 8-oxo-dG pair proceeded more efficiently compared to its dC counterpart indicating that once misincorporation occurs the stable G-A mispair is not recognised by proofreading and will persist. If the 8-oxo-dG lesion is not excised (e.g. by formamidopyrimidine glycosylase, also known as FAPyG) before DNA replication proceeds, or if dATP or 8-oxo-dGTP is mistakenly incorporated at the apurinic site that results from excision of the modified base, the mutation resulting from the 8-oxo-dG mispairing will be a G:C to T:A transversion (see Fig.1.1). Since a high frequency of G:C to T:A mutations in the *ras* oncogene have been observed in tumours of sun exposed skin, it has been postulated that 8-oxo-dG formation may contribute to some of these mutations and thus may be carcinogenic (Hattori-Nakakuki et al., 1994).

Pyrimidine photoproducts have been reported following UVA irradiation of *E.Coli*, but a 6-fold greater energy input is required at 365 nm compared to 254 nm in order to achieve the same order of magnitude of lesions (Tyrrell, 1973). Pyrimidine dimer formation in keratinocytes has also been reported after irradiation with visible light between the wavelengths of 400 and 500 nm (Pflaum et al., 1998), these lesions were postulated to occur by direct absorption of light, rather than through other intermediates. Peak et al. (1987a, b) demonstrated the induction of DNA single strand breaks (SSBs) in human cells in vitro by UVA exposure.

UVA irradiation of cells in a deuterium oxide (D_2O) environment enhanced these SSBs. It is possible therefore, that singlet oxygen might be a mediator of these breaks as the decay of this ROS is slowed down by an order of magnitude compared with H_2O. Roza and collegues (1985) also observed UVA-induced SSBs after irradiating human fibroblasts with UVA. However, it was shown that by adding catalase before irradiation, almost all of these breaks were eradicated, indicating that H_2O_2 is produced, and may be responsible for the induction of these lesions. The hydroxyl radical has also been implicated in the production of SSBs in isolated *Bacillus subtilis* DNA after 365 nm UVA irradiation (Peak and Peak, 1990), as hydroxyl radical quenchers such as acetate, mannitol, formate, and azide were shown to protect against these breaks. Finally, the requirement for oxygen in the light-mediated (380-490 nm) induction of DNA-protein cross-links (DPCs) was demonstrated in studies by Gantt et al. (1979). Peak et al. (1985) subsequently demonstrated that production of these DPCs by radiation at 405 nm could either be enhanced or reduced by irradiating in either D_2O or hypoxic conditions respectively. DPC can result in the interference of chromatin unfolding, DNA repair, replication and transcription.

1.3.4 *Lipid Peroxidation and UVA-Induced Damage to Biological Membranes*

Lipid peroxidation is the oxidative deterioration of polyunsaturated lipids (reviewed by Bucala, 1996). Polyunsaturated fatty acids (PUFAs) contain two or more carbon-carbon double bonds. The major constituents of biological membranes (organelle and plasma membranes) are lipids and proteins, thus during lipid peroxidation it is possible that membrane proteins may also get damaged. Cell and organelle membranes tend to be

(amphipathic) lipid bilayers with proteins inserted within them. The fluidity of a membrane is known to be essential for its proper functioning and usually it is determined by its unsaturated and PUFA side chains. These side chains lower the melting point of the interior of the membrane thus damage to PUFAs can result in a compromise of membrane function.

Any species that is sufficiently reactive to abstract a hydrogen atom (H) from a methylene (-CH2-) group of an unsaturated or PUFA can cause initiation of lipid peroxidation (Fig. 1.2). The more double bonds present in a fatty acid, the more prone that fatty acid is to H atom abstraction. The hydroxyl radical ($OH^{\bullet}$) can readily initiate lipid peroxidation and travel into the interiors of membranes producing a carbon radical ($-C^{\bullet}H-$) and H_2O. Superoxide on the other hand is insufficiently reactive to abstract H atoms from PUFAs. The carbon radical formed by H atom abstraction is stabilised to form a conjugated diene and there are different reactions that can proceed. For example, if two carbon radicals collide, the side chains of fatty acids can become cross-linked. Under aerobic conditions the most likely fate of a carbon radical is it will combine with O_2 to give a peroxyl radical ($LOO^{\bullet}$). This reaction is particularly favoured because O_2 is a hydrophobic molecule that can concentrate in the interior of membranes. However, under low oxygen concentrations, alternative pathways may be favoured, such as reaction with protein thiols (-SH groups). The next stage of lipid peroxidation is called the propagation stage. This is where a peroxyl radical abstracts an H atom from another lipid molecule thus producing a lipid hydroperoxide (LOOH) and another carbon radical, thus allowing the chain of lipid peroxidation to continue.

Fig. 1.2. The top part of this diagram represents a lipid bilayer made up of phospholipids (grey cirlcles with black tails). Inserted in this bilayer is cholesterol (white circular structures) which is mostly found in the plasma membrane, and in and around the bilayer are proteins (spotted oblong structures). The dark grey structure is an α-tocopherol molecule. The schematic below the lipid bilayer picture shows an idealised representation of the initiation and propagation of lipid peroxidation of a fatty acid with three double bonds (source: Halliwell and Gutteridge, 1999).

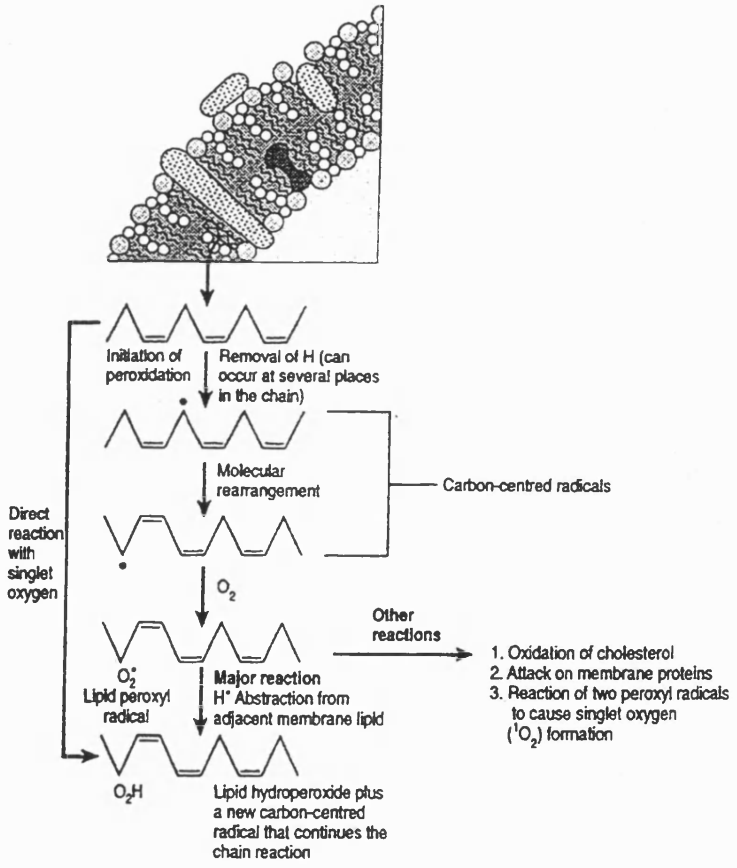

Iron plays a detrimental role in the process of lipid peroxidation. Not only can Fe^{2+} catalyse the formation of the hydroxyl radical, it can also catalyse the decomposition of lipid hydroperoxides (LOOH) to produce the alkoxyl radical ($LO^{\bullet}$). Alkoxyl radicals are capable of abstracting H atoms from PUFAs and lipid hydroperoxides producing carbon radicals and peroxyl radicals, which can continue to propagate lipid peroxidation. Alternatively, Fe^{3+} can decompose peroxides to peroxyl radicals, which also can continue the propagation of lipid peroxidation. There are quite a number of iron chelates that can stimulate lipid peroxidation, some of which include simple chelates (e.g. Fe^{2+}-ADP) and haemproteins (e.g. cytochromes) (Halliwell and Gutteridge 1999).

Singlet oxygen is capable of causing rapid lipid peroxidation, and the production of peroxides occurs via the reaction of singlet oxygen directly with carbon-carbon double bonds. This is known as an *ene* reaction. Within the hydrophobic interior of lipid membranes the lifetime of singlet oxygen is much greater than if it was in an aqueous solution. Production of singlet oxygen by excitation of photosensitisers, such as porphyrins, has been shown to induce rapid peroxide formation (reviewed by Girotti, 1990). Singlet oxygen can also be formed during lipid peroxidation e.g. by the reaction of two peroxyl radicals to form a cyclic intermediate, which subsequently decomposes to give singlet oxygen. This, itself, could form more lipid peroxides. There are a number of different peroxide decomposition products including epoxides, aldehydes, ketones and hydrocarbons. One of the more common products is malondialdehyde (MDA), which can attack proteins and introduce mutagenic lesions in DNA. 4-Hydoxy-2-*trans*-nonenal (4-HNE) is another common product, which can inhibit DNA and protein synthesis. At

high enough concentrations it can cause membrane blebbing followed by cell lysis (see Halliwell and Gutteridge, 1999, and references cited therein).

UVA has been shown to induce lipid peroxidation in a number of studies (reviewed by Tyrrell, 1994). UVA (365 nm) radiation was shown to lyse the membranes of isolated rat liver lysosomes, this was measured by protein release from these organelles (Desai, 1964). Using an enzymatic assay with yeast, cell membrane damage was shown to occur after UVA irradiation (Ito and Ito, 1983). More recently, lipid peroxidation and membrane damage has been shown to occur in a number of cultured human cell lines such as fibroblasts and keratinocytes after UVA treatment (Morliere et al., 1991; Moysan et al., 1993; Gaboriau et al., 1993; Vile and Tyrrell, 1995; Applegate et al., 1995). Lipid peroxidation was determined from the level of thiobarbituric acid-reactive species (TBARS) and membrane damage was evaluated using the lactate dehydrogenase (LDH) leakage assay. In one of the studies (Gabroriau et al., 1993), fluorescence anisotropy of a membrane-bound probe demonstrated reductions in cell membrane fluidity as a function of UVA irradiation.

1.3.5 *UVA Radiation and Oxidative Protein Damage*

Oxidative damage to proteins can occur directly by ROS or indirectly by end products of lipid peroxidation such as MDA and HNE. Hydrogen peroxide and superoxide, at physiological levels, tend to have little or no direct affect on proteins. The hydroxyl radical and singlet oxygen, on the other hand, can generate a wide range of end-products upon attack of proteins, some examples of which are briefly discussed below (Halliwell

and Gutteridge, 1999). Thiol groups of cysteine and methionine are easily oxidised by many ROS to form either thiyl radicals or disulphides. Methionine is readily oxidised to methionine sulphoxide. Oxidation of histidine can often cause inactivation of enzyme active sites, which appears to be important in protein cross-linking as well as 'marking' proteins for proteolysis. Tryptophan residues are powerful singlet oxygen scavengers and are sensitive to hydroxyl radical attack forming fluorescent products such as *N*-formylkynurenine. Tyrosine residues in proteins can be attacked by the hydroxyl radical to form dihydroxyphenylalanine (DOPA), this forms a part of melanin synthesis. Tyrosine radicals can end up crosslinking with one another to form bityrosine, which conceivably could inhibit signal transduction by blocking tyrosine phosphorylation. It is well known that damaged proteins become 'marked' for proteolytic degradation and the destruction of these unwanted proteins, in eukaryotes, mostly occurs in proteosomes which are multicatalytic protease complexes (some proteins are also degraded in lysosomes).

Relatively little attention has been paid to protein damage caused by UVA irradiation. This may be because proteins are readily re-cycled through degradation and synthesis. However, just from irradiating cultured cells with UVA and measuring protein content by the Bradford procedure (1976), it is clear that there is significant protein degradation occurring in a dose-dependent manner (R.D. Watkin, unpublished observation). There have been studies showing that UVA radiation is capable of inactivating certain enzymes, including catalase, pepsin, amylase and tyrosinase, in an oxygen dependent manner (reviewed by Tyrrell, 1991). Haem-containing antioxidant enzymes, such as catalase and

peroxidases, are UVA absorbing chromophores (the absorption maximum of catalase is in the UVA range). Catalase was shown to be directly destroyed by solar simulated radiation in human fibroblasts (Shindo et al., 1994). Kramer and Ames (1987) showed that catalase is rapidly inactivated by UVA radiation in *Salmonella typhimurium*. They also showed that certain strains of this bacterium, which constitutively overexpress certain proteins such as catalase and alkyl hydroperoxide reductase (a flavin-containing protein that is a bifunctional catalase-peroxidase), are significantly more sensitive to UVA-induced cell killing compared to the wild type. In addition, an *Escherichia coli* strain that overexpresses catalase, by virtue of a *kat G* plasmid, is considerably more sensitive to UVA killing than the strain not carrying the plasmid, despite being more resistant to H_2O_2 (Eisenstark and Perrot, 1987). These studies suggest that catalase (and other UVA absorbing enzymes) may not only be inactivated by UVA radiation, but might also act as endogenous photosensitisers (reviewed by Tyrrell, 1991). More recently it was shown that UVA caused a dose-dependent oxidation of sulphydryl groups of bovine serum albumin and human γ-globulin in vitro, and of proteins in primary human fibroblasts (Vile and Tyrrell, 1995). The in vitro studies showed that the UVA-mediated protein oxidation was iron-dependent and involved singlet oxygen and hydrogen peroxide, but not the hydroxyl radical. Similar observations were made for the fibroblasts.

1.3.6 *Patholgical Consequences of UVA Radiation (320–380 nm)*

Until recently (the past 15 years), very little attention was paid to the harmful affects of UVA radiation (320–380 nm), which is very abundant in natural sunlight. In fact, UVA was considered to be innocuous and of little or no concern to dermatologists, because of its relative inability to cause noticeable effects such as erythema. In 1974, the development of a treatment that used psoralens plus UVA (PUVA) for the photochemotherapy of psoriasis and other skin diseases led to an increased interest in UVA radiation. The availability of high intensity UVA-emitting systems for use in PUVA treatment contributed to growth of the tanning industry. The industry blossomed throughout the Western world from the mid-1970s and early 80s, and it became increasingly evident that through recreational and cosmetic purposes, people were exposing themselves to much greater amounts of UVA radiation, without realising its potentially acute and chronic harmful effects. In the past 15 years, the understanding of the effects of UVA has increased rapidly, and it now evident that UVA is not safe and can produce many of the harmful effects that are produced by UVB. Ironically, UVA exposure has increased with the use of sunscreens. This is because some sunscreens are designed to reduce erythema (sunburn) essentially blocking out UVB, but not UVA to allow melanogenesis (tanning) to occur. People spend longer times in the sun because the discomfort of sunburn is no longer there as a deterrent. Additionally, most UVA sunscreens have complications making them unsuitable. This is because they are either an irritant, cosmetically unacceptable, photolabile (unstable), or block out only part of the UVA spectrum.

The amount of solar UVA radiation that reaches the earth's surface is significantly greater than that of UVB throughout the year. This is because, unlike UVB, UVA is not filtered or attenuated by stratospheric ozone, and is less affected by the solar zenith angle and seasonal variation. Of the total solar irradiance at sea level, approximately 5–7% is UV and greater than 90% of this is UVA (Pathak, 1997). Transmission of UVA into the dermis is much greater than UVB because it is absorbed less by biological macromolecules in the epidermis. UVA radiation can penetrate deep in to the skin to a depth of 160–250 μm, compared to UVB radiation that can only penetrate to a depth of 17–49 μm (Pathak, 1997). In untanned, fair-skined people, approximately 50% of UVA rays reach the dermis. In pigmented people (people with darker skin), the amount of UVA rays that reach the dermis is less, but is still a significant amount (approximately 30–35%). Physiologically, this means that UVB can induce structural and functional changes only as deep as the superficial papillary dermis, whereas UVA can exert its effects throughout the skin, deep into the reticular dermis. Therefore epidermal keratinocytes, melanocytes and Langerhans cells are affected by UVA, along with dermal components such as fibroblasts, structural fibres (collagen and elastin), lymph and blood vessels (and cells within them) and nerves (Kumakiri et al., 1977; Beitner, 1986; Lavker et al., 1995).

Some of the harmful, damaging effects observed after UVA exposure are similar to those observed after UVB exposure. UVA has been found to be photocarinogenic. In experiments using hairless mice, UVA radiation was shown to induce non-melanoma skin tumours (Sterenborg et al., 1990; Kelfkens et al., 1992; Bech-Thomsen and Wulf,

1995; de Laat et al., 1997). It was hypothesised recently (Moan et al., 1999) that UVA may be also be responsible for melanoma induction in humans as it has been shown in the Xiphophorus fish (Setlow and Woodhead, 1994). There are lines of evidence that suggest that UVA radiation can be either immunosuppressive or immunoprotective (depending on irradiation conditions). In mice irradiated with chronic low-dose UVA, Bestak and Halliday (1996) showed that local suppression of contact hypersensitivity CHS, Langerhans cell depletion and T suppressor cell activation occurred. It has also been demonstrated, however, that UVA can be photoprotective at physiologically relevant doses. In experiments with mice, it was shown that UVA abrogated the immunosuppressive effects of UVB and UCA (Reeve and Tyrrell, 1999).

UVA radiation has been strongly implicated as a cause of photoaging. In a study by Kligman and collegues (1985), hairless mice irradiated with UVA over a 34-week period developed a significant degree of elastosis. Although the deposition of elastic fibres was less dense than that produced by UVB, the elastosis not surprisingly extended much deeper into the dermis. UVA irradiation with a light source that only emitted wavelengths between 340 and 380 nm (UVA I) failed to cause significant elastosis, even after huge doses. This suggests that it is the wavelengths of 320–340nm (UVA II) that are mainly responsible for this UVA-induced photodamage. In experiments with human models, irradiation of skin with UVA resulted in a decrease in elastic tissue whereas solar simulated UV (UVA and UVB) produced a slight increase (Lowe et al., 1995). In a study using hairless mice, Menter and colleagues (1996) showed that narrow-band UVA (320–355 nm) caused marked dermal collagen damage (but only moderate elastosis) and

broadband UVA has been found to stimulate collagenase synthesis in human dermal fibroblasts (Petersen et al., 1992).

1.4 *Defence Against UVA-Induced Oxidative Stress*

There are a number of different ways a cell is protected against oxidative stress. These include, antioxidant molecules, antioxidant enzymes, metal sequestering proteins and inducible responses such as haem oxygenase induction. In this section, some of the important components of cutaneous antioxidant defence will be briefly discussed.

1.4.1 *Antioxidant Molecules*

Glutathione (GSH), is an endogenous tripeptide that is the most abundant thiol found in most tissues. It plays an extremely important role in the cellular defence against oxidative damage and GSH depletion by D, L-buthionine-(*S,R*)-sulfoximine (BSO) treatment strongly sensitises cells to the lethal action of UVA and UVB radiations (Tyrrell and Pidoux, 1986). GSH is a powerful free radical scavenger and quenches radicals by hydrogen atom donation resulting in the formation of GSH disulphide (GSSG or oxidised glutathione), and is regenerated by glutathione reductase with NADPH acting as a hydrogen donor. GSH also functions as a hydrogen donor for several other antioxidants such as ascorbate, which in turn regenerates α-tocopherol (Shindo et al., 1994). GSH has also been shown to protect calf thymus DNA and chinese hamster ovary cells (CHO) against 8-OHdG formation after UVA exposure (Fischer-Neilsen et al., 1992; Fischer-Neilsen et al., 1993).

α-Tocopherol (vitamin E) is a lipophilic endogenous antioxidant that provides protection against UV-induced oxidative membrane damage. α-Tocopherol functions as a chain breaking antioxidant, is a scavenger of lipid peroxide radicals (see Halliwell and Gutteridge, 1999), and has been shown to protect against UVA-induced lipid peroxidation in cultured human fibroblasts (Morliere et al., 1990; Gaboriau et al., 1993) and keratinocytes (Djavaheri-Mergny et al., 1996). α-Tocopherol has also been shown to be a physical quencher and chemical scavenger of singlet oxygen, with the irreversible oxidation of a-tocopherol to its α-tocopheryl quinone (reviewed by Fryer, 1993).

Ascorbate (vitamin C) has been shown to protect against 8-OHdG formation in either, CHO cells after UVA irradiation (Fischer-Neilsen et al., 1992), or mouse keratinocytes after UVB irradiation (Stewart et al., 1996). The mechanism of ascorbate protection is thought to be two-fold. Either ascorbate directly quenches or reacts with singlet oxygen, hydroxyl radicals and superoxide anions (Njus and Kelley, 1991; Darr et al., 1992) or it restores the antioxidant properties of oxidised α-tocopherol by regenerating tocopheroxyl radicals (Leung et al., 1981; Njus and Kelley, 1991).

β-carotene is a precursor for vitamin A and is a member of the carotenoid family of antioxidants. It is capable of quenching excited triplet states and singlet oxygen, and scavenging peroxide radicals (Krinsky et al., 1982). There are contrasting views on the effectiveness of β-carotene as a photoprotectant. It would appear from most of the studies to date, that β-carotene itself is limited in its protective effects, unless in the presence of other antioxidants (reviewed by Edge, 1998). In the presence of antioxidants

(such as α-tocopherol, ascorbate and GSH), β-carotene appears to reduce the induction of cancer development as determined by in vitro and in vivo studies (reviewed by Toma et al., 1995). There are many other antioxidants that have been shown to be photoprotective, including the endogenous molecule ubiquinol (coenzyme Q) and certain exogenous flavenoids, these however are not discussed here.

1.4.2 *Antioxidant Defence Enzymes*

In addition to antioxidants, the cell is also protected from oxidative stress by enzymatic antioxidants, some of which are briefly discussed. Glutathione peroxidase (GPX) is a selenium dependent enzyme that is active against H_2O_2 and lipid hydroperoxides by coupling the reduction of these compounds with the oxidation of reduced glutathione (GSH), forming water and an alcohol respectively. GPX is dependent on the presence of selenium in each of the four subunits of the enzyme a sufficient supply of GSH, which is the unique hydrogen donor for this enzyme. Selenium deficiency was found to cause a decrease in GPX activity and increased lipid peroxidation in cultured human fibroblasts after UVA exposure (Moysan et al., 1995). In human skin fibroblasts, Leccia and colleagues (1993) showed that incubation with selenium increased GPX and decreased UVA-induced lipid peroxidation. As mentioned above, glutathione reductase reduces oxidised glutathione (GSSG) back to GSH using NADPH, thus recycling GSH that is oxidised by GPX activity.

Catalase is another enzyme that scavenges H_2O_2 in the skin, but unlike other peroxidases, catalase catalyses the direct decomposition of H_2O_2 to ground state oxygen and water,

without the use of another substrate. As discussed previously in this chapter, catalase activity is strongly reduced after UVA exposure, probably due to oxidative damage to the enzyme. Compared to GPX, catalase is thought to be less important as an antioxidant enzyme because fibroblasts deficient in catalase activity did not show decreased survival after a single dose of solar simulated UV (Shindo et al., 1994). However, catalase was found to reduce damage to other antioxidant enzymes (GPX and superoxide dismutase) and thus maintain their activity during chronic UV exposure (Shindo et al., 1994).

Superoxide dismutases (SODs) all essentially catalyse the same reaction, which is the reduction of superoxide anion to less reactive H_2O_2. In the skin, the enzyme is present in forms such as Cu-Zn-SOD and Mn-SOD. SOD activity has been found to be reduced by solar simulated UV irradiation in human skin fibroblasts (Shindo et al., 1994) and by UVA irradiation in human keratinocytes (Punnonen et al., 1991). However, inactivation of this enzyme is thought to occur indirectly by ROS rather then directly as was found with catalase (Shindo et al., 1994). Zinc addition (one of the metals in the active site of Cu-Zn-SOD) to cultured human fibroblasts resulted in a reduction in lipid peroxidation and an increase in survival, yet no increasee in Zn-SOD activity was observed (Leccia et al., 1993). Similarly, Parat and colleagues (1995) found that addition of manganese (the metal in the active site of Mn-SOD) to cultured human fibroblasts protected these cells from oxidative injury by UVA irradiation; but this was not accompanied by an increase in Mn-SOD activity. In contrast to this however, it has recently been shown that cultured fibroblasts repetitively exposed to UVA radiation (200 kJ/m^2 per day for three days) actually developed an adaptive response, marked by an increase in Mn-SOD mRNA

levels and Mn-SOD activity after the third exposure (Poswig et al., 1999). Since the product of SOD activity is H_2O_2 (which is toxic), increases in SOD activity are ideally accompanied an increases in catalase and/or GPX (Amstad et al., 1991; Yohn et al., 1991). However, if SOD activity exceeds that of H_2O_2 scavengers, it has been shown that the toxicity of superoxide increases due to an accumulation of H_2O_2 formed by SOD activity (Amstad et al., 1991).

Haem oxygenase, the principal mammalian enzyme responsible for haem catabolism, is an enzyme that can either be inducible (HO-1) or constitutive (HO-2). The enzyme is involved in the breakdown of haem to biliverdin, which is then converted to bilirubin by biliverdin reductase, both of which are antioxidants (Stocker et al., 1987). UVA irradiation (and treatment with other agents that induce oxidative stress such as H_2O_2 or sodium arsenite) of cultured human fibroblasts and keratinocytes leads to induction of HO-1 activity (Keyes and Tyrrell, 1987, 1989; Appelgate et al., 1991) suggesting that HO has some role in the protection of cells. Under conditions where the levels of cellular antioxidant systems are inadequate to cope with oxidative stress the levels of HO-1 are induced. For example, the depletion of GSH levels correlated with an increase in both the constitutive and oxidant-inducible accumulation of HO mRNA levels (Lautier et al., 1992). The induction of HO-1 activity by UVA irradiation was linked to the induction of the iron storage protein ferritin (Vile and Tyrrell, 1993). Addition of the HO inhibitor tin-protoporphyrin IX prior to UVA irradiation prevented an increase in ferritin levels suggesting a HO-dependent mechanism. More recently, Kvam et al. (1999) showed that UVA irradiation resulted in the release of 'free' haem intracellularly and Pourzand et al.

(1999) also showed that the levels of 'free' iron also increased immediately after UVA irradiation. The increase in free haem would explain HO-1 induction, and both free haem and free iron would account for an increase in ferritin to sequester potentially toxic 'free' iron in a relatively inert form, thus preventing the formation of the highly toxic hydroxyl radical (see Chapter 5). Sequestration of redox active metals is another line of antioxidant defence and other proteins that can bind potentially oxidant metals, such as transferrin and metallothioneins may also be considered to have antioxidant properties. After chronic UV exposure, the level of non-haem iron of skin has been found to be elevated (Bissert et al., 1991), an increase in ferritin might help reduce the potential toxicity of this iron increase. Ferris et al. (1999) showed that in murine cells either overexpressing HO-1 or that were HO-1 deficient, HO-1 activity regulated iron accumulation and efflux. In experiments where ^{55}Fe was added to cells overexpressing HO-1 activity, iron uptake was reduced and iron efflux was increased compared to normal cells or HO-1 deficient cells, suggesting another possible cytoprotective role for HO.

1.5 *Objectives of this Project*

The objectives of each individual study are presented at the end of each chapter introduction (Chapters 2-5) so they will not be discussed in detail here. The overall aims and scope of this project are twofold. Firstly, to investigate the importance of protoporphyrin IX as an endogenous chromophore in the UVA-mediated inactivation of human cells. Identification of UVA absorbing chromphores that account for the radiation wavelength dependence of deleterious effects in the skin remains elusive. Several have been postulated, including porphyrins, flavins and quinones, though none have been proven to be the chromophore that is responsible for UVA-mediated damage.

It was recently demonstrated in our laboratories that exposure of cultured human fibroblasts to UVA radiation resulted in an increase in intracellular 'free' iron levels (Pourzand et al., 1999). In light of this, the second part of this project concentrated on gaining a better understanding into the changes in iron levels as a result of UVA irradiation, and to further investigate the source of iron release. Included in the iron studies was also the investigation into what effect UVA irradiation of cells with altered PPIX levels had on changes in intracellular 'free' iron. The purpose of this was to determine if PPIX was effective in promoting iron release in UVA irradiated cells.

Overall, the intention of this project was to enhance the current understanding and knowledge of the effects of UVA radiation. By achieving this, it is hoped that some contribution may be made, at least in the long term, to the prevention of the pathological consequences of UVA radiation such as photocarcinogenesis and photo-induced ageing.

2. Study of the relationship between endogenous protoporphyrin IX concentration in human cells and inactivation by UVA radiation

2.1 Introduction

2.1.1. *PPIX Biosynthesis and Cellular Distribution*

Protoporphyrin IX (PPIX) is the immediate precursor of haem in the haem biosynthetic pathway (Fig. 2.1). In the first, and rate limiting, step of this pathway, δ-aminolevulinic acid (ALA) is formed from glycine and succinyl CoA by the pyridoxyl phosphate-requiring enzyme ALA synthase (ALAS). The last step in the formation of haem is the incorporation of iron into PPIX and it takes place in the mitochondria under the action of the enzyme, ferrochelatase. Administration of exogenous ALA effectively bypasses the rate limiting ALA synthesis step in this pathway in mammalian cells leading to the accumulation of the endogenous chromophore PPIX. PPIX also accumulates because of the limited capacity of ferrochelatase. The intracellular distribution (Peng et al., 1997 and references cited therein) of PPIX after ALA stimulation tends to follow a general pattern as a function of time, with an initial localisation in the mitochondria where it is formed. PPIX gradually migrates to other subcellular compartments and their membranes (including the perinulcear region, endoplasmic reticulum, and lysosomes) over time, eventually localising in the plasma membrane. There are a variety of factors that determine and affect the affinity of porphyrins for biological membranes and intracellular compartments. These factors include the hydrophobicity of the molecule, charge and aggregation state, pH, and the physicochemical properties of the microenvironment the porphyrin is in (Riccheli, 1995, and references cited therein).

Fig. 2.1. The haem biosynthetic pathway. The synthesis occurs partly in the mitochondria (as indicated on the left side of the figure) and partly in the cytoplasm. B6, pyridoxyl-5'-phosphate; ALA, α-aminolevulinic acid; PGB, porphobilinogen; URO'GEN, uroporphyrinogen; COPRO'GEN, coproporphyrinogen; PROTO'GEN, protoporphyrinogen; Ac, acetate; Pr, propionate; Vi, vinyl (source: Ponka, 1997).

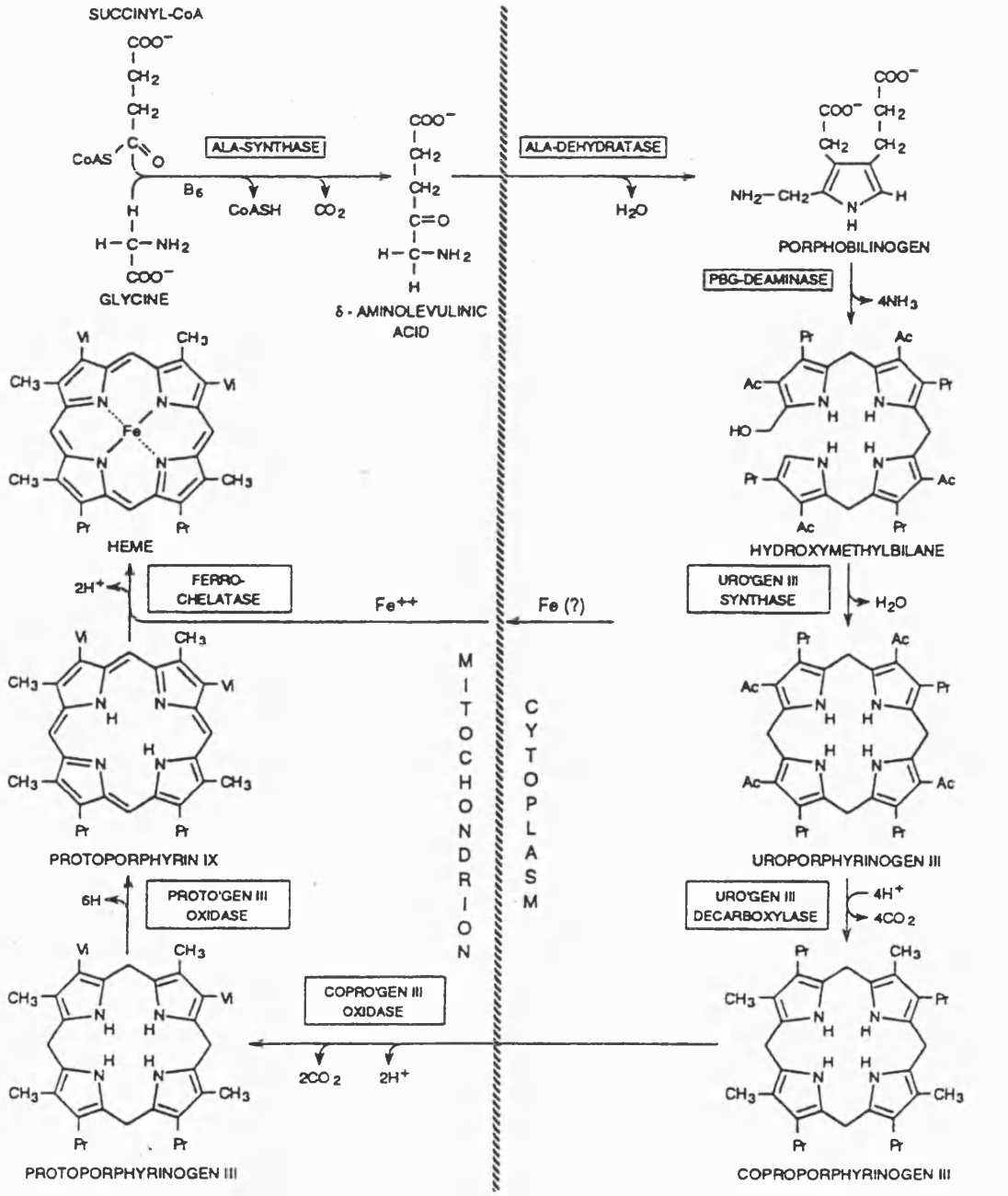

2.1.2 *Intracellular Effects of UVA Irradiation*

UVA radiation (320-380nm) generates reactive oxygen species (ROS) by photochemical reactions which cause lipid peroxidation, DNA damage, protein oxidation and inactivation of enzymes, and cell death (Tyrrell, 1991 and references cited therein; Vile et al., 1995). UVA is also known to induce several genes in a variety of different cell types (reviewed by Tyrrell, 1994, 1996), in particular, the major stress protein HO-1 in human skin fibroblasts (Keyse and Tyrrell, 1987).

2.1.3 *Intracellular Effects of ALA-PDT*

ALA based photodynamic therapy (ALA-PDT) is a clinical cancer treatment that is based on the administration of ALA to tumour tissues in order to generate photosensitising concentrations of PPIX. Activation of PPIX by light of an appropriate wavelength induces a photochemical reaction that is intended to destroy tumour cells and tissues (Kennedy and Pottier, 1992). It is generally accepted that the main activated oxygen species produced during PPIX photosensitisation is $^1O_2$, though other ROS may also be involved (He et al., 1995). Singlet oxygen has only a limited range of action 0.01-0.02 μm because of a short lifetime of 0.01-0.04 μs (Moan and Berg, 1991), therefore initial sites of damage are generally restricted to the immediate locality of the photosensitiser that generates it (e.g. PPIX). PPIX is produced mitochondrially so it is not unexpected that mitochondria have been shown to be damaged after ALA-PDT. Some forms of damage that have been documented include swelling of the mitochondria (Iinuma et al, 1996); morphological alterations, decreases in cellular ATP levels, and disruption to various mitochondrial enzymes and functions (Salet and Moreno, 1990); inactivation of mitochondrial ferrochelatase (He et al., 1995); and reduced oxygen consumption (Shevchuk et al., 1996). Owing to

PPIX localisation, ALA-PDT has been shown to damage other cellular compartments. Uberriegler and colleagues (1995) described endoplasmic reticulum decomposition, production of large cytoplasmic vacuoles, and the nucleus breaking down into several, partially compartmentalised smaller masses. Damage to lysosomes and release of acidic hydrolases induced by exogenous addition of PPIX and subsequent photosensitisation has been documented in mouse fibroblasts along with lipofuscin formation (Morliere et al., 1987). Gaullier et al. (1995) showed lysosomal damage, lipofuscin formation, and membrane blebbing in keratinocytes and fibroblasts that had been treated with ALA followed by exposure to targeted light. It was recently demonstrated that increasing the intracellular PPIX content of human skin fibroblasts by incubation with ALA significantly lowers the threshold for induction of HO-1 gene activation by UVA radiation (Ryter and Tyrrell, 1998). Neutrophils exposed to PPIX and UVA irradiation have exhibited inactivation of various soluble cytosolic enzymes and also exhibited leakage of potassium ions (K) and lactate dehydrogenase as a result of plasma membrane damage (Sandberg et al., 1981). Ionic alterations involving K leakage accompanied by Na, Cl, and Ca influx have also been observed in melanoma cells (Schoenfeld et al., 1995). Finally ALA-PDT has been also observed to cause cell inactivation by both apoptosis and necrosis and the type of death process depends on cell type (Noodt et al., 1996; Webber et al., 1996).

2.1.4 *UVA Absorbing Chromophores and the Objectives of this Study*

Identification of UVA absorbing chromophores that account for the radiation wavelength dependence of deleterious effects in the skin remains elusive. Riboflavin has been implicated as a critical chromophore by Sato and coworkers (1995; Minami et al., 1999). They have shown that addition of riboflavin (vitamin B_2) to normal

human fibroblasts significantly increases their sensitivity to UVA and the cytotoxic action of riboflavin is exerted primarily through the generation of H_2O_2 upon and after UVA irradiation. It is noteworthy however, that the concentration of riboflavin used in these studies was 100 μg/ml which is considerably higher than the level of 0.2 μg/ml which they document has been measured in normal human whole blood (Sato et al., 1995). The same group has also investigated UVA-induced pyridoxine (vitamin B_6) photosensitisation (Sato et al., 1993). This study showed that whilst a high concentration was used (100 μg/ml), the addition of pyridoxine also markedly enhanced the photosensitivity of normal human fibroblasts to UVA radiation. The mode of cytotoxicy of pyridoxine was reported to occur through photoproducts of this compound rather than through an intermediate such as H_2O_2.

In our study we have tested the hypothesis that PPIX may be a critical chromophore in the UVA inactivation of the human lymphoblastoid cell line, TK6 and the primary human fibroblast, FEK4. To achieve this objective it was necessary to determine the rate of cell inactivation by UVA as a function of intracellular PPIX concentration. PPIX was extracted by a method of acid extraction (Schoenfeld et al., 1995) and the concentration determined by spectrofluorimetry. Inactivation of TK6 cells was measured by assaying for clone forming ability 14 days post-irradiation (Tyrrell et al., 1984). Inactivation of FEK4 cells was measured by microscopically counting surviving populations 24 h post-irradiation (see methods), described by Gibson et al. (1997).

The rate of inactivation was derived from the slope of the dose response curve. Since cell inactivation was close to exponential it can be expressed by the mathematical relationship:

$$N/N_0 = e^{-kD}$$

Where N/N_0 is the surviving fraction after dose D, and k is the slope of the curve. The k value in this study is referred to as the inactivation rate constant.

2.1.5 *The MTS Assay*

The MTS (3-(4, 5-dimethylthiazol-2-yl)-5-(3-carboxymethoxyphenyl)-2-(4-sulphophenyl)-2H-tetrazolium, inner salt) assay was investigated as a possible method for determining ALA-induced phototoxicity. This particular method is more advanced, but effectively based on the same principle as the MTT assay, an assay that has and is being widely used to investigate the number of viable cells in proliferation or cytotoxicity assays. Mosman (1983) initially developed the MTT assay, based on the reduction of the tetrazolium salt, MTT (3-(4,5-dimethylthiazol-2-yl)-2,5-diphenyltetrazolium bromide) by actively growing cells to produce a blue formazan product. Despite its acceptance, the actual biochemical mechanisms or subcellular localisation of MTT reduction were actually unknown. For a period it was accepted that the cellular reduction of the MTT occurred in the mitochondria, the inner membrane mitochondrial enzyme succinate dehydrogenase being mostly responsible. In contrast to this, data produced more recently (Berridge and Tan, 1993) suggested most cellular MTT reduction occurred outside the inner mitochondrial membrane and involved pyridine nucleotide cofactors NADH and NADPH-dependent mechanisms,

possibly occurring in microsomes and on the outer mitochondrial membrane. The MTS assay works on a similar principle to that of the MTT assay, but is more advanced. The MTS tetrazolium compound, when used with an electron transfer reagent such as phenazine methosulphate (PMS), has the advantage of producing a soluble coloured formazan compound when bioreduced by viable cells (Fig. 2.2). The corresponding MTT formazan product, on the other hand, is insoluble and requires an additional solubilisation step, which can be particularly inconvenient when using suspension cell lines. The solubilisation step involves removing the original reagent, washing the cells, then adding an organic solvent such as dimethyl sulphoxide to solubilise the insoluble MTT formazan crystals, before adding the solution to a 96-well plate for reading. The convenience of using the MTS reagent is that the cells and the reagents are placed in a 96-well plate and can be recorded directly on a plate reader after a specified period. Fig 2.2 shows the schematic of the metabolism of MTS to its chracteristic coloured formazan product.

Fig. 2.2. Reduction of MTS to its formazan product by metabolically active cells. Dehydrogenase enzymes are thought to generate reducing equivalents such as NADH and NADPH which can transfer their electrons to the electron transfer reagent (ETR) phenazine methosulphate (PMS). The reduced PMS, in turn can directly interact with and reduce the MTS tetrazolium compound producing the coloured formazan product detectable at 490 nm (source: Promega technical bulletin #TB169, 1996).

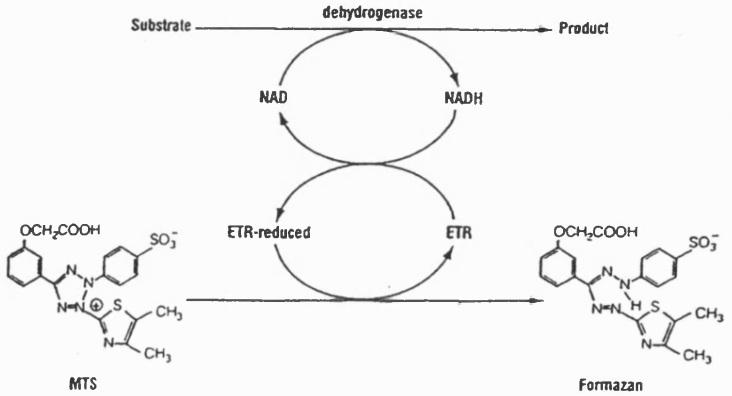

After testing the MTS method for suitability as a phototoxicity assay in response to UVA radiation, we became concerned that this type of assay might not be suitable for ALA-induced photosensitisation studies. This was because of a chemical reaction that occurs between ALA and MTT resulting in a characteristic blue formazan product (Campbell et al., 1996). In our study, we test for a similar reaction between ALA and MTS to determine if this assay is suitable for evaluating ALA-induced phototoxicity.

2.2 Methods

2.2.1 *Chemicals*

All chemicals were from Sigma Chemical Co. (UK) unless stated otherwise. Cell culture materials were from Gibco (UK), except foetal calf serum (FCS) which was from PAA Laboratories (Australia) and isotonic phosphate-buffered saline (PBS) which was from Oxoid (UK).

2.2.2 *Cell Culture*

The human lymphoblastoid cell line TK6 (Thilly, 1979) was cultured in RPMI 1640 supplemented with 10% FCS, L-glutamine, sodium bicarbonate, penicillin and streptomycin. Under these conditions the cells doubled approximately every 18-20h. Cultures were grown at 37°C in a 5% CO_2 incubator and were maintained in exponential growth phase by diluting to 2 x 10^5 cells/ml every 1 or 2 days. For all experiments, TK6 cells were diluted to 2 x 10^5 cells/ml and grown for 24h. The primary human skin fibroblast cell line FEK4 (Tyrrell and Pidoux, 1986) was cultured in Earle's modified minimal essential medium (EMEM) supplemented with 15% FCS, L-glutamine, sodium bicarbonate, penicillin and streptomycin. Cells were passaged by trypsinisation once a week and were used for experiments between passages 9 and 15. For all experiments, FEK4 cells were seeded into plastic culture dishes and grown for 3 days to approximately 80% confluency.

2.2.3 *Induction of PPIX Synthesis*

PPIX levels in TK6 and FEK4 cells were modulated by addition of ALA to the culture media in concentrations up to 400 μM and 200 μM respectively, for 4 and 18 hours in the dark. Subsequent handling of cells was performed under low light.

2.2.4 *Extraction of Porphyrins*

After ALA incubation, porphyrins were extracted according to the method described by Schoenfeld *et al.* (1994) as follows: Approximately 1 x 10^7 cells were collected and centrifuged for 5 min at 1000 rpm. TK6 could be directly spun from their culture media, but FEK4 needed to be washed with PBS and trypsinised from the plates before being collected. After spinning down, cells were washed with PBS, centrifuged again, then re-suspended in 0.75 ml of glacial acetic acid. This suspension was briefly sonicated, after which 2.25 ml of ethyl acetate was added. The mixture was vortexed, centrifuged at 2500 rpm for 5 min and the supernatent collected. PPIX was back extracted into 1ml of 1.5M HCl by vortexing the supernatent with the HCl and centrifuging as before. The organic phase (top) was aspirated and the acid phase (bottom) containing the porphyrins was retained for spectrofluorimetric measurement.

2.2.5 *Fluorimetric Determination of Porphyrin Levels in the Extract*

A commercial PPIX standard (Sigma Chemical Co., UK) was prepared for a calibration curve, which was measured using a spectrofluorimeter (Kontron SFM25, Switzerland). The PPIX (MW 606.6) was initially dissolved in DMSO at a concentration of 10 μg/ml and subsequently serially diluted in 1.5 M HCl for calibration standards. Fluorescence of the extracts was measured at an excitation of 404 nm and emission of 604 nm (maxima were determined by doing a wavelength scan of the excitation and emission spectra of the commercial PPIX standard, Fig. 2.5). PPIX concentration of the extracts was determined in relation to the fluorescence of the PPIX standard.

2.2.6 *UVA Source and Irradiation Conditions for TK6 and FEK4 Cells*

Irradiation was performed at a temperature between 20 and 24°C using a broad spectrum Sellas 4 kW UVA lamp (Germany), the spectral output of this lamp is shown in Fig. 2.3. The UVA dose rate was measured using an IL1700 radiometer (International Light, USA). TK6 cell suspensions were irradiated at a density of 5 x 10^5 cells/ml in PBS supplemented with 0.01% Ca^{2+} and Mg^{2+}(Keyse and Tyrrell, 1989). Cells were irradiated in quartz vessels (Scientific Laboratory Supplies Ltd, England) that were agitated using a mixing platform (IKA Laboratechnik,Germany). Sham- irradiated cells were treated in the same manner. 80% confluent FEK4 cells were irradiated in the dishes they were cultured in. Prior to irradiation, media was removed and cells were washed with isotonic phosphate-buffered saline (PBS). Cells were then covered in PBS supplemented with 0.01% Ca^{2+} and Mg^{2+} and irradiated. Sham-irradiated cells were treated in the same manner.

Fig. 2.3. UVA lamp profile. The spectral output of the UVA Sellas lamp is divided in to two parts, 200-400 nm (below) and 400-700 nm (p. 42). Note the relative emission intensity (y-axis) is in much smaller units in the second part of the emission spectrum (p. 42).

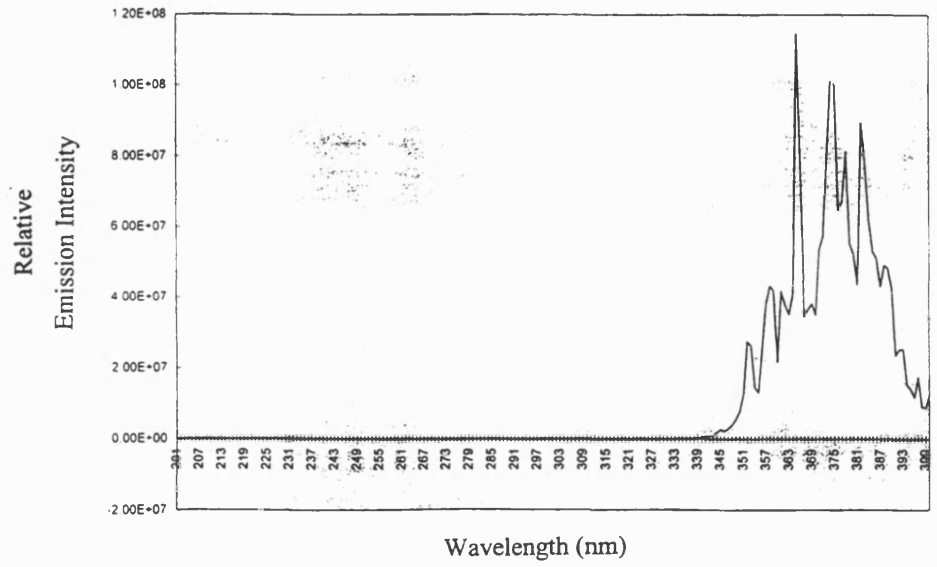

Fig. 2.3. continued.

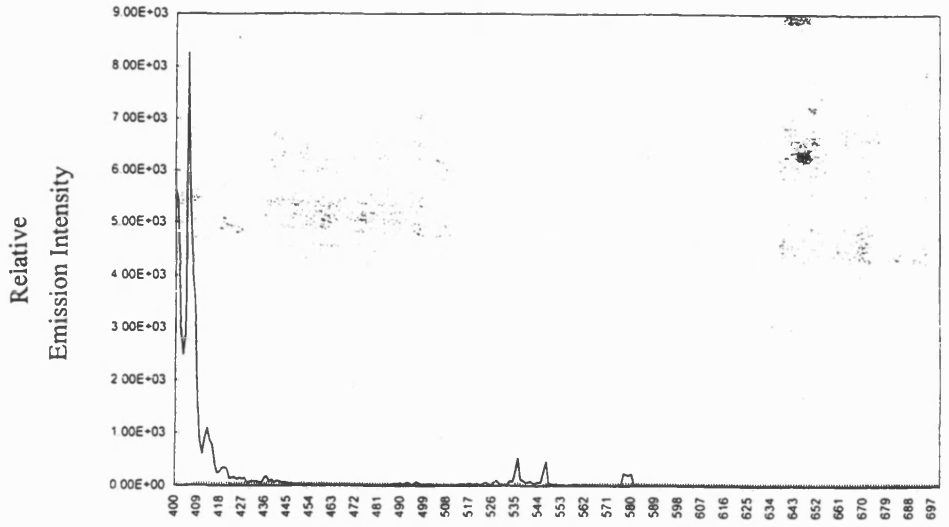

2.2.7 *Determination of Phototoxicity in TK6 Cells as a Result of UVA Irradiation as Determined by the CellTiter 96® AQueous One Solution Cell Proliferation Assay*

The CellTiter 96® AQueous One Solution Cell Proliferation Assay (Promega, UK) was optimised for TK6 cells (data not shown) so that phototoxic effects of UVA could be investigated (the principle of this assay is described in section 2.1.5). A solution was made up in Milli-Q water (Millipore, UK) containing MTS tetrazolium compound at a concentration of 133 μg/ml and 25 μM phenazine methosulphate (PMS). The MTS/PMS solution was distributed in a 96-well plate (Helena Bioscience, UK), 20 μl per well. After irradiation (up to 500 kJ/m^2 UVA), the TK6 cells were collected, centrifuged for 5 min at 1000 rpm, then re-suspended at a density of 1 x10^6 cells/ml in serum free medium. 100 μl of this cell suspension was added to each well of the 96-well plate containing the MTS/PMS solution. The 96-well plate was then incubated for two hours at 37°C to allow formation of the soluble MTS

formazan product. The reaction was stopped by adding 25 µl of 10% SDS to each well. Absorbance was recorded at 490 nm using a microplate reader and corrected using a blank (reagents minus cells). There was a linear response between number of viable cells and the amount of MTS formazan compound produced at 490 nm (Fig 2.4). Absorbance of UVA irradiated cells was compared to those of sham-irradiated cells and expressed as percentage of viable cells.

Fig. 2.4. The effect of cell number on absorbance at 490 nm using the CellTiter 96® AQ_{ueous} One Solution Assay. Various numbers of TK6 human lymphoblastoid cells in 100 µl of RPMI were added to wells of a 96-well plate each containing 20 µl of the MTS/PMS solution (see text). After 2 h at 37°C in a humidified 5% CO_2 atmosphere, the absorbance was recorded at 490 nm using an ELISA plate reader. Each point represents the mean ± S.D. of 4 independent experiments. The correlation coefficient was 0.99938, indicating that there was a linear response between viable cell number and absorbance at 490 nm. The background absorbance for blank and cell number and was corrected for.

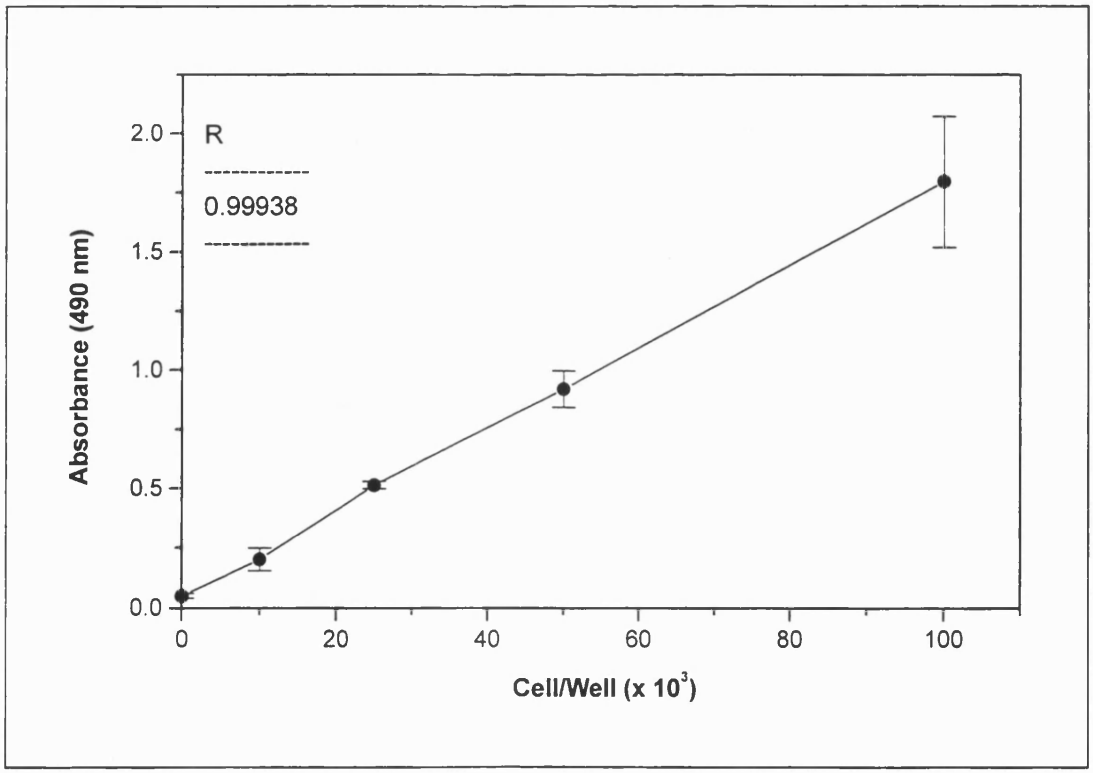

2.2 8 *Investigation of the Interaction Between ALA and MTS*

This investigation was performed using the method described in section 2.2.7. Instead of measuring absorbance of the MTS formazan produced by cells, absorbance of the MTS formazan produced as a result of interaction between the MTS tetrazolium salt and ALA was measured, as a function of ALA concentration. Results were displayed as fold increase in absorbance over control. The control used was reagents minus ALA. ALA was prepared in serum free media in concentrations up to 120 μM.

2.2.9 *Determination of Phototoxicity in TK6 Cells Using the Cloning Assay*

The cloning assay was performed according to Tyrrell et al., (1984). TK6 cell suspensions were diluted in fresh complete media to a concentration of 10 cells per ml and were distributed in 96-well microtiter plates at a volume of 200 μl per well (i.e. 2 cells/well). Cells were incubated at 37°C in a humidified 5% CO_2 atmosphere and after a minimum of 14 days, colonies were scored microscopically. The original cloning efficiency was calculated assuming poisson distribution of the clone forming units over the wells using the formula:

$$\text{Cloning efficiency} = -\ln P_0/n$$

Where P_0 is the fraction of wells with no clone present and n is the average number of cells originally distributed per well. Under our conditions, the cloning efficiency of TK6 human lymphoblastoid cells on the plastic microtiter plates was approximately 70-80%. ALA-treated and UVA-irradiated cells as described above, and surviving fractions were calculated with reference to the sham-irradiated controls.

2.2.10 *Determination of Phototoxicity in FEK4 Cells*

Phototoxicity was determined in FEK4 cells according to a method described by (Gibson et al., (1997). After irradiation, the buffer was removed and conditioned media added to the plates. Cells were incubated for 24 h after which the conditioned media was removed and the plates washed with PBS. Cells were trypsinized and re-suspended in 1 ml of complete media. Cell counts were performed microscopically; ALA-treated and UVA-irradiated surviving fractions were determined relative to the sham-irradiated levels.

2.2.11 *Determination of the Inactivation Rate Constant, k*

The inactivation rate constant was determined as described in section 2.1.4.

2.3 Results

2.3.1 *PPIX Calibration for Spectrofluorimetry*

The excitation and emission maxima were determined by running the appropriate wavelength scans of the commercial PPIX standard (Fig. 2.5a). These maxima were then used to measure the fluorescence of the serially diluted PPIX standard in order to construct the calibration curve (2.5b). The concentration of PPIX in prepared extracts was subsequently measured using identical conditions.

Fig. 2.5. (a) Excitation and emission spectra of PPIX in HCl. **(b)** A typical calibration curve of a PPIX standard, measured using spectrofluorimetry.

(a)

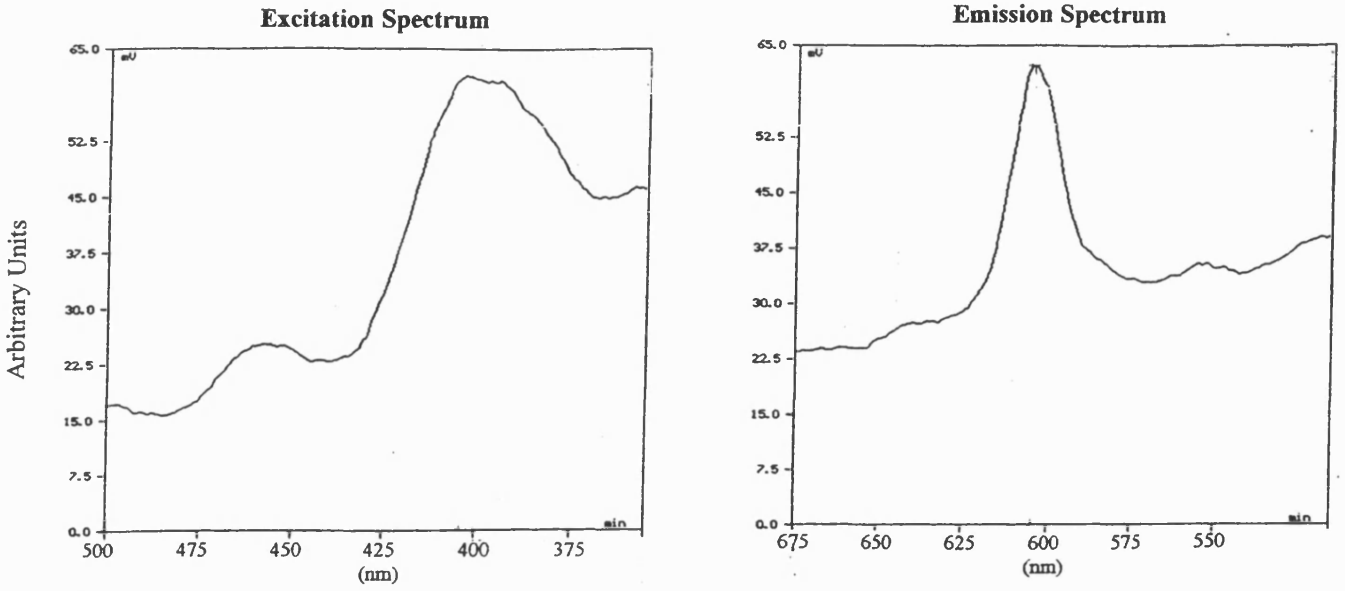

(b)

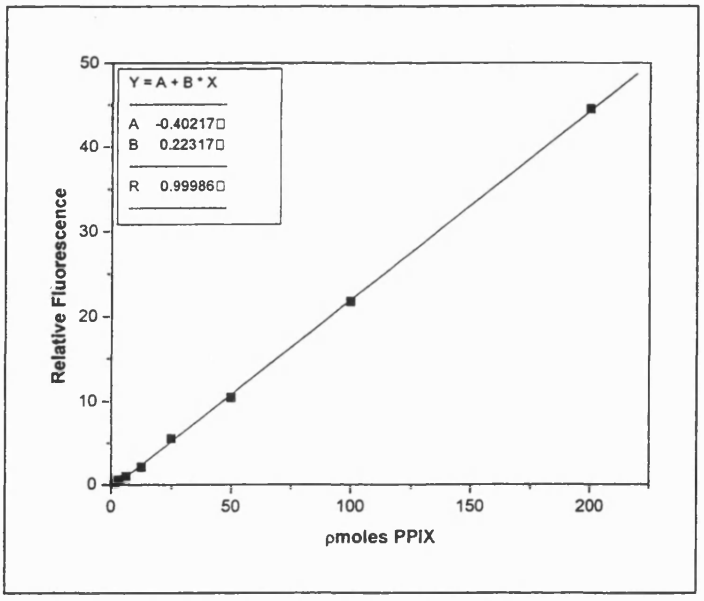

2.3.2 *PPIX Biosynthesis in TK6 Human Lymphoblastoid Cells*

Porphyrin synthesis was stimulated by ALA treatment of the cells at concentrations between 100 and 400 μM for 4 and 18 hours (Fig. 2.6). No ALA dark toxicity was observed using these conditions (data not shown). PPIX was extracted from the cells and measured using spectrofluorimetry. The porphyrin accumulation in these cells appeared to be ALA dose dependent. Both incubation periods yielded similar quantities of intracellular PPIX with the range of ALA concentrations used. When porphyrin synthesis was stimulated (with ALA concentrations ranging from 100 to 1000 μM) up to 18 hours and PPIX extracted at different times during this period, total intracellular PPIX content appeared to reach a maximum at approximately 8 h (Fig.2.7). Between 8 and 18 hours, total intracellular content of PPIX decreased due to efflux of the molecule from the cell.

Fig. 2.6. Biosynthesis of PPIX by TK6 cells as a function of ALA concentration in the culture medium. The graph shows the amount of PPIX in the cells after 4 (●) and 18 hours incubation (O) with ALA. Data represent the mean of 3-5 independent experiments (± S.D.).

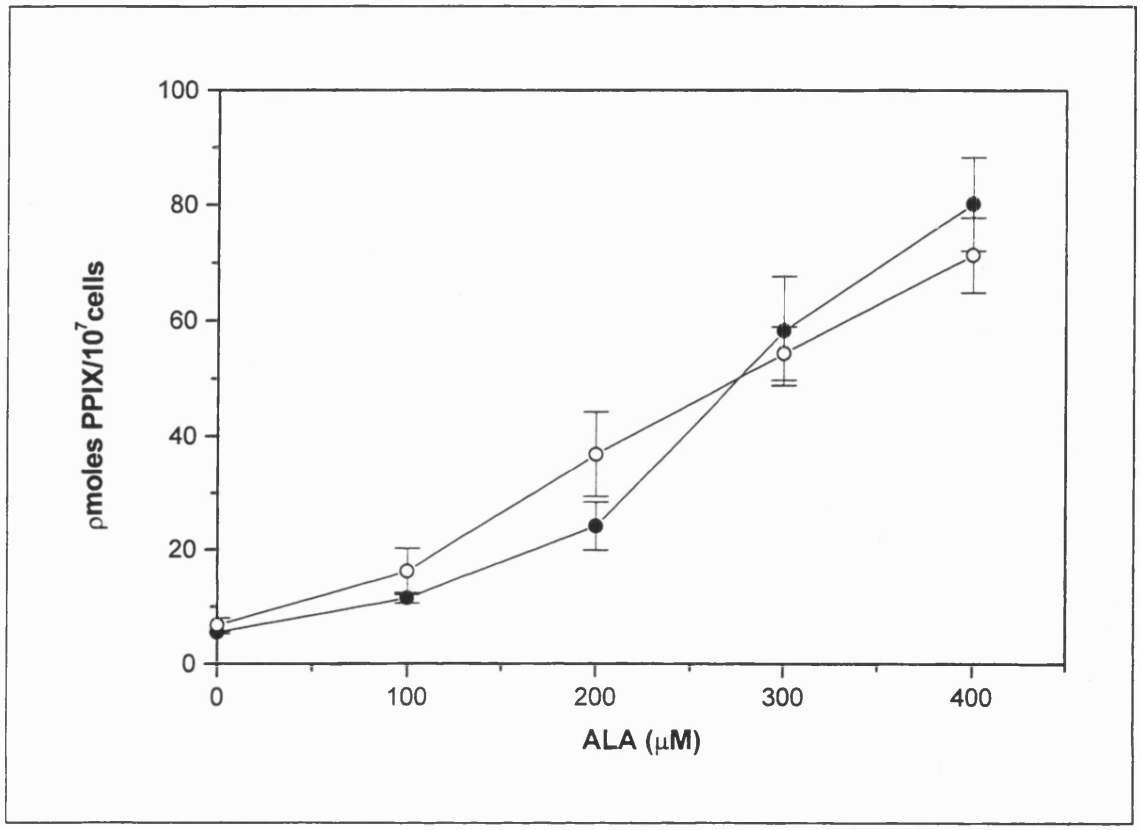

Fig. 2.7. Biosynthesis of PPIX by TK6 cells as a function of incubation time and ALA concentration in the culture medium. The graph shows the amount of PPIX in the cells over time after incubation with either no ALA (▼), 100μM (∇), 400μM (●), or 1000μM (O) ALA. Data represent the mean of 3-5 independent experiments (± S.D.).

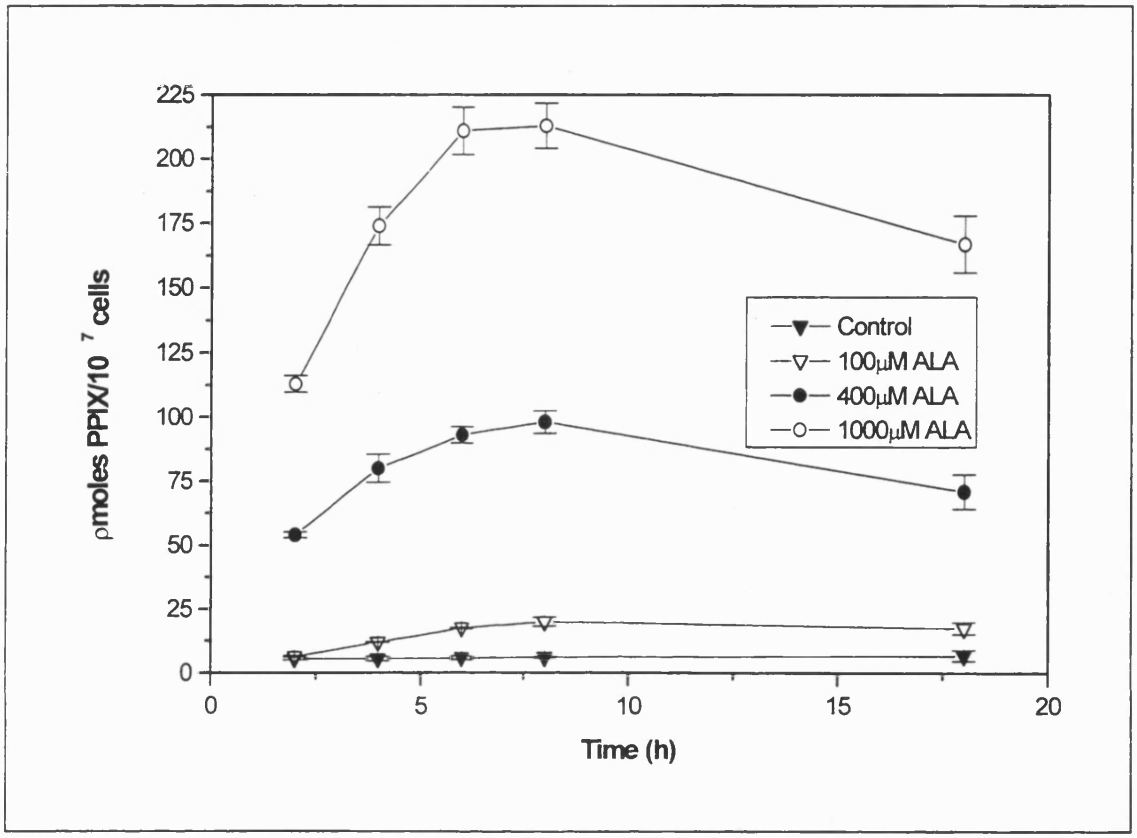

2.3.3 *PPIX Biosynthesis in FEK4 Primary Human Skin Fibroblasts*

Porphyrin synthesis was stimulated by ALA treatment of the fibroblasts at concentrations between 50 and 200 μM for 4 and 18 hours (Fig. 2.8). No ALA dark toxicity was observed using these conditions (data not shown). The porphyrin accumulation in these cells also appeared to be ALA dose dependent. Unlike TK6, the 18 h incubation yielded significantly higher intracellular PPIX concentrations compared to 4 h with the range of ALA concentrations used. As ALA dose increased, the PPIX ratio between the two incubations also increased. Incubation with ALA for 18 h at a concentration of 50 μM produced a 1.765-fold higher intracellular PPIX concentration compared to the 4 h incubation, whereas 200 μM ALA produced a 4.778-fold higher PPIX level after 18 h than after 4 h.

Fig. 2.8. Biosynthesis of PPIX by FEK4 cells as a function of ALA concentration in the culture medium. The graph shows the amount of PPIX in the cells after 4 (●) and 18 hours incubation (O) with ALA. Data represent the mean of 3-4 independent experiments (± S.D.).

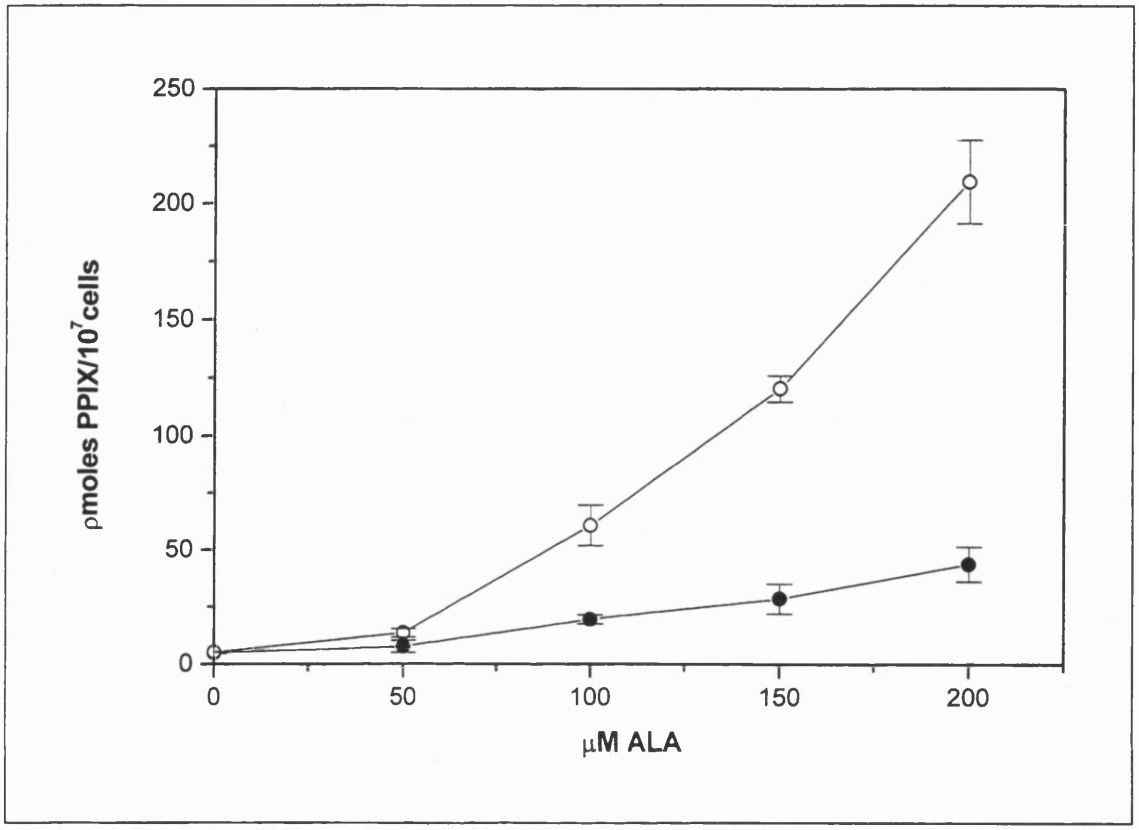

2.3.4 *MTS – A Viability Marker to Quantify UVA-induced Phototoxicity*

TK6 cells were irradiated with UVA doses up to 500 kJ/m^2 and then incubated with the MTS tetrazolium salt. Production of the soluble coloured MTS formazan product (as a result of bioreduction of the tetrazolium salt by viable cells), as measured at 490 nm, is directly proportional to the number of living cells in culture (Fig.2.4) so this assay was employed to evaluate UVA-induced phototoxicity. Fig 2.9 shows the UVA dose response observed using this assay.

Fig. 2.9. Percentage of viable cells at a series of UVA doses as estimated using the MTS assay. Following irradiation, 1 x 10^5 cells (were incubated for 2h at 37°C in (100 µl of) serum free media containing 133 µg/ml MTS formazan salt. Data represent the mean of 3 independent experiments (± S.D.).

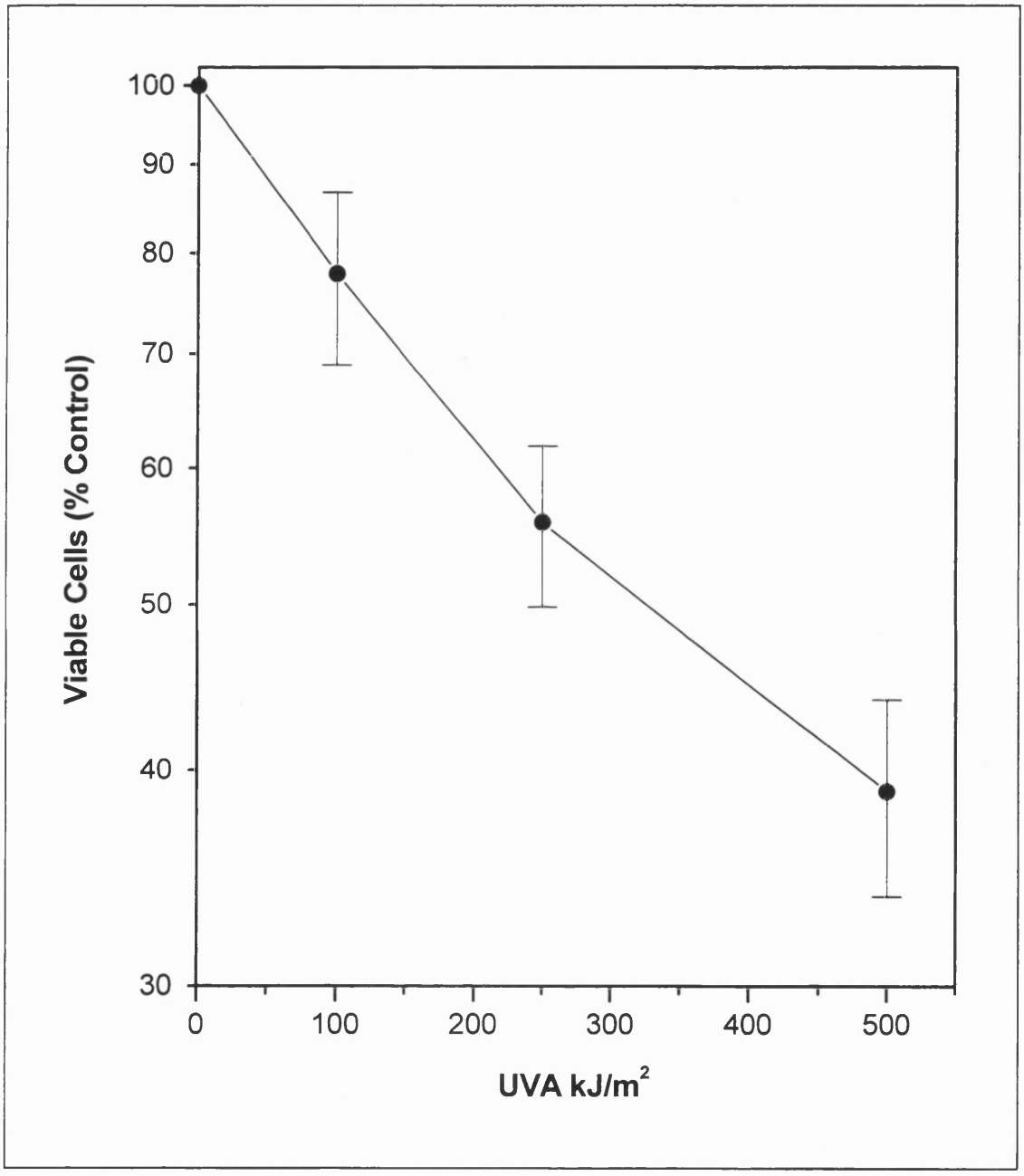

2.3.5 *MTS Tetrazolium Salt and its Interaction with ALA*

It was previously reported (Campbell *et al.,* 1996) that the value of the colourimetric MTT (methyl-thiazol-tetrazolium) assay for use in evaluating phototoxicity as a result of ALA-induced photosenstisation was limited due to a chemical reaction between ALA and MTT resulting in a blue formazan product. The MTS and MTT are very similar reagents so the interaction of ALA and MTS was investigated to determine if this assay could be used for further phototoxic investigations involving cells treated with ALA. Fig. 2.10 shows the fold increases in absorbance over control (at 490 nm) as a result of an interaction between MTS and ALA as a function of ALA concentration in a cell-free system. From this graph, it is clear that somewhere between 7.5 and 15 μM ALA there is a sharp increase in the absorbance measured at 490 nm.

Fig. 2.10. Changes in absorbency measured at 490 nm as a result of the interaction between ALA and MTS formazan salt after 2h incubation at 37°C. The reaction was performed in a cell-free, serum-free medium. Data represent the mean of 3 independent experiments (± S.D.).

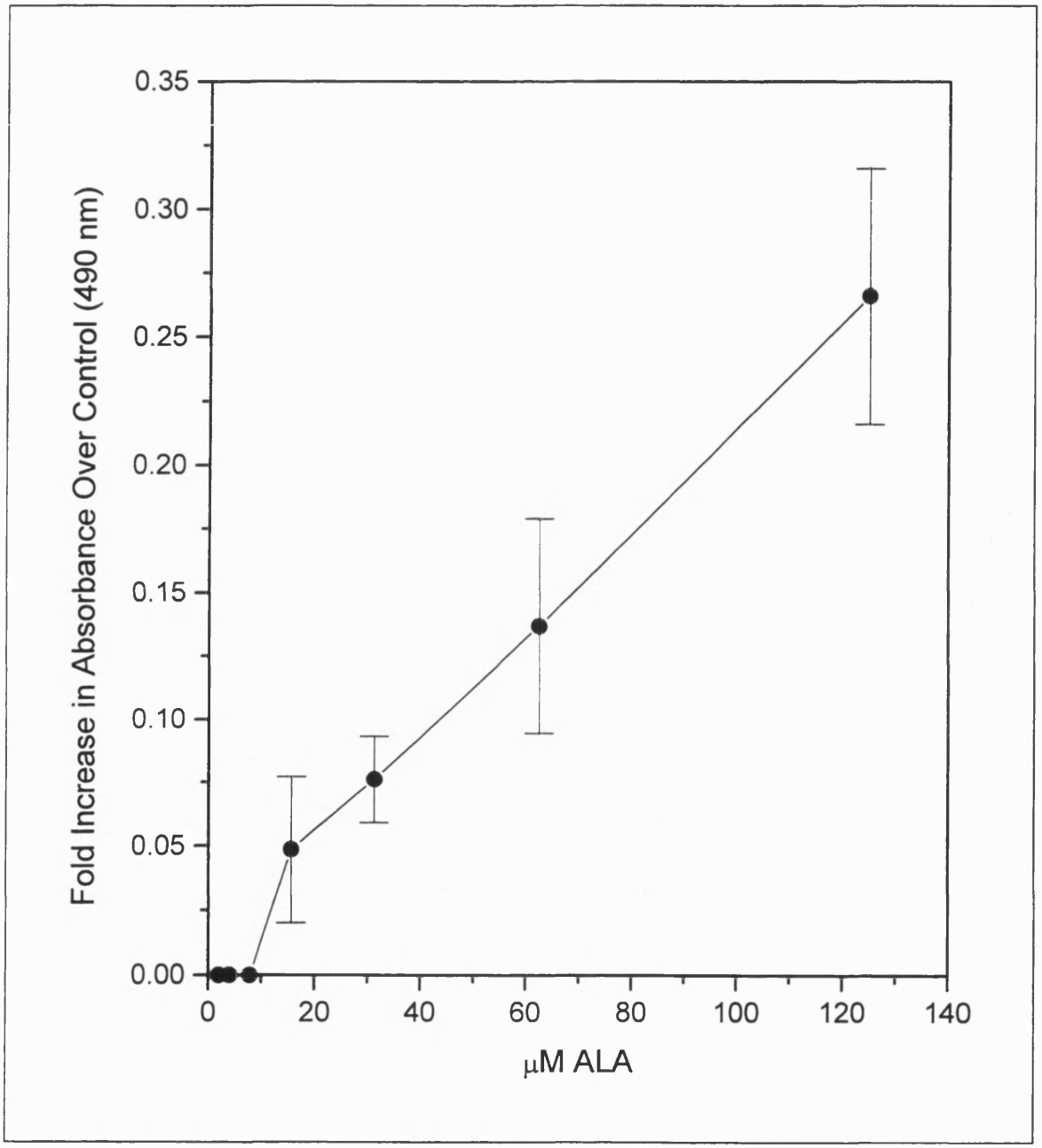

2.3.6 *UVA-induced Porphyrin Toxicity in TK6 Human Lymphoblastoid Cells*

Figs. 2.11 and 2.12 display the UVA dose response curves for TK6 cells with various intracellular PPIX concentrations. Cells were stimulated with ALA for 4 (Fig. 2.11) and 18 hours (Fig.2.12) then exposed to graded doses of UVA. Following irradiation, cells were assayed for colony forming ability (see methods). This data clearly shows that the degree of UVA-induced toxicity increases as a function of intracellular PPIX content in these cells. However, there is no simple correlation between total intracellular PPIX concentration and the rate of UVA-induced cell inactivation. The relative rates of cell inactivation appears to be more efficient after the 4 h ALA incubation than after 18 h (see Fig.2.16).

Fig. 2.11. UVA dose-dependent inactivation of clone-forming ability of TK6 cells with ALA-induced PPIX. Cells were incubated with ALA for **4h** followed by UVA irradiation, then assayed for clone-forming ability. The legend indicates the intracellular PPIX concentration as a result of ALA treatment. Data represent the mean of 3-4 independent experiments (± S.D.).

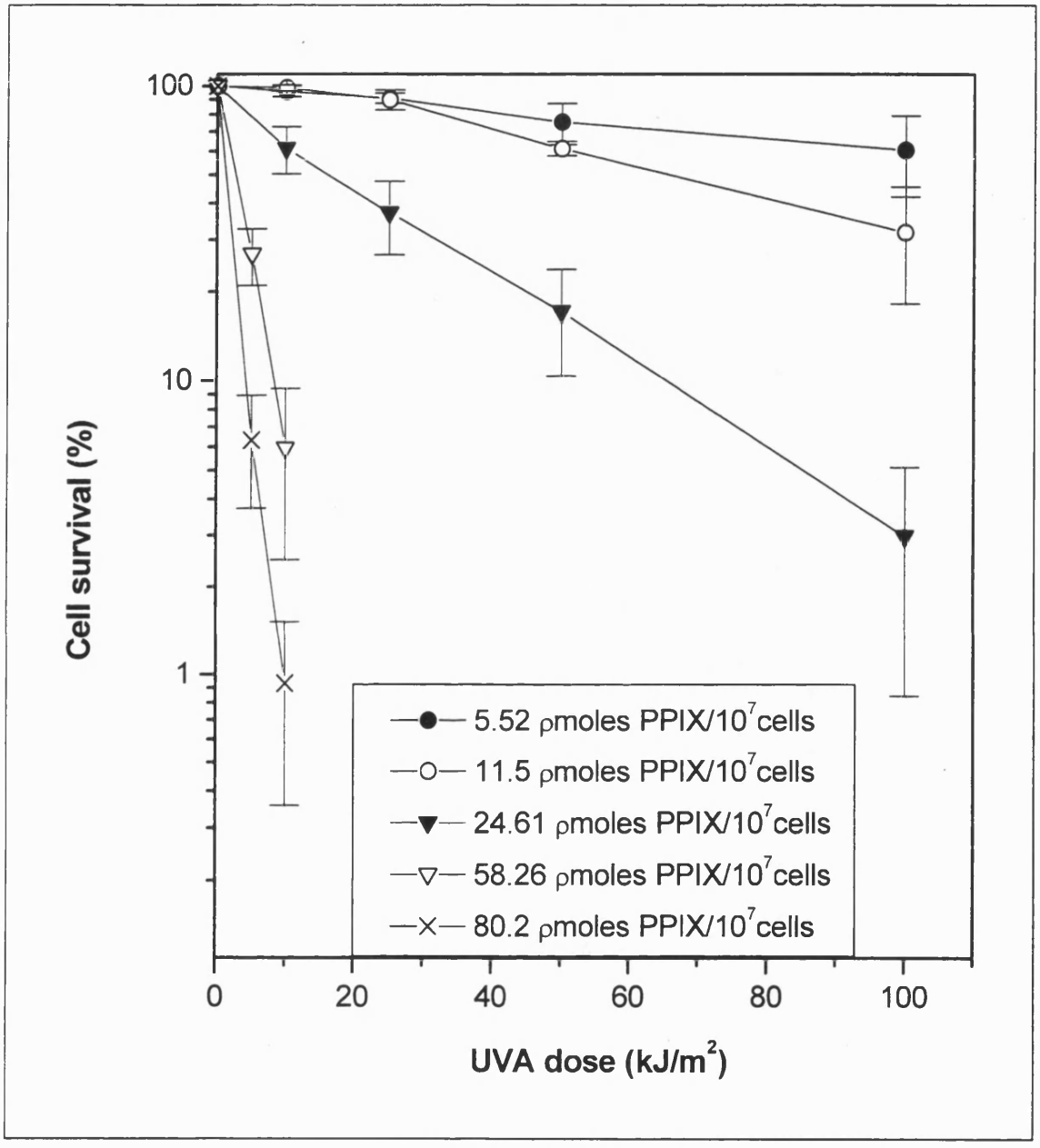

Fig. 2.12. UVA dose-dependent inactivation of clone-forming ability of TK6 cells with ALA-induced PPIX. Cells were incubated with ALA for **18h** followed by UVA irradiation, then assayed for clone-forming ability. The legend indicates the intracellular PPIX concentration as a result of ALA treatment. Data represent the mean of 3-4 independent experiments (± S.D.).

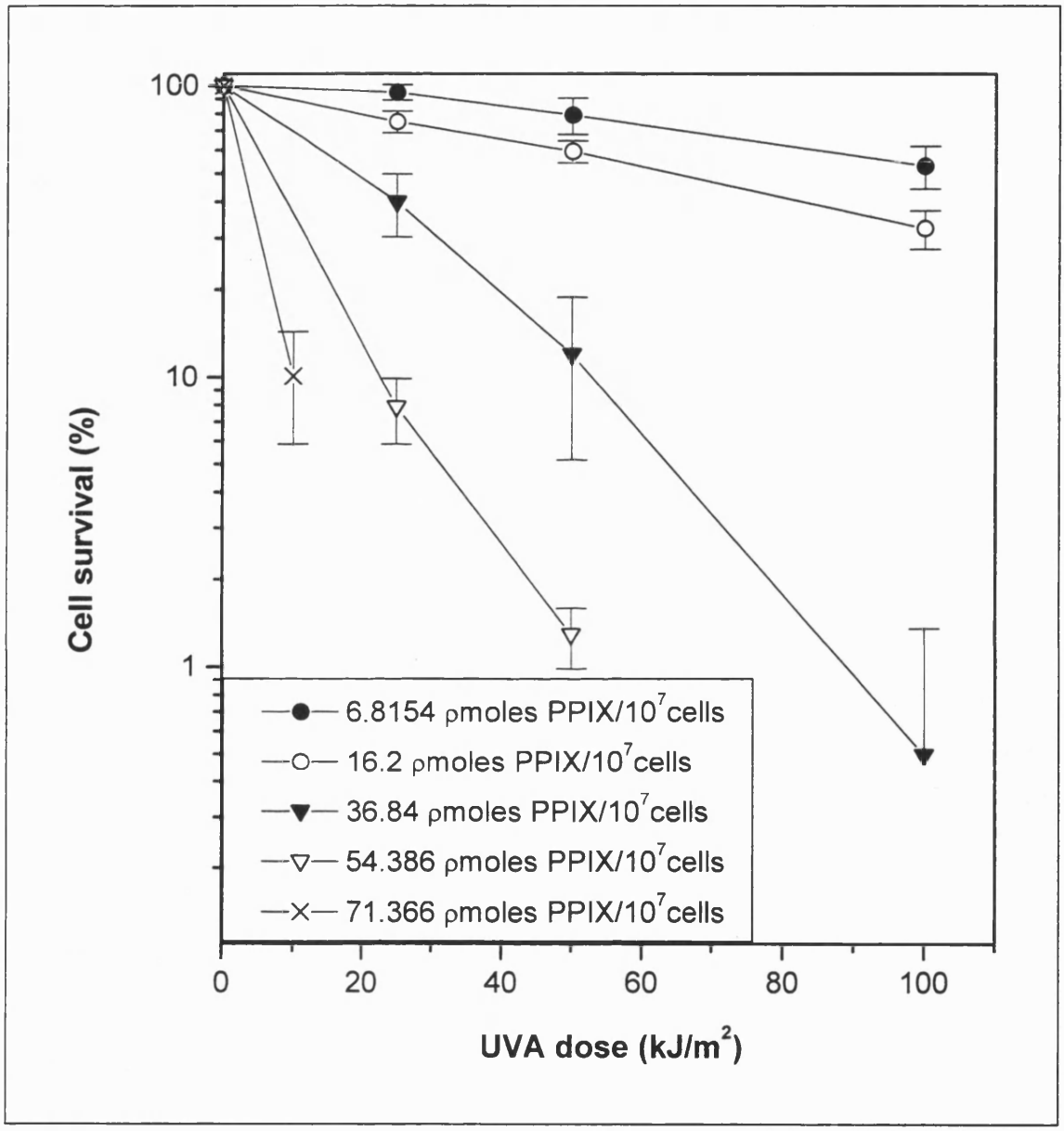

2.3.7 *UVA-induced Porphyrin Toxicity in FEK4 Primary Human Skin Fibroblasts*

Fig. 2.13 shows the dose response of 80% confluent untreated FEK4 cells to UVA after doses up to 500 kJ/m^2. As the graph shows, the highest UVA dose in this study resulted in a 50% survival 24 h post-irradiation. Figs. 2.14 (4 h ALA) and 2.15 (18 h ALA) display the UVA dose response curves for FEK4 cells with various intracellular PPIX concentrations. Cells were stimulated with ALA for 4 and 18 hours then exposed to graded doses of UVA. Following irradiation, cell survival was measured 24 h later (see methods). Similar to TK6, this data shows that the degree of UVA-induced toxicity increases as a function of intracellular PPIX content in these cells. However, also like the TK6, there is no simple correlation between total intracellular PPIX concentration and the rate of UVA-induced cell inactivation (see Fig. 2.17).

Fig. 2.13. UVA dose-dependent cell killing of FEK4 fibroblasts. Cells were grown to approximately 80% confluency followed by UVA irradiation; survival was determined after 24 h. Data represent the mean of 4 independent experiments (± S.D.).

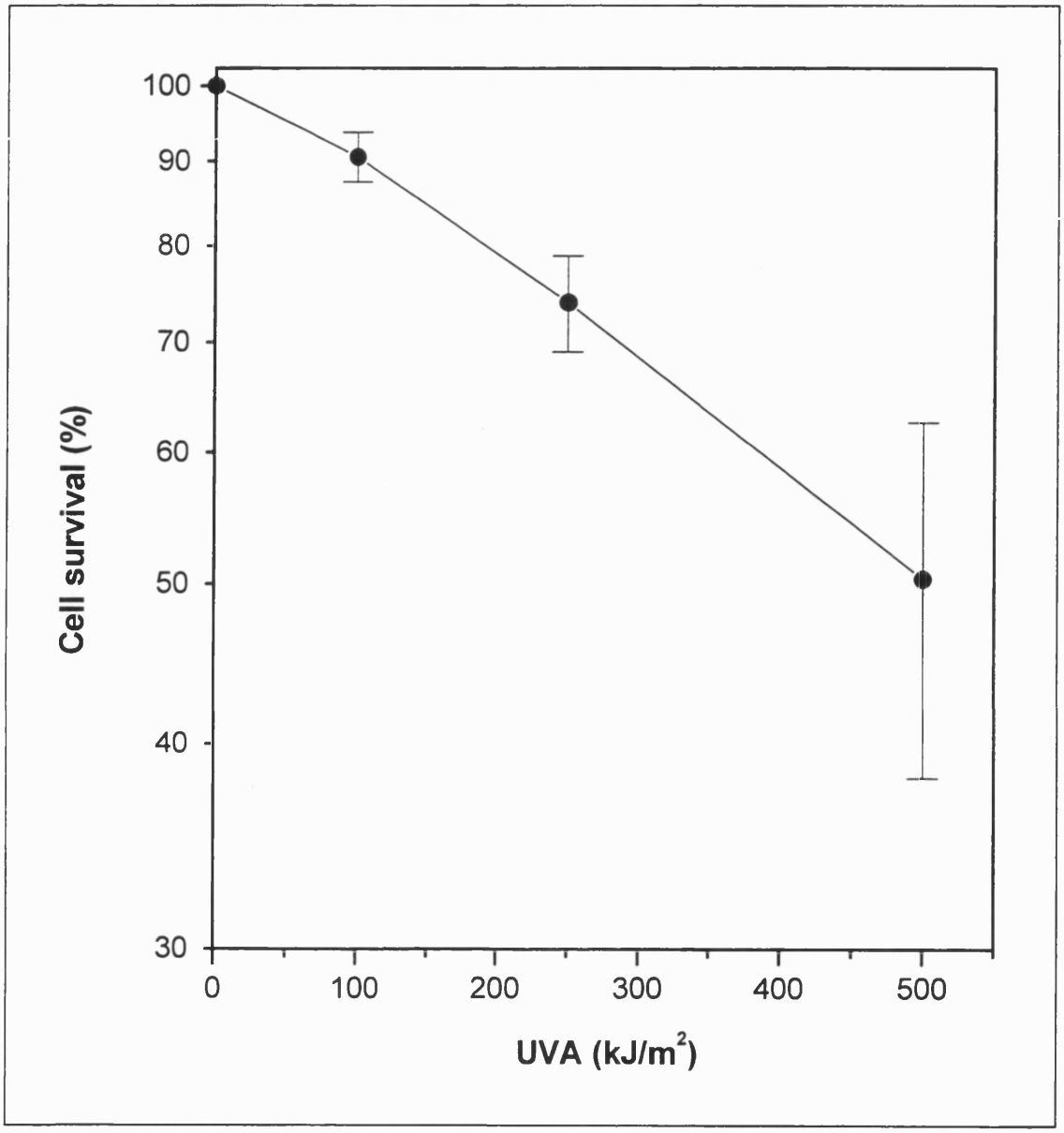

Fig. 2.14. UVA dose-dependent cell killing of FEK4 fibroblasts with ALA-induced PPIX. Cells were incubated with ALA for **4h** followed by UVA irradiation; survival was determined after 24h. The legend indicates the intracellular PPIX concentration as a result of ALA treatment. Data represent the mean of 4 independent experiments (± S.D.).

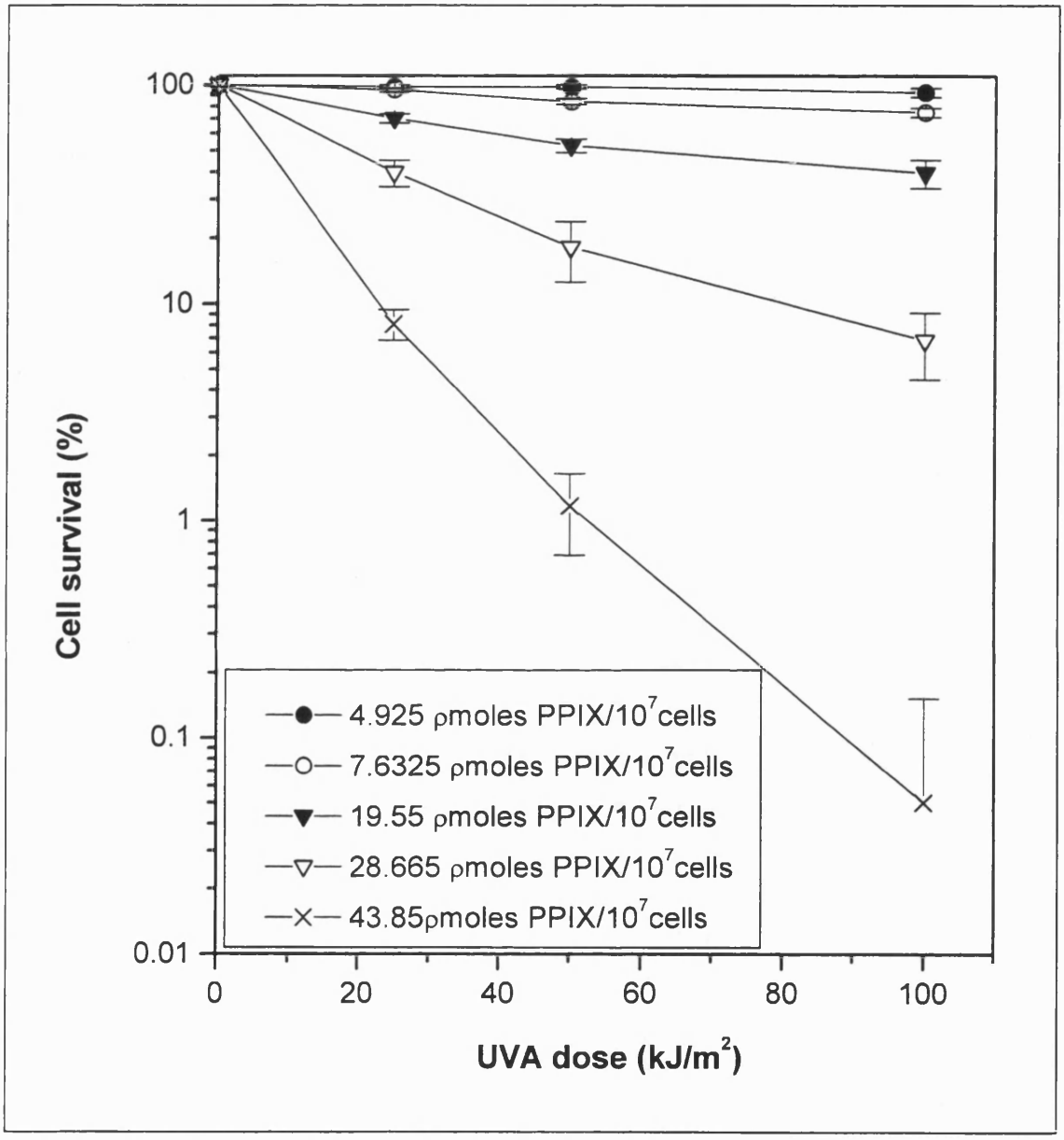

Fig. 2.15. UVA dose-dependent cell killing of FEK4 fibroblasts with ALA-induced PPIX. Cells were incubated with ALA for **18h** followed by UVA irradiation; survival was determined after 24h. The legend indicates the intracellular PPIX concentration as a result of ALA treatment. Data represent the mean of 4 independent experiments (± S.D.)

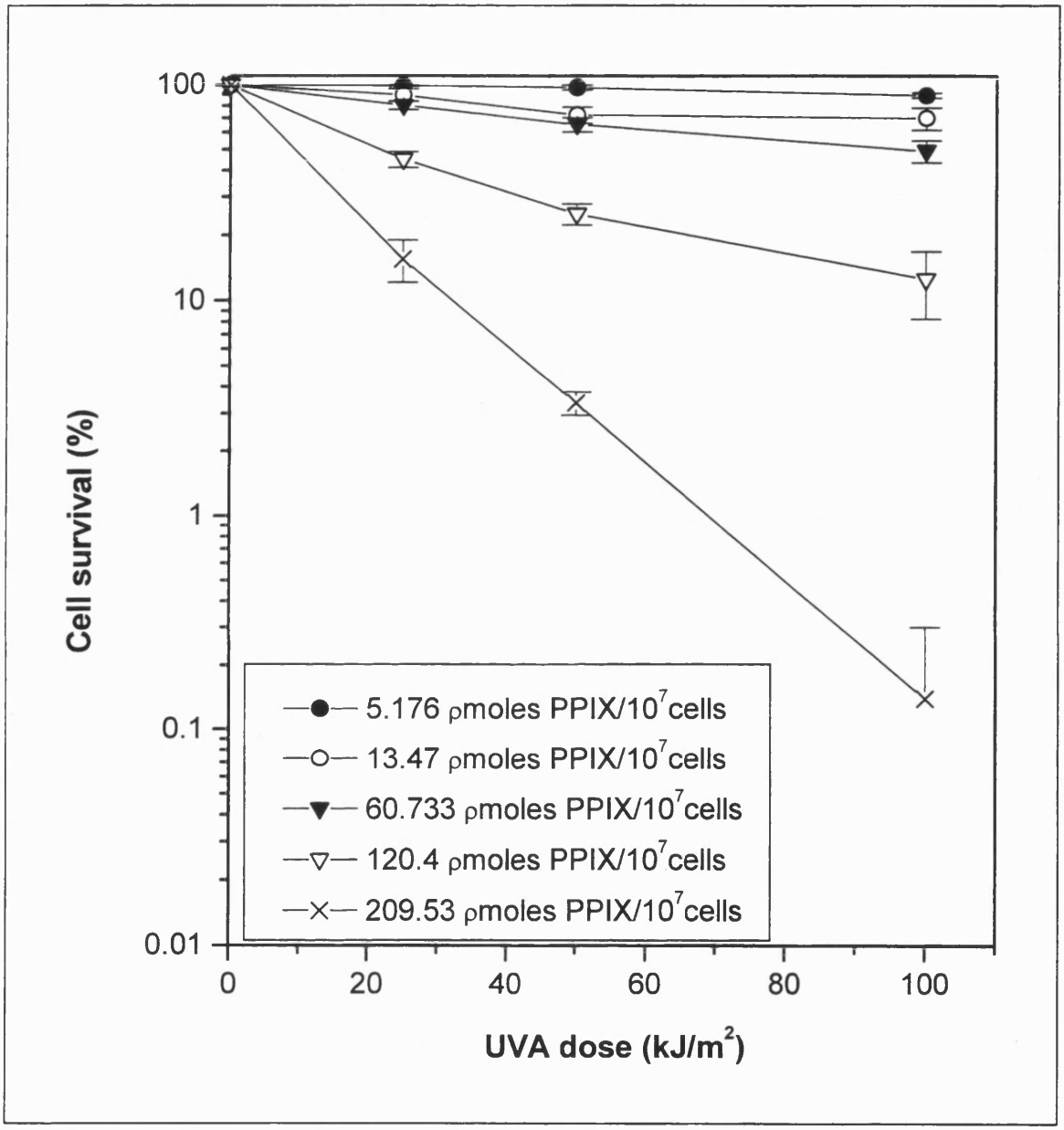

2.3.8 *Inactivation of TK6 Cell Populations by UVA as a Function of PPIX Concentration*

Fig. 2.16 depicts the rate of inactivation of TK6 cell populations plotted as a function of intracellular PPIX concentration. This data shows that the rate of inactivation of these cells with modulated PPIX levels is generally higher after 4 h ALA incubation than it is after 18 h. By examining the relationship between the inactivation rate constants at different intracellular PPIX concentrations, an estimate of the basal content of PPIX that would be necessary to lead to significant cell death following UVA irradiation can be derived by back extrapolating the linear portion of the curve to the abscissa. The estimate of the appropriate concentration of PPIX after 4 and 18 hours ALA incubation was approximately 20 and 40-45 pmoles/10^7 cells respectively. The estimated basal content of PPIX in the TK6 cells varied between 5.5 and 7 pmoles/10^7 cells (see discussion).

Fig. 2.16. Rates of inactivation of TK6 cells by UVA radiation as a function of intracellular PPIX concentration. The graph shows the inactivation rate constants (k) of cells incubated for 4 (●) and 18 hours (O) with ALA followed by UVA irradiation, verses intracellular PPIX concentration. Data represent the mean of 3-4 independent experiments (± S.D.).

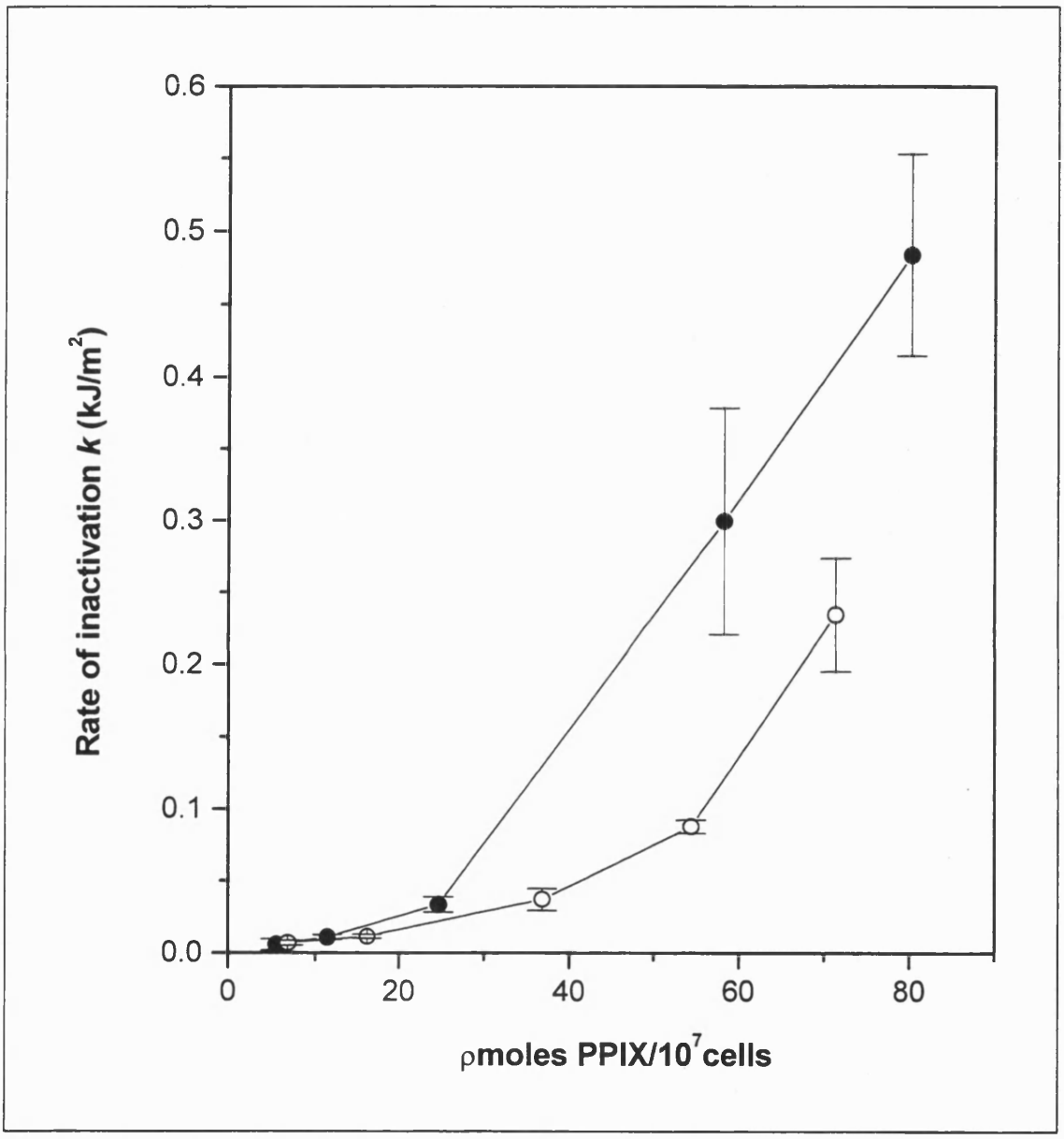

2.3.9 *Inactivation of FEK4 Cell Populations by UVA as a Function of PPIX Concentration*

Fig. 2.17 depicts the rate of inactivation of FEK4 cell populations plotted as a function of intracellular PPIX concentration. This data shows that the rate of inactivation of cells is greater as a function of intracellular PPIX concentration after 4 h ALA incubation compared with 18 h incubation. Estimation of the basal content of PPIX that would be necessary to lead to significant cell death following UVA irradiation in FEK4 cells was performed in the same manner as it was for TK6 (see section 2.3.8). The estimate after 18 hours ALA incubation was approximately 10-20 pmoles/10^7 cells. In contrast to the 18 h incubation (and to the TK6 data), the estimate for 4 h ALA incubation was within the linear portion of the curve. The measured basal content of PPIX in the FEK4 cells varied between 4.925 and 5.176 pmoles/10^7 cells (see discussion).

Fig. 2.17. Rates of inactivation of FEK4 cells by UVA radiation as a function of intracellular PPIX concentration. The graph shows the inactivation rate constants (k) of cells incubated for 4 (●) and 18 hours (O) with ALA followed by UVA irradiation, verses intracellular PPIX concentration. Data represent the mean of 3-4 independent experiments (± S.D.).

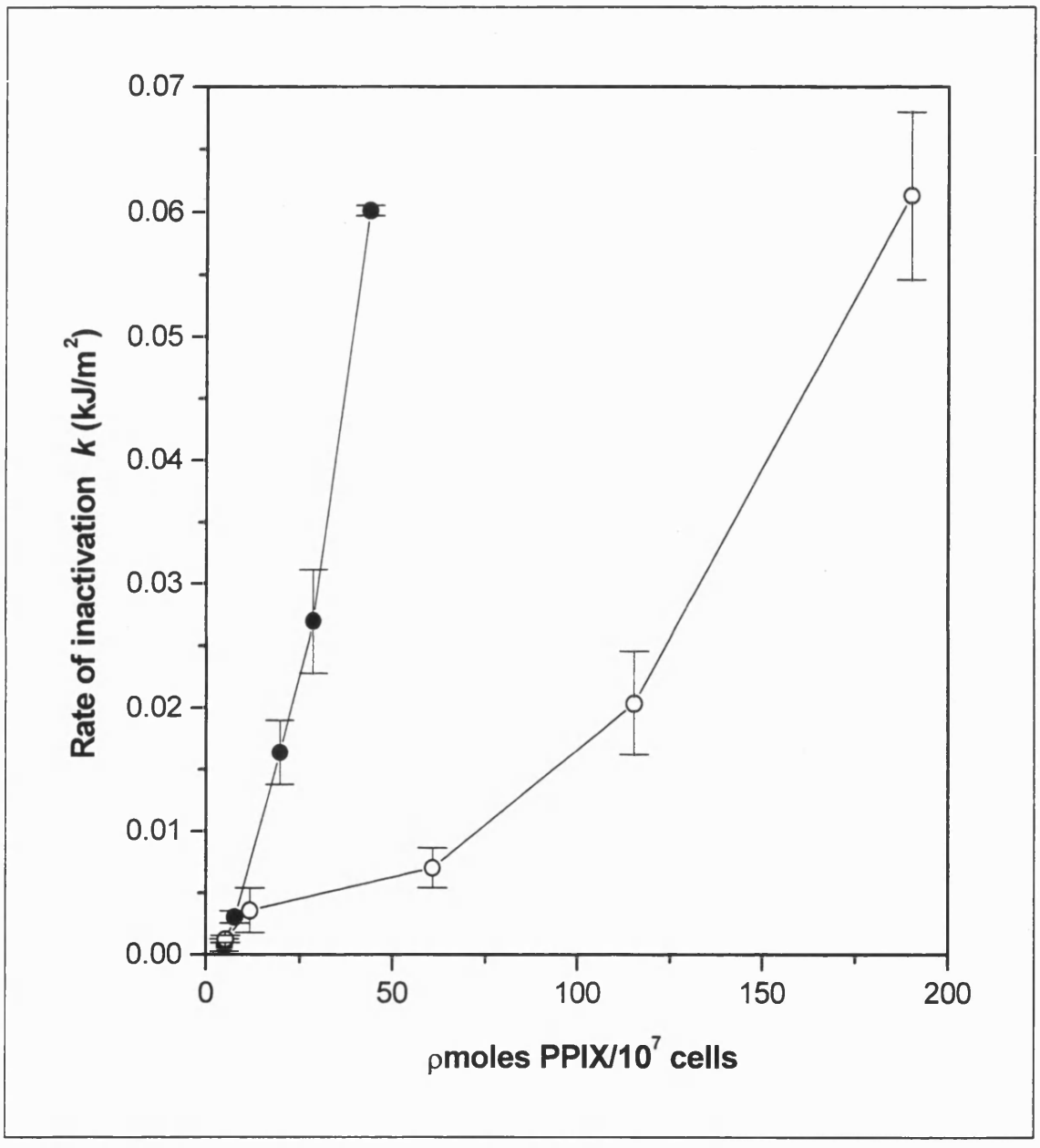

2.4 Discussion

To determine if PPIX is a crucial chromophore in UVA-mediated inactivation of the human lymphoblastoid cell line TK6 and the primary human skin fibroblast cell line FEK4, we have studied how the rate of cellular inactivation by UVA radiation varies as a function of intracellular PPIX concentration. In TK6, although incubation with ALA for 18 h of ALA would be expected to yield higher cellular porphyrin content than incubation for 4 h, Fig. 2.6 shows that the two ALA incubation periods result in similar intracellular PPIX concentrations. This is probably explained by the efflux of PPIX from the cells which occurs through diffusion and is influenced by the level of serum protein in the culture medium (Iinuma et al., 1994), in particular albumin (Steinbach at al., 1995). With this cell line (under the conditions detailed in the methods section, which involves culturing the cells for 24 h in medium containing 10% FCS, then adding ALA) we have demonstrated that total intracellular PPIX reaches a maximum after about 8 h (possibly indicating saturation) and then decreases between 8 and 18 hours (Fig. 2.4). This decrease suggests that between 8 and 18 hours, the rate of porphyrin synthesis in TK6 may be lower than the rate of efflux. It was reported that mammalian epithelial cells which were cultured in media containing a high serum content (10% FCS), when stimulated with ALA, showed a considerably higher release of porphyrins into the medium compared with cells cultured in media containing a low serum content (1% FCS) (Fukuda et al., 1993). A similar result was observed using the same cell line, but comparing PPIX efflux from cells cultured in media containing 10% FCS with cells cultured in media that was serum-free (Washbrook et al., 1997). These two reports do however differ with regard to the rate of tetrapyrrole synthesis as a function of serum content in the culture medium. Fukuda and collegues (1993) showed that the rate of porphrin synthesis, with 10%

FCS in the culture medium, was over twice that which occurred when the serum content was 1% serum after incubation with 0.6 mM ALA for 6 h. Reasons for this are not clear, but they suggest either stimulation of enzymes in tetrapyrrole synthesis or a transport mechanism (presumably involving ALA) playing a role. In contrast, Washbrook and collegues (1997) showed that the rate of porphyrin synthesis was approximately 30% lower in 10% culture media compared to that of serum free medium. They argue that serum in the medium decreases ALA uptake by either inhibiting influx of ALA or increasing its efflux.

Unlike TK6, incubation of FEK4 with ALA for 18 h leads to a considerably higher content of intracellular PPIX compared with incubation with ALA for 4 h (Fig. 2.8). The reason for the discrepancy between the two cell lines is probably explained by the large volume of the fibroblast compared with the lymphoblastoid cell, which would permit a larger amount of intracellular PPIX to accumulate after the longer incubation period. When comparing the two cell lines after 4 h ALA incubation, the intracellular content of PPIX appears similar in both cell types (under the 100 and 200 μM conditions). This comparison can only be made loosely though, as the serum content may be different in the media when the cells were drugged with ALA. The study undertaken here was aimed at looking at intracellular PPIX content after ALA stimulus and not extracellular porphyin levels as a result of efflux. However, in retrospect, studying porphyrin efflux would have been useful to ascertain and compare the rate of porphyrin production in the two cell lines.

MTS was initially investigated to use a simple but rapid assay for obtaining phototoxicity data to compliment the clonogenic assay. The MTS technique was

optimised for the lymphoblastoid cells and then used to obtain dose response data for irradiation with UVA up to 500 kJ/m^2 (Fig. 2.9). It was then intended to use this assay to investigate the response of cells that had different porphyrin levels to irradiation with UVA radiation. However, in a previous study, Campbell and colleagues (1996) reported that the MTT tetrazolium salt could interact with ALA to produce a characteristic blue formazan product. Based on this observation, a cell free system was devised to investigate the reaction, if any, MTS had with ALA. Fig.2.10 clearly shows that at low ALA concentrations a formazan product is produced, which is detectable at 490 nm. This suggests that ALA leads to the reduction of the MTS tetrazolium salt. It has been demonstrated in vitro that ALA can cause iron release from ferritin (Otieza et al., 1995). In the presence of iron and under aerobic conditions, ALA can be oxidised to 4,5-dioxovaleric acid (DOVA) (Carvalho et al., 1997). This reaction may be responsible for the MTS reduction. In conclusion, neither MTS tetrazolium salt or the MTT tetrazolium salt would appear to be suitable for use in determining ALA-induced photosensitisation effects because of the coloured formazan compound produced as a result of the interaction between the tetrazolium salt and ALA.

Fig. 2.13 illustrates the dose response of untreated FEK4 cells to UVA radiation after doses up to 500 kJ/m^2. This particular method of determining phototoxicity (Gibson et al., 1997) had not been previously investigated in our laboratories, so this preliminary study was carried out to test the sensitivity of this technique. From this result, it was concluded that this method was suitable to carry out further phototoxicity studies.

Figs. 2.11-2.12 and 2.14 – 2.15 show that while an increase in intracellular PPIX concentration does increase the sensitivity of the TK6 and FEK4 cell lines to UVA-induced phototoxicity, there is no absolute correlation between intracellular PPIX content and UVA inactivation. This observation is consistent with data produced by other groups (Iinuma et al., 1994; Gibson et al., 1997). Despite this, Iinuma and colleagues (1994) concluded that there might be a threshold of intracellular PPIX necessary before ALA-induced phototoxicity was observed. The 4 h ALA incubation in our study resulted in a greater efficiency of cell killing by UVA radiation compared to that with 18 h incubation in both cell lines (Figs.2.11-2.12 and 2.14-2.15). This observation may have implications for the optimisation of ALA-PDT, but why should this shorter incubation lead to greater phototoxicity? Malik et al. (1996) have demonstrated using fluorescence and spectral imaging and mapping that after incubation with ALA, the monomeric fraction of PPIX was primarily in the plasma membrane and the membranes of cytoplasmic organelles. On the other hand, aggregated species of PPIX were located in the cytoplasm and vesicular compartments including the mitochondria and endoplasmic reticulum. It was also shown that dimerisation may be induced after excess PPIX is produced by ALA induction. In another study, it has been shown that compared with longer incubation periods, shorter incubation times with exogenously added PPIX produce a larger fraction of the rapidly bleached monomeric form of PPIX, as measured by fluorescence decay measurements (Strauss et al., 1998). A concomitant dramatic effect on cellular phototoxicity was also observed using these shorter incubations. Bezdetnaya and colleagues (1996) demonstrated that photobleaching of monomers is more likely to occur compared with the aggregated species when solutions of both PPIX and HpD are irradiated. In the aggregated species fluorescence and intersystem

crossing is reduced due to an increased internal conversion, which is the nonradiative pathways of energy loss within a molecule. This appears consistent with the observation that the fluorescence and triplet state yields are much reduced in the aggregated form of Hp compared to the monomeric component (Smith, 1985). Finally, aggregation of the photosensitiser Hp has been found to reduce the singlet oxygen yield and thus, essentially it's phototoxic capacity (Tanelian and Heinrich, 1995).

One other factor that may play a role in the ability of PPIX to inactivate cells is its localisation after ALA treatment. There are several studies that have used fluorescence microscopy to monitor PPIX localisation ALA treatment (reviewed by Peng et al., 1997, and refs. cited therein), and it would appear that the localisation pattern is primarily affected by the time that cells are incubated with ALA. The majority of these studies document a similar pattern that changes with time, which is the initial appearance of PPIX in the mitochondria (where it is formed), followed by its localisation in the membranes of organelles and eventually the plasma membrane. Some groups have also observed PPIX staining in the cytoplasm (Gaullier et al, 1995; Uberriegler et al., 1995). Thus, the primary sites of PPIX photosensitisation may be restricted by the pattern of PPIX localisation and accumulation, which in turn may affect the inactivation of cells. In conclusion, distribution of the porphyrin, concentration, and aggregation state may all have crucial effects on the ability of PPIX to sensitise cells to UVA.

Finally, an estimation of the basal content of PPIX necessary to mediate significant cell killing by UVA was made from the relationship between the inactivation rate

constants and the intracellular PPIX concentration in both cell lines (Figs. 2.16 and 2.17). The method used to estimate the basal content necessary to contribute to significant cellular inactivation is derived by back extrapolating the linear portion of the curve, which is produced by plotting inactivation rate constants against PPIX concentration, back to the abscissa. The estimated value essentially indicates a threshold of intracellular PPIX required, after a particular incubation, before a significant contribution is made to UVA-induced cell killing. This threshold does not necessarily indicate the total concentration of intracellular PPIX, but rather a concentration of PPIX species (monomeric, dimeric and aggregated forms) that are able to generate a sufficient amount of ROS in order to result in significant cell inactivation after UVA irradiation. The slow rate of increase in inactivation over the non-linear part of the curve (Figs. 2.16 and 2.17) shows that an increase in PPIX concentration is not accompanied by a significant relative increase in the rate of inactivation. This suggests that, either insufficient ROS species are generated because of a lack of total PPIX, insufficient quantities of an efficient photosensitising fraction of PPIX (i.e. monomers) to generate these ROS, or that the antioxidant capacity is sufficient to protect the cell. When this threshold is reached, the rate of inactivation increases in a linear manner and at a much greater rate. This is because whatever limiting factor or factors were effective before the threshold was reached, are no longer inhibiting the increase in rate of inactivation, as a function of PPIX concentration.

Under our conditions, it was determined that the basal content of PPIX is insufficient to make a significant contribution to UVA-mediated inactivation of the human lymphoblastoid cell line TK6 and therefore it is unlikely to be a critical UVA

chromophore in this cell line under normal conditions (Fig. 2.16). Whilst incubation of FEK4 cells with ALA for 18 h cells would appear to give a similar result as that for TK6 cells, the incubation of FEK4 with ALA for 4 h appears to produce quite a different outcome (Fig. 2.17). The basal content of these cells lies within the back extrapolate of the linear portion of this curve, suggesting that it is sufficient to make a significant contribution to UVA-mediated cell inactivation. We conclude from this study that the basal content of PPIX in FEK4 fibroblasts appears to implicate this molecule as a critical chromophore in the UVA-mediated inactivation of this cell line.

Chapter 3. Study of the effects of δ-aminolevulinic acid-induced protoporphyrin IX and UVA irradiation on the cytoplasmic aconitase activity of iron regulatory protein-1 in human skin cells

3.1 Introduction

3.1.1 *Iron Homeostasis*

Iron is an essential nutrient and is important for a variety of cellular processes including respiration and cell division. Despite iron playing a critical role in such processes, when in excess, it is potentially highly toxic because it can catalyse the formation of free radicals through mechanisms such as the Fenton and Haber Weiss reactions (Halliwell and Gutteridge, 1999). In mammalian cellular systems, there is a tightly regulated system that is responsible for acquisition, utilisation, and storage of iron. The genes that comprise this system are themselves modulated by levels of intracellular iron.

Cellular iron homeostasis in non-erythroid mammalian cells is maintained primarily through the co-ordinated regulation of the synthesis of the two proteins, transferrin receptor (TfR) and ferritin. Iron acquisition (reviewed by Richardson and Ponka, 1997) occurs through the binding of di-ferric transferrin (Tf) to the cell-surface transferrin receptor (TfR). This complex is internalised within enclosed endocytic vesicles. Acidification of the endosome results in release of the Tf bound iron; the apo-Tf/TfR complex is returned to the cell surface where it dissociates for recycling of the same process. This released iron is subsequently exported to the cytoplasm where it is either incorporated into a number of iron-containing/requiring proteins, transported to the

mitochondria for haem synthesis, or stored in the cytoplasmic iron storage protein ferritin. Ferritin is composed of 24 subunits encoded by two highly homologous genes, in which up to 4500 iron atoms can be stored in the Fe^{3+} form (reviewed by Bridges, 1990; Harrision and Arosio, 1996; see Chapter 5).

Two cytoplasmic RNA-binding proteins known as iron regulatory protein-1 and -2 (IRP-1 and IRP-2) control the rate of ferritin and TfR synthesis through the regulation of translation, and through the stabilisation of their mRNAs (Henderson and Kuhn, 1995). Under conditions of iron deprivation the IRPs are capable of binding to stem-loop structures, known as iron-responsive elements (IREs), in the 5'-untranslated region (5'-UTR) of the ferritin mRNA and in the 3'-untranslated region (3'-UTR) of the TfR mRNA. Binding of the IRPs to the 5'-UTR of the ferritin mRNA results in repression of translation of the ferritin protein (Gray and Hentze, 1994). In contrast, binding of the IRPs to the 3'-UTR of the TfR mRNA results in its stabilisation, thus allowing translation to proceed (Casey et al., 1989). When iron supply to cells is increased IRP-1 becomes post-transcriptionally inactivated and IRP-2 is degraded. Intracellular iron levels affect the rate of synthesis of both IRPs, through the activity of IRP-1 and through the stability of IRP-2. Thus, when the intracellular iron level is low, the production of ferritin is low while the production of TfR is high. On the other hand, when the intracellular iron level is high the production ferritin is high, whilst the production of TfR is low (reviewed by Hentze and Kuhn, 1996; Haile, 1999). Purification of the human IRP-1 protein led to the discovery that it displays a marked homology with mitochondrial aconitase (Rouault et al, 1991; Hentze and Argos, 1991). Mitochondrial aconitase is an iron sulphur protein

that catalyses the reversible isomerisation of citrate to isocitrate via *cis*-aconitate in the citric acid cycle. A cubane sulphur-cluster ([4Fe-4S]), like that of the mitochondrial aconitase, was found in the IRP-1 (Kennedy et al., 1992) and analysis of recombinant IRP-1 led to the observation that the protein functioned as a cytosolic aconitase in iron-replete cells (holoprotein), inactive in IRE-binding. In iron-deficient cells however, the apoprotein (without the cluster) accumulates and binds to IREs exhibiting no aconitase activity. Thus, IRP-1 is a bifunctional regulator possessing the two mutually exclusive functions, RNA-binding and aconitase activity, depending on the levels of intracellular iron (Henderson and Kuhn, 1995). An IRE element has been also been identified in the 5'-UTR of mammalian mitochondrial aconitase (Kim et al., 1996). The level of translation of this protein has been shown to be regulated by IRP/IRE-binding so that iron levels may regulate mitochondrial aconitase, and hence the function of the citric acid cycle.

3.1.2 *What is the Function of Cytoplasmic Aconitase Activity?*

While the role of the mitochondrial aconitase (m-aconitase) functioning as one of the enzymes of the Kreb's cycle is well characterised and understood, the role of the of the cytoplasmic aconitase (c-aconitase) in the metabolism of cytoplasmic citrate remains largely unclear. Philpott and colleagues (1994) confirmed that the enzymatic activity is not necessary for cluster assembly/disassembly or regulated RNA binding as previously suggested by Klausner and colleagues (1993). Philpott and colleagues suggested that the cytoplasmic aconitase function and concomitant citrate metabolism are directly regulated by iron. Hence, the role of citrate (and its metabolism) in intracellular iron trafficking

may provide the key to the cytoplasmic aconitase function. Paraskeva and Hentze (1996) also postulate a relationship between citrate and iron transport. They suggest that a co-regulatory function of both the mitochondrial and cytoplasmic aconitases in response to iron levels may exist, and that iron level may affect the catalytic turnover of citrate. Since citrate can bind iron and might serve as intracellular iron transporter, both the RNA-binding and the enzymatic activity of IRP-1 may collaborate in the regulation of intracellular iron transport. Gray and colleagues (1993) discussed the possibility of a link between the two aconitases, again with reference to citrate. They speculate that in iron starved cells repression of both aconitases may lead to preservation of citrate which is an intracellular carrier of iron to the mitochondria (Frausto da Silva, 1991). This may also aid the liberation of iron stored within cells (O'Connell et al., 1989). Alternatively, iron overload in cells may be aided by reduction in citrate levels from increased aconitase activity, thus reducing iron mobilisation from iron stores. Clearly the elucidation of the role of cytoplasmic aconitase requires further experimental investigation.

3.1.3 *Response of IRPs to Oxidative Stress*

In the attempt to understand how the iron-sulphur-cluster may function as a sensor of intracellular iron levels, the influence of oxidants on the iron-sulphur cluster of IRP-1 assembly, as well as iron availability, must also be understood. The iron-sulphur cluster of IRP-1 is positioned in a solvent filled cleft where it may be susceptible to oxidant destabilisation. The nature of the nitric oxide (NO) interaction with aconitase is controversial, some groups suggest peroxynitrite is the reactive species (Hausladen and Fridovich, 1994; Castro et al, 1994), whereas others have suggested that NO itself is

sufficient to destabilise the cluster (Kennedy et al., 1997; Gardner et al., 1997; for a review see Cooper, 1999). Treatment of cells with NO or NO producing reagents has been shown to result in IRE-binding (Weiss et al., 1993; Drapier et al., 1993). Treatment of cells with hydrogen peroxide leads to activation of RNA-binding activity and concomitant loss of cytoplasmic aconitase activity, as would be expected if oxidative stress was responsible for cluster disassembly (Martins et al., 1995; Pantopolous and Hentze, 1995; Gardner et al., 1995). It is tempting to assume direct chemical attack on the iron sulphur cluster of the IRP-1 protein resulting in the reduction of cytoplasmic aconitase activity, as has been postulated (Rouault and Klausner, 1996; Hentze, 1996). However, there is evidence that suggests ROS may also play a signalling role in the induction of IRP-1 (Pantopoulos et al., 1997). Although the level of iron might have negligible influence on iron-sulphur cluster disassembly, iron level does determine whether the cluster can be assembled and thus will control the transition from apoprotein to holoprotein. The holoprotein can function as a sensor of oxidants, while the apoprotein can function as a sensor of iron levels. The actual mechanisms of assembly and disassembly of the dynamic iron-sulphur clusters are still poorly understood and remain to be delineated. In turn, this will provide the understanding of how iron-sulphur proteins can serve as sensors of both iron and oxidants (for reviews see Rouault et al., 1996; Haile, 1999).

3.1.4 *The Basis and Objectives of This Study*

In this study we investigate the effects of ALA and UVA on cytoplasmic aconitase activity (other consequences of UVA and/or ALA treatment are discussed in previous

chapters). There is only a sparse amount of data in this particular area, with no data existing to the knowledge of this author connecting both ALA and UVA treatment with cytoplasmic aconitase activity. In human keratinocytes exposed to UVA, Giordani and colleagues demonstrated UVA inactivation of cytoplasmic aconitase activity by UVA radiation alone (Giordani et al., 1997), although they were uncertain as to what led to the inactivation. Carvalho and colleagues (1997) have shown (in a variety of different cell lines) an ALA-induced activation of IRP-1/IRE binding. They propose that ALA alone affects the IRP-1 activity and not through other indirect mechanisms such as production of ROS or synthesis of PPIX or haem. The concentration range of ALA used in this study was between 0.5 and 8mM. Exogenous addition of PPIX to erythroleukemic cells has been shown to activate IRP-1 RNA-binding (Coccia et al., 1997). This group suggested that PPIX acts through a similar mechanism to that exerted by an iron chelator. Our work investigates the effect of UVA on the cytosolic aconitase activity in human fibroblasts and keratinocytes. We also study the effects of ALA treatment on the cytosolic aconitase activity in the fibroblasts, both before and after UVA irradiation (controls are included in the form of haemin and desferal treatment). This assay was developed with the intention not only to compliment data obtained using the IRP-1 RNA-binding assay, but also to help gain a better understanding of the mechanisms occurring during the transition from holoprotein to apoprotein (and vice-versa) after various treatments such as UVA irradiation.

3.1.5 *Measurement of Cytosolic Aconitase Activity*

The cytoplasmic aconitase assay has been performed in many different ways (documented within references cited in this chapter). All the different variations of this assay effectively measure the same thing, which is the activity of the cytoplasmic enzyme in response to intracellular iron and oxidant levels. The method used in this study (Giordani et al., 1998) measures spectrophotometrically the aconitase activity in the cytoplasmic fraction as a function of substrate disappearance/consumption (i.e. *cis*-aconitate) at 240 nm. The addition of the substrate marks the start of the reaction. *Cis*-aconitate acid is the substrate intermediate in the aconitase-catalysed conversion of citrate to isocitrate (source: Stryer, 1988):

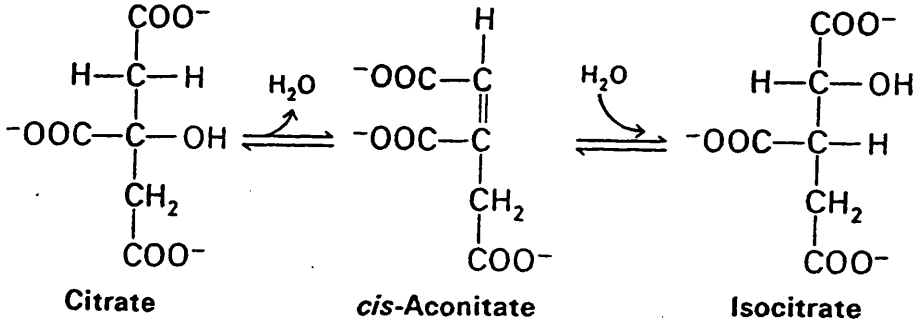

Subcellular fractionation was achieved using centrifugation and a special method of lysis involving the compound digitonin. Digitonin was used to selectively permeablise the plasma membrane since it is cholesterol-rich compared to the mitochondrial membrane. Digitonin reacts specifically with cholesterol so that the plasma membrane is damaged while the mitochondrial membranes remain intact (Zuurendonk and Tager, 1974). The

quality of the cytosolic fraction was tested for using succinate dehydrogenase as the mitochondrial marker enzyme.

3.2 Methods

3.2.1 *Cell Culture*

The human lymphoblastoid cell line, TK6, and the primary human fibroblast cell line, FEK4, were cultured as described in section 2.2.1. The immortalised human keratinocyte cell line HaCaT (Boukamp et al., 1988) was cultured in Dulbecco's minimal essential media high glucose (Gibco, UK), supplemented with 10% FCS, L-glutamine, sodium bicarbonate, penicillin and streptomycin. Cells were trypsinised once a week. For all experiments HaCaT cells were seeded into plastic culture dishes for 3 days to approximately 80% confluency.

3.2.2 *Chemical Treatments and Irradiation Conditions*

FEK4 cells were treated with ALA as described in section 2.2.3. Positive controls for the modulation of the cytoplasmic aconitase activity were prepared for the FEK4 in the form of the haem analogue haemin and the iron chelator desferal. Solutions of 50 μM haemin or 100 μM desferal (Ciba Geigy, Switzerland) were made using conditioned cell culture media. These solutions were added back to the cells, which were incubated at 37°C for either 2 h with haemin or 18 h with desferal. Both FEK4 and HaCaT cells were UVA-irradiated as described in section 2.2.6.

3.2.3 *The Cytoplasmic Aconitase Assay*

The cytoplasmic aconitase assay was performed according to Giordani and co-workers (1998). After irradiation (or treatment with either haemin or desferal), cells were collected. The TK6 cells were centrifuged for 5 min at 1000 rpm, washed with PBS and

centrifuged again. The FEK4 and HaCaT cells were washed with PBS, then scraped from the plates and collected in 3 ml of PBS and centrifuged for 5 min at 1000 rpm. Pellets from all cell types were re-suspended in 10 ml of ice-cold buffer containing 0.25-M sucrose, 100 mM Hepes and 0.007% digitonin (Bouton et al., 1997). The digitonin stock solution was stored in dimethyl sulphoxide (DMSO) at room temperature. Cell lysates were centrifuged for 10 min at 1500 g. The supernatant was transferred to a fresh tube and centrifuged for 10 min at 12500 g with a Beckman J-25 centrifuge (Ireland). Aconitase activity was immediately assayed in the cell-free extracts at 25°C in the presence of 0.02% BSA after the final centrifugation using the method described by Drapier and Hibbs (1986). The reaction was started with the addition of 0.2mM cis-aconitic acid and the disappearance of cis-aconitic acid was measured at 240 nm using absorption spectrophotometry with a Kontron Uvikon 922 spectrophotometer (Switzerland). A typical reaction measurement is shown below in Fig. 3.1:

Fig. 3.1 A typical aconitase activity measurement using spectrophotometry. This kinetic study shows the disappearance of the substrate *cis*-aconitate measured at 240 nm. Absorbance was set to zero at the start of the reaction, which explains the negative absorbance values observed during the reaction as the substrate is consumed.

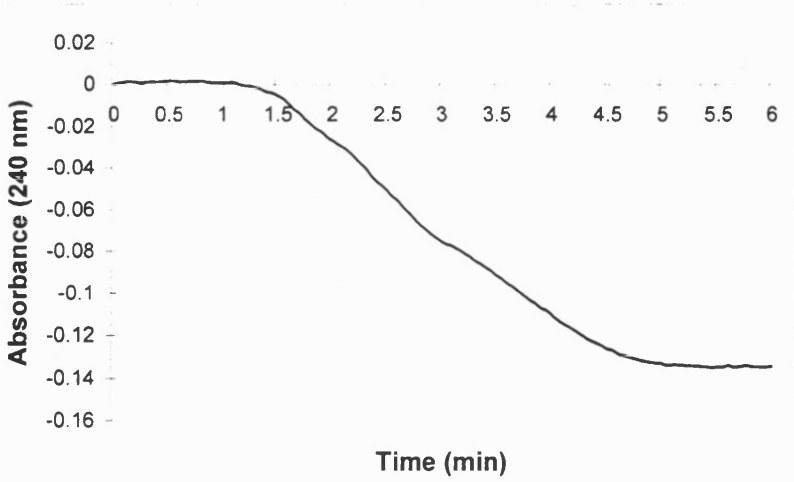

Both the BSA and cis-aconitic acid stock solutions were made up using the Hepes-sucrose buffer described above. A molar absorption coefficient of 3410 cm^{-1} mM^{-1} was used for cis-aconitic acid (Henson and Cleland, 1967). Under the experimental conditions described here, one unit of IRP-1 aconitase activity is defined as 1 μmol cis-aconitate consumed min^{-1} mg $protein^{-1}$ (Sigma catalogue). Enzyme activity was calculated using the following equation (Segel, 1976):

$$\text{Activity} = \frac{(\Delta O.D._{240}/3410) \times (v)}{(\mu g \text{ protein}) \times (t)}$$

Where $\Delta O.D._{240}$ is the change in optical density measured at 240 nm, 3410 corresponds to the molar absorption coefficient for *cis*-aconitic acid (cm^{-1} mM^{-1}), v is volume of the reaction mixture (ml), and t is time (min). Protein concentration was determined using the method described by Bradford (1976) with the BioRad reagent kit (UK). BSA was used for calibration and adsorption measurements were obtained using a microplate reader at 595 nm.

3.2.4 *Succinate Dehydrogenase Activity - Test for Mitochondrial Contamination of the Cytoplasmic Fraction*

Succinate dehydrogenase (SDH) activity was assessed by the ability of the cytoplasmic fraction and total homogenate to reduce 2-(4-iodophenyl)-3-(4-nitrophenyl)-5-phenyl-tetrazolium chloride (INT) in the presence of the electron coupling reagent phenazine methosulphate (PMS) (Porteous and Clark, 1965). The incubations (1 ml) contained (in

μmoles) sodium phosphate, 50; sodium succinate, 10; INT, 0.4; PMS, 0.33; and Triton X-100, 0.0001%. The cytoplasmic fraction and the total homogenate were assayed. The electron acceptors (INT and PMS) were added after a 6 min pre-incubation at 30°C. Absorbance increase was followed at 540 nm (reaction proceeded at 30°C) using a Kontron Uvikon 922 spectrophotometer (Switzerland). The reference incubation contained 10 μmoles sodium malonate instead of sodium succinate. Mitochondrial contamination of the cytoplasmic fraction was expressed as a percentage of the activity of SDH in the total homogenate.

3.3 Results

3.3.1 *Basal Cytoplasmic Aconitase Levels*

The basal cytoplasmic aconitase activity in the FEK4 primary human fibroblasts and the HaCaT immortalised human keratinocytes is shown in Fig 3.2. The fibroblast cell line displayed over 2-fold higher basal cytoplasmic aconitase activity compared to the keratinocyte cell line (0.825 ± 0.093 and 0.3935 ± 0.054 U/mg protein respectively). Mitochondrial contamination of the cytoplasmic fraction was determined by comparing the activity of the mitochondrial enzyme succinate dehydrogenase in both the cytoplasmic fraction and the total cell homogenate (section 3.2.4). Contamination was tested for after all the treatments discussed in this chapter. Succinate dehydrogenase activity was never greater than 10% that of the total activity in the cell homogenate.

Fig. 3.2. Basal cytoplasmic aconitase activity of FEK4 primary human fibroblasts and HaCaT immortalised human keratinocytes. Data represent the mean of 3-6 independent experiments (± S.D.).

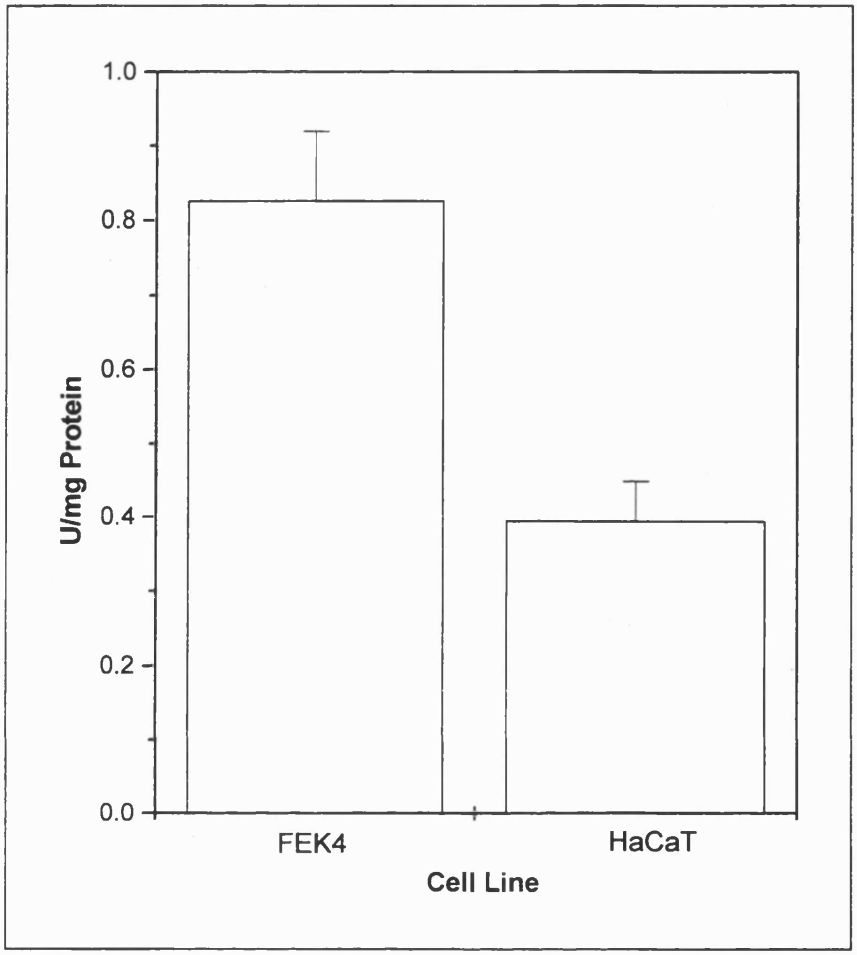

3.3.2 *Effects of UVA Irradiation on the Cytoplasmic Aconitase Activity of FEK4 Primary Human Fibroblasts and HaCaT Immortalised Human Keratinocytes*

The cytoplasmic aconitase activity of the FEK4 primary human fibroblasts and HaCaT immortalised human keratinocytes in response to graded doses of UVA radiation are shown in Tables 3.1 and 3.2 respectively. The response to UVA is similar for both cell lines, but the changes observed are greater in the fibroblasts compared with the keratinocytes. As the tables show, the cytoplasmic aconitase activity rises steadily up to about 250 kJ/m^2 UVA where the activity peaks. The activity then decreases between 250 and 500 kJ/m^2 UVA. After a UVA dose of 500kJ/m^2, the cytoplasmic aconitase activity measured had dropped to below the control levels. Concerning the modulation of cytoplasmic aconitase activity by UVA radiation, both the results for the FEK4 fibroblasts and the HaCaT keratinocytes contrast sharply with those obtained by Giordani et al. (1998) with NCTC 2544 keratinocytes.

Table 3.1. Dose response of cytoplasmic aconitase activity of FEK4 primary human fibroblasts exposed to UVA radiation. Data represent the mean of 4-6 independent experiments (± S.D.).

Treatment	Aconitase Activity (U/mg protein)	% Activity (Relative to Control)
Sham-irradiated	0.825 ± 0.093	100
50 kJ/m^2 UVA	0.867 ± 0.025	105.125 ± 3.112
100 kJ/m^2 UVA	0.961 ± 0.039*	116.5 ± 4.795
250 kJ/m^2 UVA	1.2 ± 0.051*	145.515 ± 6.293
500 kJ/m^2 UVA	0.615 ± 0.044*	74.6 ± 5.396

Statistical analyses were made using an unpaired *t* test. *, Significantly different from non-irradiated control ($p < 0.05$ level).

Table 3.2. Dose response of cytoplasmic aconitase activity of HaCaT immortalised human keratinocytes exposed to UVA radiation. Data represent the mean of 3-4 independent experiments (± S.D.).

Treatment	Aconitase Activity (U/mg protein)	% Activity (Relative to Control)
Sham-irradiated	0.3935 ± 0.054	100
50 kJ/m^2 UVA	0.399 ± 0.0181	101.6 ± 4.615
100 kJ/m^2 UVA	0.441 ± 0.012*	112 ± 3.162
250 kJ/m^2 UVA	0.506 ± 0.0216*	128.68 ± 5.505
500 kJ/m^2 UVA	0.339 ± 0.0239*	86.2 ± 6.039

Statistical analyses were made using an unpaired *t* test. *, Significantly different from non-irradiated control ($p < 0.05$ level).

3.3.3 *Effects of ALA Treatment and UVA Irradiation on the Cytoplasmic Aconitase Activity of FEK4 Primary Human Fibroblast Cells*

The cytoplasmic aconitase activity of FEK4 cells in response to treatment with ALA for 4 and 18 hours was investigated (Table 3.3). As one can see from the table, after both incubation times, the aconitase activity decreases in a dose-dependent manner. The maximum decrease in aconitase activity after ALA treatment was approximately 35%, and this was observed after a treatment of 200 μM for 4 h. Application of graded doses of UVA to the ALA treated populations had a dramatic effect on the cytoplasmic aconitase activity in these cells compared to their untreated (without ALA) counterparts (Tables 3.1 and 3.2). As Table 3.3 shows, all irradiated ALA treated populations expressed a marked increase in cytoplasmic aconitase activity. Interestingly, the 50 kJ/m^2 UVA dose showed an increase in cytoplasmic aconitase activity that correlates with an increase in intracellular PPIX concentration (Fig. 2.8). In contrast to this, a 100 kJ/m^2 UVA dose appears to indicate a saturation of the cytoplasmic aconitase activity measured, as there is no significant difference between the activities of the samples irradiated with this dose. The maximum activity observed under our conditions was just over 200% higher that of the untreated control; this was measured after an incubation with 200 μM ALA for 18 h followed by a 100 kJ/m^2 UVA dose. Mortality of the cells 24 h after ALA treatment and UVA irradiation are shown in Figs. 2.14 and 2.15.

Table 3.3. Dose response of cytoplasmic aconitase activity of FEK4 primary human fibroblasts exposed to ALA and UVA radiation. Data represent the mean of 4 independent experiments (± S.D.).

Treatment	Aconitase Activity (U/mg protein)	% Activity (Relative to Control)
Non-ALA treated, non-irradiated	0.825 ± 0.093	100
4 h 100 μM ALA, non-irradiated	0.639 ± 0.068	77.5 ± 8.109
4h 100 μM ALA50 kJ/m^2 UVA	1.237 ± 0.198*	150 ± 24.055
4 h 100 μM ALA 100 kJ/m^2 UVA	2.345 ± 0.197*	284.25 ± 23.894
4 h 200 μM ALA, non-irradiated	0.545 ± 0.055	66.124 ± 6.733
4 h 200 μM ALA, 50 kJ/m^2 UVA	1.536 ± 0.1845*	186.25 ± 22.369
4 h 200 μM ALA, 100 kJ/m^2 UVA	2.369 ± 0.1787*	287.25 ± 21.156
18 h 100 μM ALA, non-irradiated	0.665 ± 0.0543	80.63 ± 6.113
18 h 100 μM ALA, 50 kJ/m^2 UVA	1.886 ± 0.297*	228.641 ± 36.039
18 h 100 μM ALA, 100 kJ/m^2 UVA	2.43 ± 0.189*	295.5 ± 23
18 h 200 μM ALA, non-irradiated	0.561 ± 0.082	68 ± 10
18 h 200 μM ALA, 50 kJ/m^2 UVA	2.161 ± 0.229*	262 ± 27.779
18 h 200 μM ALA, 100 kJ/m^2 UVA	2.602 ± 0.2138*	315.515 ± 25.926

Statistical analyses were made using an unpaired *t* test. *, Significantly different from non-irradiated control ($p < 0.05$ level).

3.3.4 *The Effects of Haemin and Desferal on the Cytoplasmic Aconitase Activity of the FEK4 Primary Human Fibroblasts*

Positive controls were used to test the efficacy of the cytoplasmic aconitase activity in FEK4 cells. Table 3.4 shows the effects of haemin and desferal incubation on the cytoplasmic aconitase activity of FEK4 cells. Haemin incubation resulted in an approximate 20% increase in activity compared to untreated cells, and desferal approximately a 50% decrease.

Table 3.4. Effect of haemin, and desferal on the cytoplasmic aconitase activity of FEK4 primary human fibroblasts. Data represent the mean of 3 independent experiments (± S.D.). The activity is expressed as a percentage of a sham-treated control.

Treatment	Aconitase Activity (U/mg protein)	% Activity
50 μM Haemin, 2 h	0.995 ± 0.029	120.6 ± 3.6
100 μM Desferal, 18 h	0.402 ± 0.055	48.8 ± 6.7

3.4 Discussion

The cytoplasmic aconitase assay was developed for this investigation not only to compliment data obtained using the IRP-1 RNA-binding assay (and other assays that may monitor levels of intracellular iron entities e.g. the calcein assay), but also to gain a better understanding of the mechanisms that occur during the transition from IRP-1 holoprotein to apoprotein (and vice versa) after various treatments such as UVA irradiation. The physiological function of the cytoplasmic aconitase is not clear, although several functions have been postulated (section 3.1.2) none have been thoroughly tested. It is well accepted and documented that UVA radiation leas to the production of ROS and these species are responsible for a variety of modifying and damaging affects (Tyrrell, 1991). We investigated in this particular study how UVA (and ALA treatment followed by UVA) affects iron metabolism in human skin cells through the use of the cytoplasmic aconitase assay.

The basal cytoplasmic aconitase activities of FEK4 primary human dermal fibroblasts and HaCaT immortalised epidermal keratinocytes are shown in Fig. 3.2. From the graph it is clear that the fibroblasts exhibit a much higher activity than the keratinocytes (approximately 2-fold higher). This is consistent with measurements of the free iron pool using the iron assay and ferritin levels (Chapters 4 and 5). When comparing different parameters that are involved in iron regulation between the two cell lines, it is interesting to find that the basal HO-1 activity in HaCaT cells is barely detectable compared with the FEK4 value. However, the basal HO-2 activity of HaCaT is 2-3-fold higher compared with FEK4 (Noel, 1995). Overall HO enzyme activity was found to be approximately

2.5-fold higher when comparing epidermal keratinocytes to their matched dermal fibroblasts (Applegate et al., 1995). Applegate and colleagues (1995) found that the basal concentration of ferritin in the keratinocytes was also approximately 2 – 3 times higher when compared with the fibroblasts. This is consistent with evidence that levels of ferritin are closely linked to HO activity (Applegate, 1995 and references cited therein). However, when comparing the fibroblast (FEK4) and the keratinocyte (HaCaT) cell lines, we found that the ferritin levels (Chapter5) and iron levels in the keratinocytes, whether measured by aconitase activity or the iron assay (Chapter 4), are much lower than in the fibroblasts. The reasons for this may to be connected with the expression of H-ferritin observed within the keratinocytes. HaCaT cells have been found recently to only express the H-ferritin subunit (C. Pourzand, unpublished observation), and it has been documented that the expression of this subunit downregulates intracellular 'free' iron levels because of its ferroxidase activity (Beaumont and Cabantchik, 1999).

Tables 3.1 and 3.2 show the modulation of cytoplasmic aconitase activity by UVA radiation in the FEK4 primary human fibroblast cell line and the HaCaT immortalised keratinocyte cell lines respectively. In both cell lines we found an increase in cytoplasmic aconitase activity in response to UVA irradiation. This increase appeared to peak around 250 kJ/m^2 UVA and the activity dropped below the control level at the higher dose of 500 kJ/m^2. In FEK4, the aconitase response correlated with a reciprocal decrease in IRP-1 RNA-binding in doses up to 250 kJ/m^2 UVA (Pourzand et al., 1999). At 500 kJ/m^2, like the cytoplasmic aconitase activity, the IRP-1 RNA-binding was lower than the control levels suggesting damage to the protein. Under circumstances such as

these, the advantages of measuring both functions of the IRP-1 protein become obvious. The increases observed in cytoplasmic aconitase activity with these two cell lines would appear to be due to iron mobilisation as a result of UVA irradiation (Pourzand et al., 1999; Watkin and Tyrrell, unpublished data). The source of this iron is not completely clear, but two possibilities arise from observations made in our laboratories (Pourzand et al.,1999; Kvam et al., 1999). It has been postulated that UVA causes oxidative damage to lysosomal membranes. In turn this allows leakage of lysosomal proteases into the cytosol where the proteolysis of ferritin occurs resulting in the immediate release of 'free' iron (Pourzand et al., 1999). Another source of iron that is also liberated immediately after UVA irradiation is that of haem from microsomal haem proteins (Kvam et al., 1999). The study of Kvam et al. (1999) demonstrated that haem was released as a result of microsomal haem protein degradation in a process that appeared to be mediated by cyclooxygenase (COX). The subsequent release of haem leads to the induction of HO-1, which in turn causes the release of 'free' iron as a result of haem catabolism. Other sources of iron may also be responsible for the affects observed on the activity of IRP, but they are as yet unidentified. Attempts at elucidating what form of iron the IRP-1 protein senses has been controversial. Iron may be either sensed directly or indirectly. Though it now widely accepted that chelatable iron has a regulatory affect on the IRP, there is still uncertainty as to what role, if any, compounds such as haem or haemin (the compound most investigated) have on IRP regulation in vivo (Rouault at al., 1993). Addition of 50 μM haemin for 2 h led to a 20% increase in the cytoplasmic aconitase activity in FEK4 (Table3.4). This increase could have been due to liberation of iron from the breakdown of haemin, though it is not definite that this effect was not caused by

haemin itself. As has been suggested (Kvam, 1999), haem added to cells, or indeed haem released from haemproteins, is conceivably chemically distinct from haemin and thus may have a different regulatory affect on IRPs in comparison to haemin. If haem (released from haemproteins) does directly regulate IRP-1 cytoplasmic aconitase activity, then this could explain why there was only partial recovery of the UVA-induced reduction of IRP-1 RNA-binding when ferritin degradation was prevented using protease inhibitors (Pourzand et al., 1999). Recognition of haem by IRPs may be of benefit to a cellular system since this could assist in the prediction of, and help manage, potentially harmful changes in the chelatable iron pool.

Previously, it has been documented (Giordani et al, 1998) that UVA radiation leads to the inhibition of cytoplasmic aconitase activity in NCTC 2544 human skin keratinocytes. Despite using various approaches (including antioxidants and iron chelation), the nature or source of this inhibition was not elucidated. In contrast to the findings of Giordani et al. (1998) we have observed quite a different response to UVA radiation in the two human cell lines, FEK4 primary fibroblasts, and HaCaT immortalised keratinocytes (Tables 3.1 and 3.2 respectively). There are a number of factors which may explain why our results differ from previous observations (Giordani et al., 1998). These factors include differences in the UV source, the dose range, the temperature of irradiation, and the exact cell lines used. Unless experimental conditions are identical, it may not be appropriate to make direct comparisons. The UVA source used in our study (for spectral output see Fig. 2.3) is composed primarily of wavelengths in the UVA I range (340-380 nm) and also some visible wavelengths up to approximately 420 nm. The source used by

Giordani et al. contained both UVA I and UVA II (320-340 nm) wavelengths. It is possible that these shorter wavelengths may result in the inactivation of the cytoplasmic aconitase activity. Determining how UVB, or a combination of UVA and UVB, affect cytoplasmic aconitase activity might also help in the understanding of the different results observed.

Table 3.3 shows the affect of ALA treatment on the cytoplasmic aconitase activity of FEK4 cells, both alone and in combination with UVA radiation. ALA treatment alone appears to drive down the aconitase activity to a similar extent after both 4 and 18 hours incubation. The treatment of cells with 100 μM desferal for 18 h was considerably more effective at reducing the cytoplasmic aconitase activity compared with a similar treatment with ALA (Tables 3.4 and Fig. 3.3). One possible explanation is that desferal chelates iron from both 'free' iron and other sources such as ferritin (Bridges, 1990) effectively removing iron for cellular functions and thereby stimulating IRP-1 RNA binding so that more TfRs are produced. ALA on the other hand, may lead to an initial sequestration of iron by stimulating haem synthesis, however this iron might be recycled through the activity of HO thus leading to a less dramatic effect on IRP regulation.

Carvalho and colleagues (1997) postulated that ALA alone is able to regulate IRPs. This was based on the observation that adding ALA or allowing its accumulation by adding the ALA dehydratase inhibitor succinyl acetone methyl ester (SAME), leads to the stimulation of IRP-1 RNA-binding intracellularly. The use of SAME leads to ALA accumulation but not haem synthesis suggesting that haem is not important in IRP

regulation. Carvalho et al. propose that ALA regulates IRP either by direct interaction of the ALA enoyl radical with the IRP iron sulphur cluster causing its disassembly, or by indirect interaction through ROS generation. This may indicate a role for ALA beyond that of an (indirect) iron chelator. However the concentrations of ALA used in the study (0.5-8 mM) and those that accumulate intracellularly were very high. When the ALA concentration is high, it is cytotoxic (Ortel et al., 1993) and capable of generating ROS (Monteiro, 1989; Fraga, 1994). It has also been shown to cause release of iron from ferritin (Oteiza et al., 1995), lipid peroxidation (Oteiza and Bechara, 1993), and DNA damage induction (Fraga et al., 1994). With such events occurring many factors may affect IRPs.

Table 3.3 also shows what happens to the cytoplasmic aconitase activity of FEK4 cells that have been treated with ALA (up to 200 μM) and subsequently irradiated with UVA (up to 100 kJ/m^2). From the data it clear that induction of PPIX, followed by UVA irradiation, has a dramatic affect on stimulating the cytoplasmic aconitase activity in FEK4 cells with a peak in activity approximately 200% higher than the control. There appears to be a degree of saturation of enzyme activity at the higher UVA dose (100 kJ/m^2), with the lower dose (50 kJ/m^2) demonstrating an increase in enzyme activity that correlates well with an increase in intracellular PPIX concentration (Fig. 2.8). The effect PPIX has in combination with UVA on the cytosolic aconitase activity would appear to complement the scenario postulated by Pourzand et al. (1999). PPIX is a hydrophobic molecule that locates preferentially deep within lipid membranes (Richelli, 1995). Upon photosensitisation by UVA, it is conceivable that membranes containing PPIX will be

subjected to lipid peroxidation (Girrotti, 1985; Korytowski et al., 1992; Oschner, 1997, and refs cited therein; see Chapter 2). Damage to lysosomes and release of acidic hydrolases induced by exogenous addition of PPIX followed by UVA irradiation has been documented in mouse fibroblasts (Morliere at al., 1987). It is possible that the huge increase in cytoplasmic aconitase activity after PPIX induction, followed by UVA irradiation, is a result of proteolytic degradation of ferritin. The release of these enzymes may be significantly enhanced under these conditions thus leading to a greater degradation and liberation of 'free' iron. Studies of ferritin in cells that have been treated with ALA and exposed to UVA radiation show that ferritin is significantly damaged (Chapter 5). It has not been determined if this damage occurs through degradation by proteolytic enzymes or directly by ROS. In experiments with horse spleen apoferritin (Precigoux et al., 1994; Michaux et al., 1996; Crichton et al., 1997), it has been shown that PPIX is able to locate within hydrophobic pockets of ferritin leading to a concomitant increase in the UVA-absorbing region (peak 370 nm). Considering the photosensitising capacity of PPIX, it is not inconceivable that upon UVA irradiation, ROS are generated within the ferritin molecule through the excitation of PPIX. This could also be responsible for the liberation of iron from ferritin. An increase in cytoplasmic aconitase activity might also occur as a result of 'free' haem release from microsomes. PPIX may localise in the membranes of microsomes, and upon photosensitisation, aid the liberation of haem into the cytoplasm by rupturing microsomal membranes. If IRPs do sense haem, this may also explain the huge increase observed after PPIX photosensitisation by UVA.

It is generally accepted that UVA radiation alone, and PPIX upon photosensitisation are able to produce singlet oxygen intracellularly (Tyrrell and Pidoux, 1989; Ryter and Tyrrell, 1999), along with other ROS. Various ROS and reactive nitrogen species (RNS), including H_2O_2 and NO, have been shown to modulate IRE binding activity and dissociate the iron sulphur cluster of the IRP holoprotein (see introduction of this chapter). We postulate that the iron release observed under our conditions is more effective in dictating the fate of the IRP under moderate doses of UVA (up to 250 kJ/m^2) than ROS or RNS. This may reflect a defence mechanism that has adapted/evolved to help cells cope better under oxidative stress. Maintenance of the integrity of the cluster prevents RNA binding and thus allows the synthesis of ferritin, which in turn leads to the sequestration of the dangerous 'free' iron species. UVA irradiation of cells with altered levels of PPIX would also appear to have little or no direct inhibition of cytosolic aconitase activity, despite these conditions being highly cytotoxic (under the more severe treatments). The inability of the ROS that have been generated by photosensitisation to inhibit or inactivate cytoplasmic aconitase activity is conceivably related to the inability of PPIX to locate near to (or within) the cytoplasmic aconitase and also to the restricted range of action of the ROS generated, particularly singlet oxygen (Moan and Berg, 1991).

4. Flow cytometry-based method of determining membrane damage and changes in the intracellular chelatable iron pool, after ALA treatment and UVA irradiation

4.1 Introduction

The average human body contains about 4 g of iron and because of its low solubility in biological mileu, there is a necessity for iron-binding proteins. The functions of these proteins are not only to bind iron in a soluble, and in some cases in a form that is can be assimilated in cells, but also to prevent the iron from catalysing unwanted, potentially cytotoxic reactions intracellularly. Iron that is not bound and kept in a relatively inert form, can generate the highly toxic hydroxyl radical ($OH^{\cdot}$) by Fenton and Haber-Weiss chemistry:

(Fenton reaction) $Fe^{2+} + H_2O_2 \rightarrow Fe^{3+} + OH^{\bullet} + OH^{-}$

(Haber-Weiss reaction) $Fe^{3+} + O_2^{\bullet -} \rightarrow Fe^{2+} + O_2$

$$\underline{Fe^{2+} + H_2O_2 \rightarrow OH^{\bullet} + OH^{-} + Fe^{3+}}$$

Iron catalyst

Net: $O_2^{\bullet -} + H_2O_2 \rightarrow OH^{\bullet} + OH^{-} + O_2$

(Source: Halliwell and Gutteridge, 1999)

A variety of iron-binding proteins have been identified, with a wide variety of functions. These include proteins that are involved in the transport and storage of iron such as transferrin and ferritin (discussed in Chapters 3 and 5); iron-containing electron-transfer

proteins of the mitochondrial respiratory chain such as cytochrome *c* and cytochrome oxidase; dioxygenases and mono-oxygenases which incorporate oxygen into substrates or use oxygen in hydroxylation reactions such as lipoxygenase and cytochrome P-450 respectively; catalase and peroxidases such as glutathione peroxidase, enzymes which reduce H_2O_2 to H_2O. Many other iron proteins exist, but most possess iron in forms such as haem and iron-sulphur clusters that mediate a range of essential biochemical processes in the mammalian cell through the versatile co-ordination and redox biochemistry of iron (reviewed by Cammack et al., 1990).

4.1.1 *The Low Molecular Weight Iron Pool (LMW-Fe Pool)*

A small amount of iron not bound to iron binding proteins has been postulated to be present in the cytosol. This pool provides the cell with a relatively accessible form of iron for incorporation into cytosolic enzymes and proteins. The constituents of this low molecular weight iron pool (LMW-Fe pool), are still unclear, but probably consist of both Fe^{2+} and Fe^{3+} ligands (reviewed by Crichton and Ward, 1992). Early studies (Bartlett, 1976, Konopka and Szotov, 1972) indicated that this LMW-Fe pool was associated with nucleotides such ATP and GTP. Evidence confirming the importance of nucleotides as ligands for the LMW-Fe pool was presented by the finding of receptors for ATP-Fe^{2+} and ATP-Fe^{3+} on mitochondria (Weaver and Pollock, 1990) which would supply iron for haem biosynthesis. Many other ligands have also been suggested as possible components of the LMW-Fe pool. These include pyrophosphates, nucleic acids, lipids, glycogen, riboflavin, ascorbate, sugars, amino acids, polypeptides, proteins, and uncharged growth factors (Crichton and Ward, 1992; and references cited therein), but none of these ligands

have been universally accepted as the major ligand for iron in the LMW-Fe pool. In a review by Richarson and Ponka (1997), it was observed that many of the studies involved in the identification of iron ligands were flawed for a variety of reasons including inappropriate and non-physiological conditions, as explained by the authors. More recently, using isolated rat liver nuclei, Gurgueira and Meneghini (1996) reported ATP-dependent uptake systems for iron-citrate and iron-ATP chelates suggesting that these may be of physiological importance.

4.1.2 *Determination of Low Molecular Weight-Fe Pool*

Attempts to quantificate and assess the LMW-Fe pool have, in the past, relied on methods that homogenise cells and tissues and the iron content is then determined using electron paramagnetic resonance (EPR) with iron chelators (Yegorov et al., 1990; Koslov et al., 1992), or used Mossbauer spectroscopy of chelated iron (St Pierre et al., 1992). All the physicochemical methods used, either required cell disruption or relatively large amounts of tissue because of the low sensitivity of the method. None of these methods involve dynamic measurements of changes in the iron pool (Epsztejn et al., 1997). One method designed to assess the LMW-Fe pool involved addition of an iron chelator, nitrobenz-furazan-desferrioxamine (NBD-DFO), that was also a fluorescent probe (Lytton et al., 1992). The method was based on the capacity of NBD-DFO to enter and extract iron from cells causing physical disruption. Binding of iron to this fluorescent probe quenched its fluorescence, and subsequent removal restored fluorescence which, in turn, could be used to provide a quantitative determination of iron content. Problems associated with this method, however, were that the probe had a low quantum yield, poor

cell tolerance, and it was difficult to assess the amount of iron bound to the probe because of its high affinity for iron (Epsztejn et al., 1997).

It was recently shown recently (Breuer et al., 1995; Breuer et al., 1995a) that calcein (CA), a fluorescein molecule with two ethylenediamine diacetate-like moieties (Fig 4.1) can serve as a metallo-sensitive probe in solution and in cells, particularly with respect to iron. This is because, upon stoichiometric binding (1:1) of an appropriate metal (i.e. iron), CA's fluorescence is quenched. CA, which has a high quantum yield, can be easily loaded into cells by its esterified, non-fluorescent analogue, calcein-AM (acetoxymethyl ester). Calcein-AM (CA-AM) crosses intact cell membranes and is cleaved by intracellular esterases to produce CA, a polar highly fluorescent molecule, that is retained in healthy cells, but can leak from cells with damaged membranes (Haugland, 1992).

Fig. 4.1. The chemical structure of (a) calcein (CA) and (b) salicylaldehyde isonicotinoyl hydrazone (SIH).

(a) **(b)**

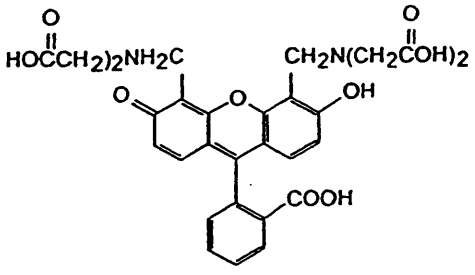

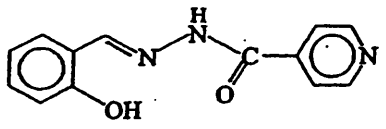

By adding a permeant chelator, such as salicylaldehyde isonicotinoyl hydrazone (SIH) (Fig.4.1), the concentration of iron that is bound to CA can be revealed (Breuer et al., 1995; Cabantchik et al., 1996). Changes in fluorescence, evoked by SIH addition, provides a basis for the dynamic monitoring of cytosolic iron in living cells using

spectrofluorimetry (Breuer et al., 1995a). These fluorescence changes can be translated, by means of calibration, to provide an estimate of the chelatable iron pool within cells (Breuer et al., 1996; Epsztejn et al., 1997) which is also known as the labile iron pool. This pool is comprised of all chelatable, rapidly exchangeable forms of iron. The liganded form of iron is in dynamic equilibrium between the Fe^{2+} and Fe^{3+} forms, though Fe^{2+} is the only soluble free-form of iron. The levels of LIP can be raised artificially by adding iron in different forms, such as diferric transferrin or ferrous ammonium sulphate. Conversely, it can be decreased artificially by the addition of iron chelators such as desferal. Addition of CA to cells will shift the equilibrium of the LIP to CA-bound forms of iron resulting in the quenching of CA fluorescence. CA has two metal binding moieties with affinity constants for Fe^{2+} and Fe^{3+} identical to EDTA, 10^{14} and 10^{24} M^{-1} respectively (Breuer et al., 1995a), and it has been deduced (Epsztejn et al., 1997) that the Fe^{2+} bound form of CA is in rapid equilibrium with Fe^{2+}. SIH is a fast (cell) permeating, high affinity (tridentate) iron chelator, which can chelate both Fe^{2+} and Fe^{3+} forms of iron and has a binding constant for Fe^{3+} of 10^{29} M^{-1} (Tsafack et al., 1996). Addition of excess SIH to cells rapidly shifts the equilibrium to the chelator bound form. This evokes a rise in CA fluorescence and gives a direct reflection of the amount of iron bound to CA.

After the development of this assay a number of different studies were performed to assess changes in the chelatable iron pool after various treatments. It was shown in human erythroleukemia cells (Breuer et al., 1996) that brief exposure to the Fe^{2+} salt, ferrous ammonium sulphate (FAS), caused a rise in the chelatable iron pool. Oxidative treatment in the form of hydrogen peroxide (H_2O_2), or reductive treatment in the form of β-mercaptoethanol (ME), both caused rises in the chelatable iron pool. These rises were

attributed to reductive iron release from ferritin. Similarly, a different study (Breuer et al., 1997) using erythroleukemia cells that were treated with diferric transferrin, and subsequently treated with the oxidants *t*-butyl hydroperoxide (TBHP) or H_2O_2, showed increases in the chelatable iron pool. The source of this increase of chelatable iron, normally undetectable using this assay, was suggested as being Fe^{3+} tightly bound to ligands such as ferritin, nucleotides, or polypetides that may be susceptible to reductive release. The viability of cells in these studies was determined using the trypan blue exclusion assay, an assay which gives an indication of cell membrane damage.

4.1.3 *Calcein as an Indicator of Membrane Damage*

The fluorescent probe CA has recently been used to assess viability in cells exposed to aminolevulinic acid (ALA), followed by exposure to light (Campbell et al., 1996). As mentioned above, CA-AM added to cells can be converted to fluorescent CA by cells with functional intracellular esterases (located on the plasma membrane) and is retained in healthy cells with intact membranes. Treatment that causes injury to cells may result in a reduction of CA fluorescence of those cells because either a lower quantity is produced by damaged esterases, or CA has leaked from the cell through a damaged plasma membrane.

4.1.4 *Objectives of this study*

In a recent study (Pourzand et al., 1999) it was demonstrated using the calcein assay, that treatment of primary human fibroblasts with UVA radiation resulted in an increase in the chelatable iron pool. UVA has also been shown to cause membrane damage and reduce the survival of cultured human fibroblasts (Gabroriau et al., 1993; Applegate et al.,

1994). The objective of this present study was to develop a method that could measure simultaneously both changes in the intracellular chelatable iron pool, and also a parameter of viability, such as membrane damage, of cells that had been treated with ALA and/or UVA irradiation. We demonstrate in this study a flow cytometry based method that can measure both of these parameters, using the fluorescent probe calcein.

4.2 Methods

4.2.1 *Cell Culture*

The primary human fibroblast cell line, FEK4, and the immortalised human keratinocyte cell line, HaCaT, were cultured as described in sections 2.2.2 and 3.2.1 respectively.

4.2.2 *Chemical Treatment and Irradiation Conditions*

FEK4 cells were treated with ALA as described in section 2.2.3. Both FEK4 and HaCaT cells were treated with desferal by preparing a 100 μM solution using the appropriate conditioned cell culture media. These solutions were then added back to the cells, which were incubated for 18 h at 37°C. Prior to irradiation, 80% confluent cells were washed with PBS and removed by trypsinsation (0.25%, 10 min). Cells were collected, spun for 5 min at 1000 rpm, then re-suspended in PBS supplemented with 0.01% Ca^{2+} and Mg^{2+} (Keyse and Tyrrell, 1989) at a density of 5 x 10^5 cells/ml. Irradiation conditions are described in section 2.2.6. Cell suspensions were UVA irradiated in quartz vessels (Scientific Laboratory Supplies, UK) that were agitated on a mixing platform (IKA Laboratechnik, Germany). Sham-irradiated cells were treated in the same manner.

4.2.3 *Loading of Cells with Calcein for Analysis using Flow Cytometry*

Immediately after irradiation, cells were collected and centrifuged for 5 min at 1000 rpm. The supernatent was then removed and cells were re-suspended at a density of 1 x 10^5 cells/ml with 0.05 μM calcein-acetoxymethyl ester (CA-AM) (Molecular Probes, USA) for 15 min at 37°C in bicarbonate-free, serum-free medium containing 1mg/ml BSA (bovine serum albumin), 20 mM Hepes, pH 7.3 (CA-AM was added from a concentrated

stock solution in DMSO). After CA-AM incubation, cells were washed of excess CA-AM using PBS, re-suspended in CA-AM free loading medium at a density of 5 x 10^5 cells/ml, and maintained on ice until flow cytometry analysis.

4.2.4 *Analysis of Calcein-Loaded Cells using Flow Cytometry*

For analysis of damage to intracellular esterases and determination of the chelatable iron pool within cells using flow cytometry, a specific set-up was designed so that during analysis, cells were stirred using a magnetic stirring bar (Merck, UK) whilst maintained at 37°C (see Fig 4.2).

Fig 4.2. Flow cytometer set-up to keep cells stirred and incubated at 37°C for analysis of damage to intracellular esterases and changes in the chelatable iron pool.

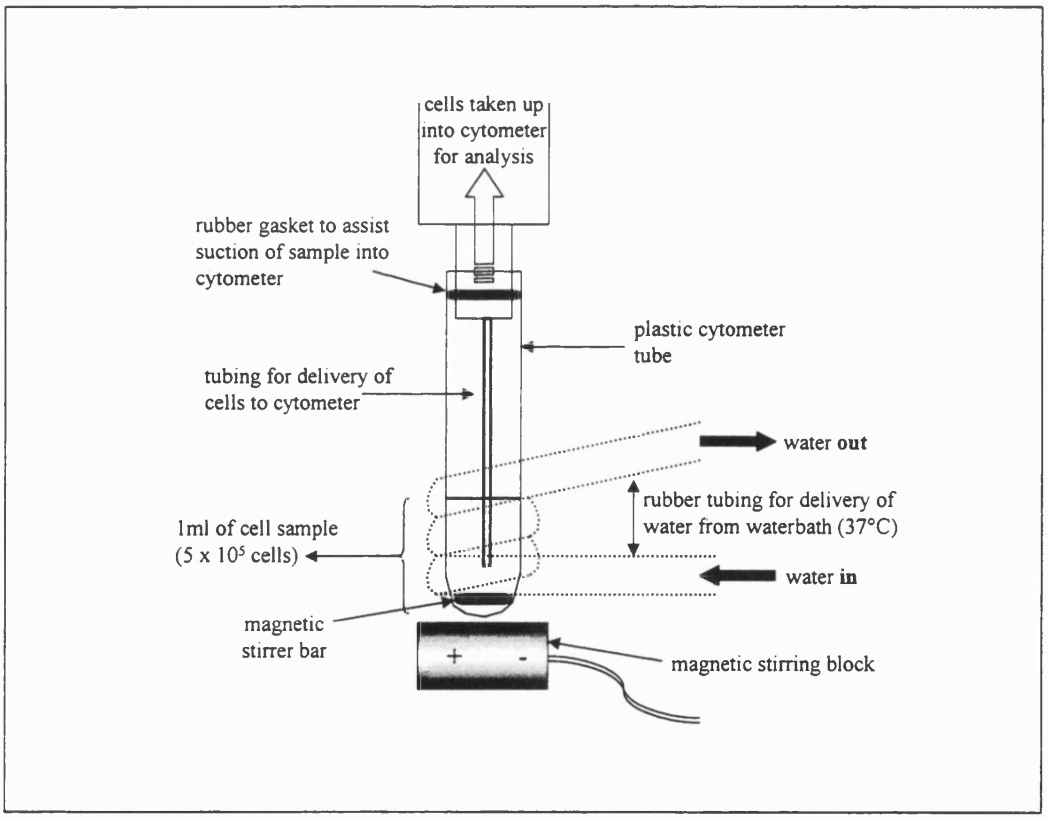

Immediately prior to measurement, 1 ml of calcein(CA)-loaded cells (5 x 10^5 cells) were centrifuged for 1 min at 3000 rpm, then re-suspended in 1 ml of pre-warmed Hepes buffered saline solution (HBS buffer), composed of PBS with 20 mM Hepes and 150 mM NaCl, pH 7.3. The cell suspension was placed in flow cytometer tube (Becton Dickinson, UK) and cells were analysed using a FACS (fluorescence activated cell sorter) Vantage flow cytometer (Becton Dickinson, UK). The flow cytometer used an argon ion laser at 488 nm (100 mW) for excitation, and measured emission fluorescence at 525 nm with a band pass filter (± 30 nm).

4.2.5 *Determination of Intracellular Esterase and Membrane Damage*

The mean CA fluorescence of 10000 cells after addition 100 μM of the cell permeant iron chelator salicylaldehyde isonicotinoyl hydrazone (SIH) (which was kindly provided by P. Ponka, Canada) was obtained for each sample. Membrane damage and intracellular esterase inactivation of UVA-irradiated cell populations was determined by comparing the fluorescence of these populations to that of the sham-irradiated controls, and expressing it as a percentage.

4.2.6 *Estimation of the Intracellular Chelatable Iron Pool*

The mean fluorescence of 10000 CA-loaded cells was obtained. The highly cell permeant iron, chelator SIH (100 μM), was then added and the increase in fluorescence (as SIH de-quenched CA fluorescence by chelating iron bound to CA) was monitored until a steady signal was obtained (usually within 2 min). The mean fluorescence of 10000 cells was obtained once more, and the mean change in fluorescence was

determined by subtracting the mean fluorescence of the cells pre-SIH treatment from the mean fluorescence of the SIH treated population. To convert this fluorescence change to a quantitative determination of intracellular chelatable iron, it was necessary to calibrate the system using iron. CA-loaded cells were prepared as mentioned above. A stock solution of ferrous ammonium sulphate (FAS) was prepared by dissolving the compound in Milli-Q water (Millipore, UK) and maintaining the solution under argon to prevent oxidation. The liquid was also bubbled with argon before use. By monitoring the fluorescence of CA-loaded cells (using flow cytometer, as described above), the calibration was performed by first adding 1 μM of the divalent metal ionophore A23187 (from a concentrated stock solution in DMSO). This substance increases the permeability of cell membranes to divalent metal ions and when the metal is added, equilibration (of the metal) occurs between the cell and the medium. Sequential additions of aliquots of FAS were added to obtain 0.25 μM step increases of metal concentration, and the discrete decreases in fluorescence elicited were monitored and recorded. The fluorescence recording of 10000 cells was not taken until a stable fluorescence signal was obtained after each FAS addition (1-2 min). Addition of 100 μM SIH results in restoration of CA fluorescence.

The data obtained by FAS titration can be fitted by a first order exponential decay function (Fig. 4.9) relating the two variables y and x which are fluorescence and FAS concentration respectively:

$$y = y_0 + Ae^{-(x/t)}$$

Where y_0, A and t are constants. By adding SIH to CA-loaded cells, de-quenching of CA fluorescence occurs which is a measure of the amount of iron that was bound to CA. By inserting this fluorescence change value into the function described above, an estimation of the concentration of chelatable iron pool was derived.

4.2.7 *Statistical Analysis*

Results are expressed as the mean ± one standard deviation. Significant differences ($p<$ 0.05) were determined by an unpaired t test.

4.3 Results

4.3.1 *Comparison of Size and Granularity of FEK4 Primary Human Fibroblasts and HaCaT Immortalised Human Keratinocytes using Flow Cytometry*

Fig 4.3 shows the forward scatter and side scatter of FEK4 and HaCaT cells as determined by flow cytometry. A laser beam is directed at a tight stream of fluid containing a dispersion of cells. As the laser beam hits the cells, the light is scattered and is registered by detectors positioned in front of (forward scatter, FSC), and perpendicular (side scatter, SSC) to the flow of cells. Forward scatter gives a measure of size and side scatter gives a measure of granularity of cells. Figs. 4.3a and b are dotplots of forward scatter verses side scatter of HaCaT and FEK4 respectively. Frequency histograms (and their mean values) are also depicted showing the forward scatter (Fig. 4.3c) and side scatter (Fig. 4.3d) of the two cell lines (HaCaT histograms are grey and FEK4 histograms are black). From this data, it can be concluded that FEK4 is a larger, more granular cell than HaCaT. From observation under a light microscope, FEK4 certainly appears larger. One thing that should also be noted is, that after trypsinisation, cells sometimes do not detach completely from one another (this is particularly noticeable with HaCaT cells). Some of the scatter picked up may therefore be from cell aggregates, thus contributing to a larger mean scatter value.

Fig. 4.3. Flow cytometry dotplots (a and b) and frequency histograms (c and d) of HaCaT immortalised human keratinocytes (a) and FEK4 primary human fibroblasts (b). Data shows the forward scatter (FSC) and side scatter (SSC) obtained from these two cell lines, which reflect size and granularity respectively. Grey histograms indicate HaCaT data and black histograms indicate FEK4 data. The mean FSC (c) and SSC (d) values of the two cell lines are also included.

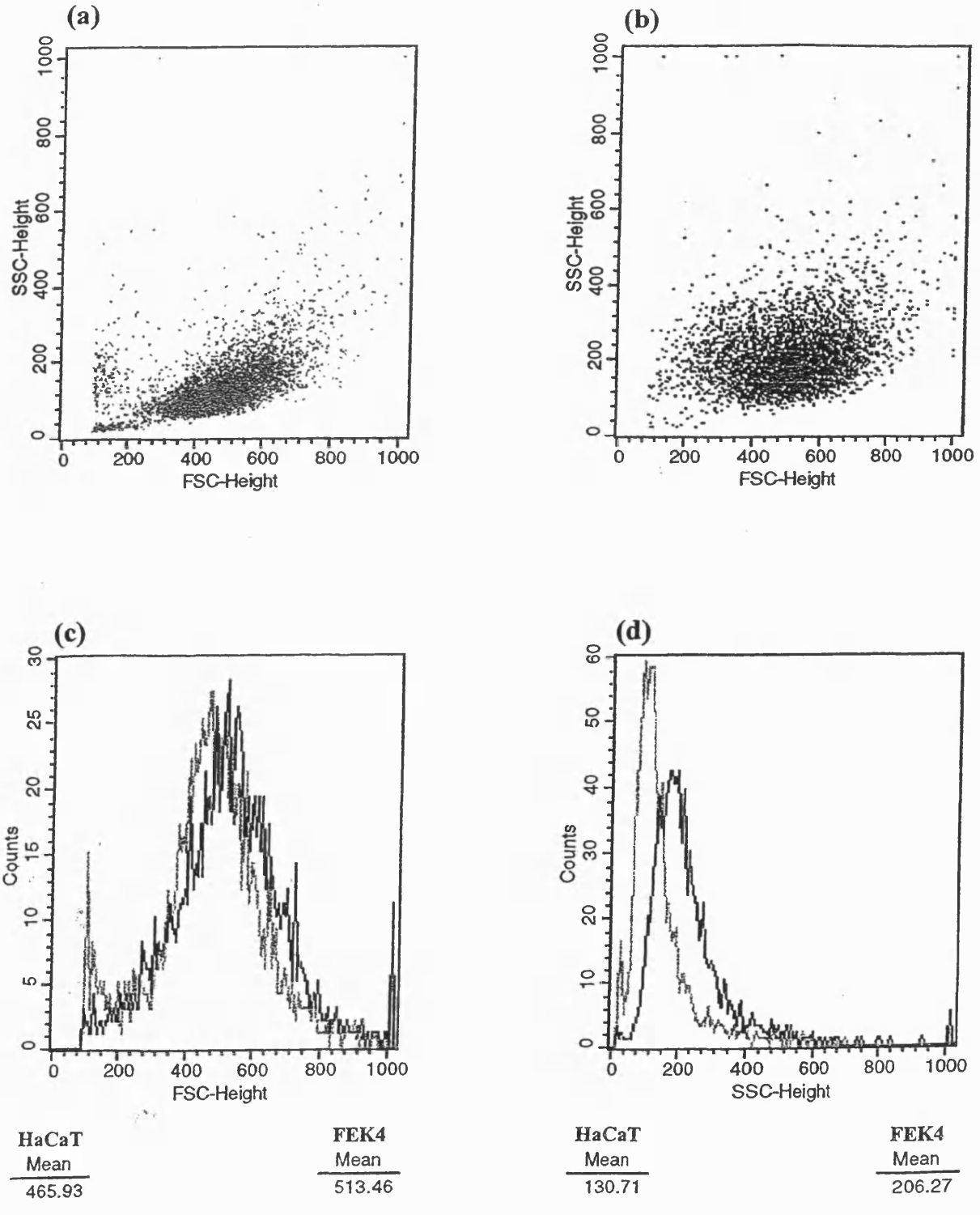

4.3.2 *Effects of UVA Irradiation on Cell Size and Granularity*

Fig. 4.4 shows forward scatter verses side scatter dotplots of a sham irradiated population of FEK4 primary human fibroblasts (Fig. 4.4a), and a population irradiated with 500 kJ/m^2 UVA radiation (Fig. 4.4b). Figs. 4.4c and d show the forward scatter (Fig. 4.4c) and side scatter (4.4d) frequency histograms of both cell populations (sham-irradiated cell histograms are black and 500 kJ/m^2 UVA irradiated cell histograms are grey). A threshold is normally set on the forward scatter, which means that any cells or particles that fall below this threshold size are not recorded. This effectively gates out debris and fragmented cells. From this data it is clear that UVA causes the cells to shrink and reduces their granularity. Although this is an extreme example of what happens to cells after UVA irradiation, the example is used to clearly show the point. Cells probably shrink and express reduced granularity because of damage to the cell membrane, which concomitantly results in leakage of intracellular components.

Fig. 4.4. Flow cytometry dotplots (a and b) and frequency histograms (c and d) FEK4 primary human fibroblasts either sham-irradiated (a) or treated with 500 kJ/m^2 UVA radiation. Black histograms and dotplots indicate sham-irradiated cells and grey histograms and dotplot indicate UVA treated cells data. The mean FSC (c) and SSC (d) values of the two cell lines are also included.

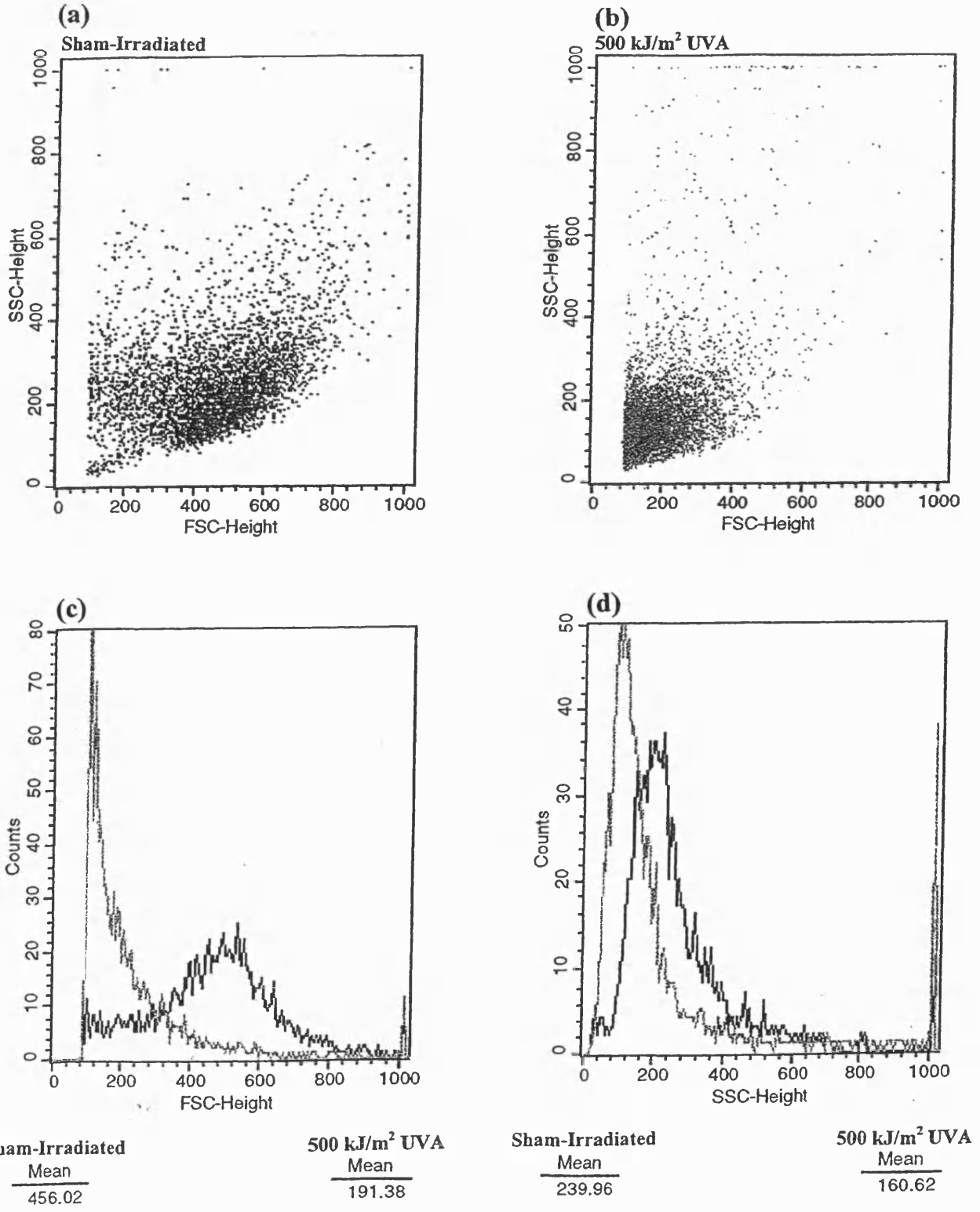

Sham-Irradiated	500 kJ/m^2 UVA
Mean	Mean
456.02	191.38

Sham-Irradiated	500 kJ/m^2 UVA
Mean	Mean
239.96	160.62

4.3.3 *An Example of the Effect of ALA Incubation and UVA Irradiation on the Production of Fluorescent Calcein by Intracellular Esterases*

As discussed in the introduction, cells with functional intracellular esterases can convert exogenously added CA-AM to fluorescent CA. This CA is retained in healthy cells with intact membranes. Treatment of cells that results in inactivation of intracellular esterases and damage to cell membranes can affect the ability of cells to produce and retain CA. Acquired intracellular fluorescence is probably the most important parameter determined by a flow cytometer. In the example shown here (Fig 4.5), cells are treated with either ALA alone, or ALA followed by UVA. The two populations are then incubated at 37°C for 15 min with CA-AM. This allows cells with functional esterases to cleave CA-AM producing fluorescent CA, and in turn, gives an indication of how healthy a population is. Intracellular CA fluorescence is measured using flow cytometry and Fig. 4.5 shows an example of fluorescence frequency histograms of cells treated with 200 μM ALA alone for 18 h (black histogram), and cells treated with ALA followed by a dose of 100 kJ/m^2 UVA (grey histogram). On the diagram, FL-1 is fluorescence intensity detected at 525 nm (± 30 nm), and calcein fluorescence emission peaks at 535 nm. The higher the FL-1 value, the greater the intracellular CA fluorescence intensity is. It is clear from the example depicted (Fig. 4.5) that ALA incubation (200 μM, 18 h) followed by UVA irradiation (100 kJ/m^2) results in a marked decrease in the mean fluorescence intensity (i.e. CA production and retention).

Fig. 4.5. Flow cytometry frequency histograms of FEK4 primary human fibroblasts treated with 200 μM ALA for 18 h and either sham-irradiated (black histogram) or irradiated with a dose of 100 kJ/m^2 UVA (grey histogram). FL-1 is a measure of calcein fluorescence intensity of the cells. The mean calcein fluorescence of the two cell populations is included.

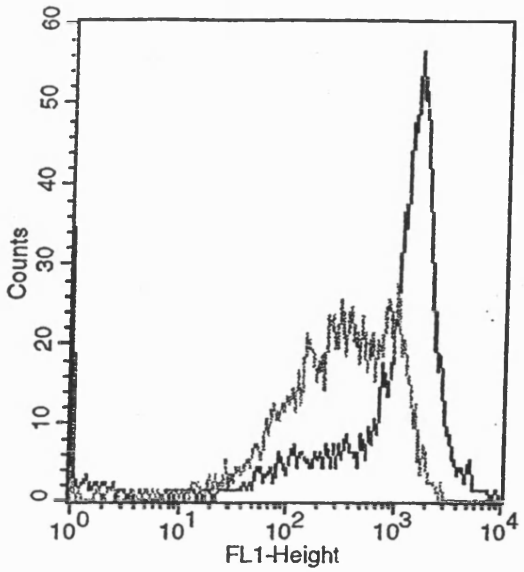

Sham-Irradiated	**100 kJ/m^2 UVA**
Mean	Mean
1272.55	466.94

4.3.4 *Effects of UVA Irradiation on Calcein Fluorescence in FEK4 Primary Human Fibroblasts and HaCaT Immortalised Human Keratinocytes*

Fig.4.6 shows the detrimental effect of graded doses of UVA radiation on the CA fluorescence in both FEK4 fibroblasts and HaCaT keratinocytes. CA fluorescence of UVA treated cells is expressed as a percentage of the CA fluorescence observed in sham-irradiated controls. The amount of CA produced intracellularly (after 15 min CA-AM incubation) in both cell lines is clearly reduced as a function of UVA dose, suggesting either that damage has occurred to intracellular esterases or that CA is lost from the cells as a result of damaged plasma membranes. The observed effect appears to be more pronounced in the fibroblasts than the keratinocytes, suggesting that the FEK4 are more sensitive to UVA-induced damage. All data that was obtained by measuring intracellular CA fluorescence reductions as a result of (ALA and/or) UVA treatment was determined after the addition of the cell permeable iron chelator, SIH, to the cells being analysed. The purpose of this was to remove any artifactual quenching of CA fluorescence by intracellular 'free' iron (see below for details).

Fig. 4.6. UVA dose-dependent reduction in calcein fluorescence reduction in FEK4 fibroblasts and HaCaT keratinocytes, as a result of intracellular esterase inactivation and loss of calcein through damaged membranes. Fluorescence is measured using flow cytometry. Data represent the mean of 3-4 experiments (± S.D.)

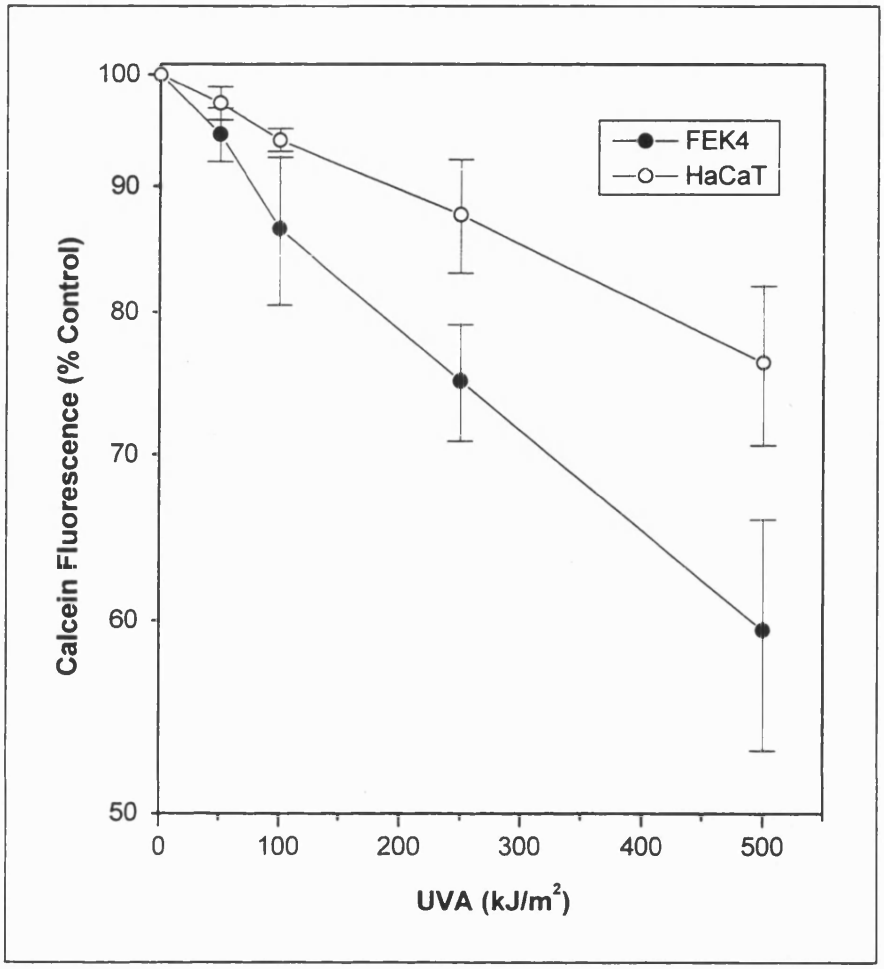

4.3.5 *Effects of ALA Incubation and UVA Irradiation on the Production of Fluorescent Calcein by Intracellular Esterases in FEK4 Primary Human Fibroblasts*

The effects of either 4 and 18 hours ALA incubation, followed by UVA irradiation (of doses up to 100 kJ/m^2) on the CA fluorescence in FEK4 cells is shown in Fig. 4.7a and b respectively. From the graphs, reduction in intracellular CA fluorescence appears to be dose dependent with respect to ALA concentration and UVA dose. The results obtained after 4 and 18 hours ALA incubation followed by UVA irradiation are not significant. Dark toxicity of ALA was tested and found to have no affect on CA levels detected compared to non-treated controls (data not shown).

Fig. 4.7. UVA dose-dependent reduction of calcein fluorescence in FEK4 fibroblasts treated with ALA for either 4 (a) or 18 (b) hours. Data represent the mean of 3-4 experiments (± S.D.).

(a) 4 h ALA

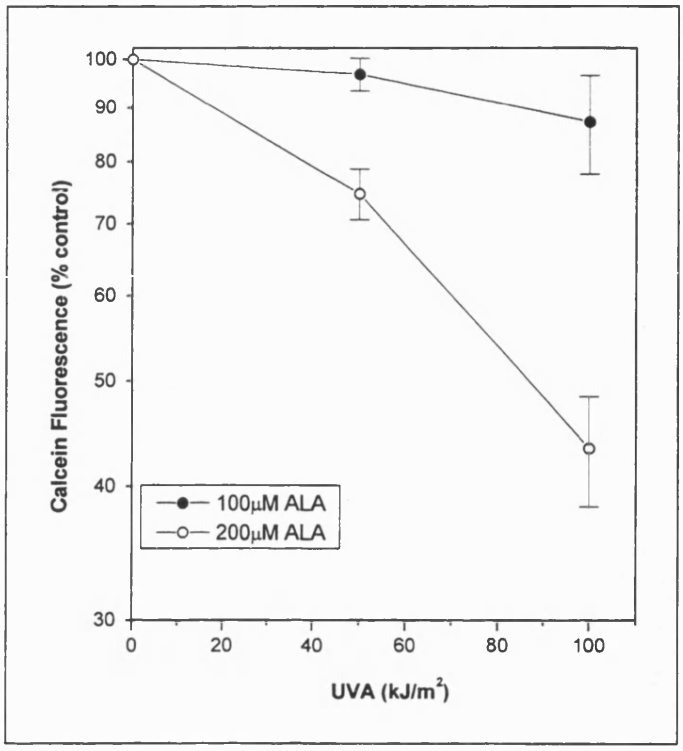

(b) 18 h ALA

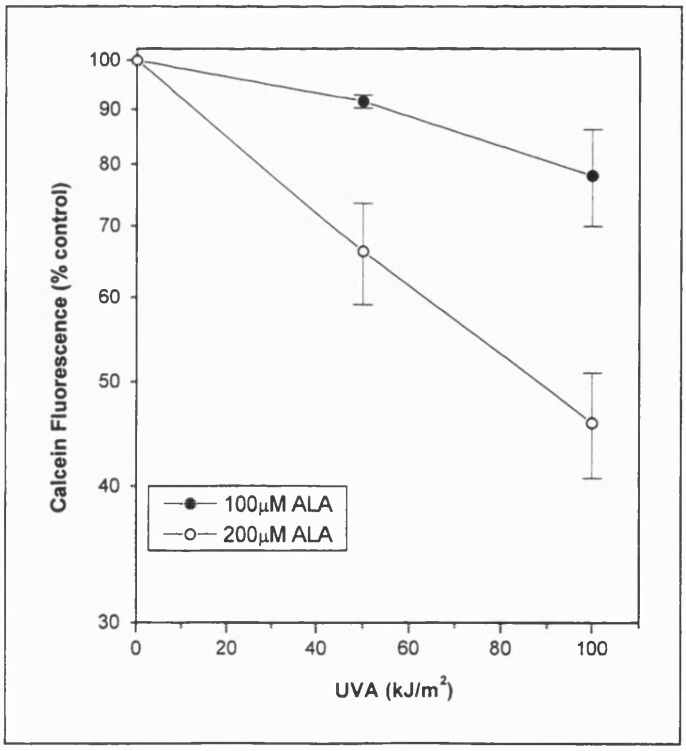

4.3.6 *Determination of the Chelatable 'Free' Iron Pool using the Cell Permeable Iron Chelator Salicylaldehyde Isonicotinol Hydrazone (SIH)*

Calcein not only gives an indication of the state of health of a cell population, it also serves as a metallo-sensitive probe. Its fluorescence is quenched due to stoichiometric (1:1) binding of iron. Addition of the cell permeable chelator SIH results in the de-quenching of CA fluorescence, by the removal of iron, because of SIH has a greater affinity for iron than CA. This, in turn, can give an indication of CA-sensitive iron levels in the cytosol, which we refer to as chelatable 'free' iron levels. Fluorescence changes can be monitored using a flow cytometer, thus changes in chelatable 'free' iron as a result of a specified treatment, such as UVA irradiation, can be estimated using this system. Fig.4.8 shows an example of the frequency histograms of CA fluorescence intensity produced by HaCaT cells after either sham-irradiation (Fig.4.8a), or after a UVA dose of 250 kJ/m^2 (Fig.4.8b). The black histograms represent the two cell populations before SIH treatment, and the grey histograms represent cells treated with 100 μM SIH. The mean fluorescence of each histogram is also included for clarification. From this data it is clear that SIH can de-quench CA fluorescence by chelating iron (seen by the increase in CA fluorescence intensity) and that UVA increases this chelatable iron pool.

Fig. 4.8. Calcein fluorescence frequency histograms of HaCaT keratinocytes either sham-irradiated (a) or have been irradiated with a dose 250 kJ/m^2 UVA radiation (b). Black histograms indicate fluorescence before SIH treatment and grey histograms indicate fluorescnce after 100 μM SIH treatment. Mean fluorescent values are included.

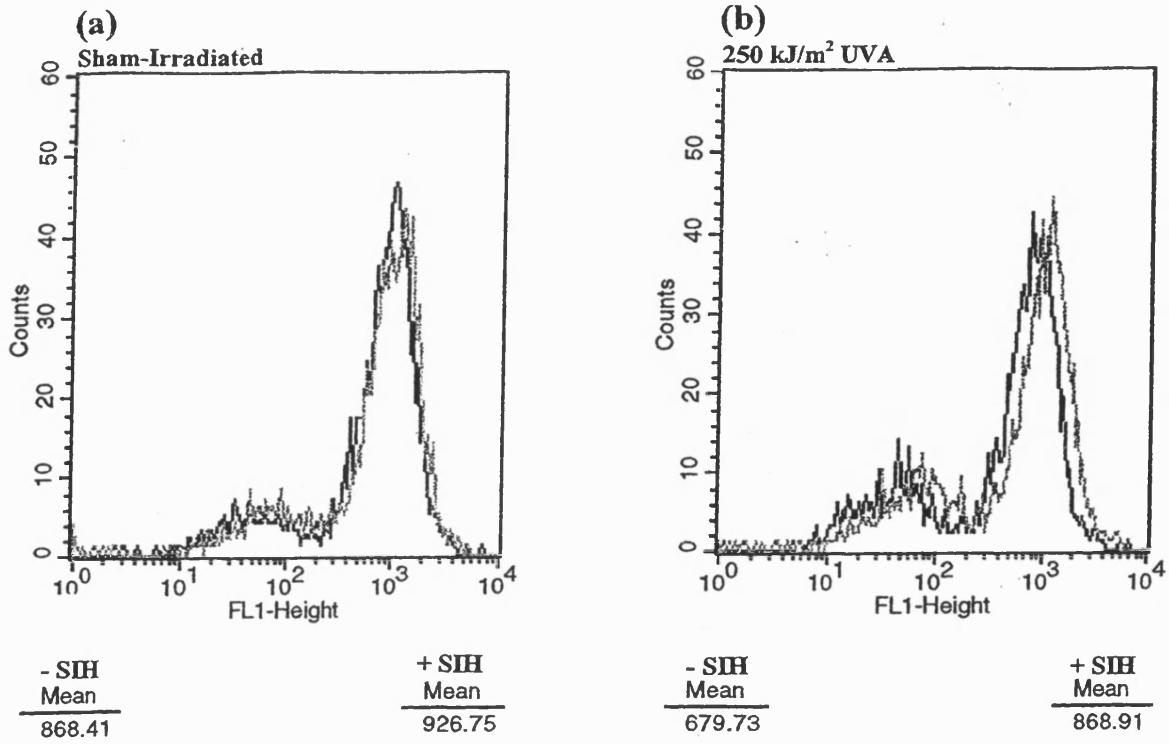

4.3.7 *Estimation of Chelatable 'Free' Iron Levels*

In order to translate the apparent change in fluorescence by the addition of SIH, to a quantitative estimate chelatable 'free' iron, it was necessary to calibrate CA-loaded cells with iron. Fig.4.9 shows an example of a typical calibration of CA-loaded cells (FEK4 fibroblasts in this example) by titration with ferrous ammonium sulphate. Sequential additions of (0.25 μM) FAS added to CA-loaded cells resulted in decreases in fluorescence and this was monitored using flow cytometry. The data obtained by the titration can be fitted by a first order exponential decay function (see 4.2.5). This function, in turn, is used to estimate of the μM concentration of the intracellular 'free' iron pool (see 4.2.5).

Fig. 4.9. Typical calibration of calcein-loaded cells (FEK4 primary human fibroblasts) with sequential (0,25 μM) aliquots of ferrous ammonium sulphate (FAS). Calcein fluorecence is monitored using flow cytometry.

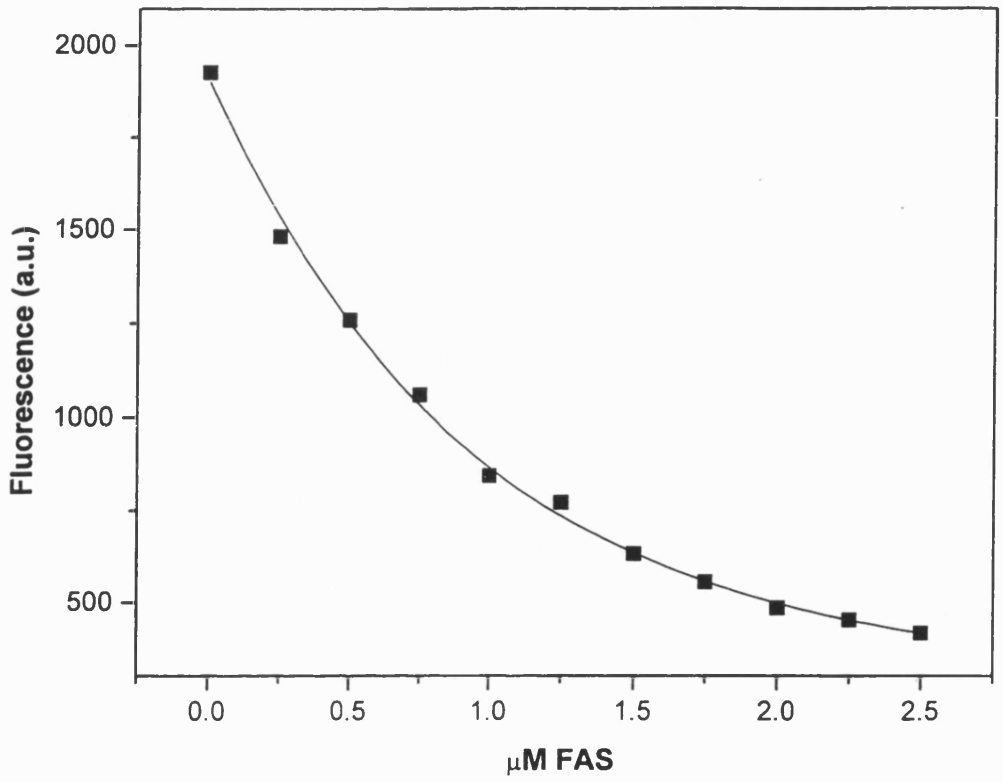

4.3.8 *Effect of UVA Irradiation on the Concentration of Chelatable Iron Pool of FEK4 Primary Human Fibroblasts and HaCaT Immortalised Human Keratinocytes*

Tables 4.1 and 4.2 show the effects of graded doses on the chelatable iron pool of FEK4 and HaCaT respectively, measured using flow cytometry. UVA radiation appears to cause a dose dependent increase in the chelatable iron pool in both cell lines. Relative increases appear lower in FEK4 compared to HaCaT, e.g. after 500 kJ/m^2 UVA, FEK4 showed approximately a 210% increase in the chelatable iron pool when compared to non-irradiated controls. A 420% increase was observed in the HaCaT cells after the same UVA dose. However, FEK4 possess a chelatable iron pool that is approximately 3 times bigger than that of the HaCaT, 0.08024 μM compared to 0.02727 μM. The absolute increases in chelatable iron that are observed in the FEK4 and HaCaT after 500 kJ/m^2 UVA, are approximately 0.16843 μM and 0.11415 μM respectively (calculation of these values is described in 4.2.5). Treatment of both cell lines with the iron chelator desferal for 18 h (100 μM) removed all chelatable iron so that there was no change in CA fluorescence after 100 μM SIH addition.

Table 4.1. The concentration of chelatable iron in the FEK4 primary human fibroblasts after UVA irradiation or desferal treatment. Measurements were performed immediately after irradiation. Data represent the mean of 3-4 independent experiments (± S.D.).

Treatment	Chelatable iron (μM)
Non-irradiated	0.08024 ± 0.01747
100 kJ/m^2 UVA	0.11179 ± 0.0126*
250 kJ/m^2 UVA	0.19903 ± 0.01612*
500 kJ/m^2 UVA	0.24867 ± 0.01629*
18 h Desferal (100 μM)	0.000 ± 0.000*

Statistical analyses were made using an unpaired *t* test. *, Significantly different from non-irradiated control ($p < 0.05$ level).

Fig 4.2. The concentration of chelatable iron in the HaCaT immortalised human keratinocytes after UVA irradiation or desferal treatment. Measurements were performed immediately after irradiation. Data represent the mean of 3-4 independent experiments (± S.D.).

Treatment	Chelatable iron (μM)
Non-irradiated	0.02727 ± 0.0645
100 kJ/m^2 UVA	0.04717 ± 0.01244
250 kJ/m^2 UVA	0.09259 ± 0.01489*
500 kJ/m^2 UVA	0.14142 ± 0.02216*
18 h Desferal (100 μM)	0.000 ± 0.000*

Statistical analyses were made using an unpaired *t* test. *, Significantly different from non-irradiated control ($p < 0.05$ level).

4.3.9 *Effects of ALA Incubation and UVA Irradiation on the Concentration Chelatable Iron Pool of FEK4 Primary Human Fibroblasts*

Table 4.3 shows the effects of incubation with ALA and irradiation with UVA, on the concentration of chelatable iron in FEK4 cells, measured using flow cytometry. Compared to the non-treated control, incubation with ALA concentrations up to 200 μM, for either 4 or 18 hours, led to a reduction in chelatable iron of up to 25%. The longer incubation reduced chelatable iron levels more effectively. Cells that were treated with 100 μM ALA for 4 h, followed by UVA irradiation of either 50 or 100 kJ/m^2, showed increases of 80% (0.06202 μM) and 130% (0.10124 μM) respectively compared to the sham-irradiated control. In contrast, cells treated with 200 μM ALA for the same period showed only an increase of approximately 20% (0.01323 μM) after 50 kJ/m^2 UVA, and a decrease of almost 40% (0.02655 μM) after 100 kJ/m^2, compared to the sham-irradiated control. The 18 h ALA incubations resulted in similar trends to those observed after 4 h, though the changes were less dramatic. For example, the 18h, 100μM ALA incubation resulted in a dose dependent increase in chelatable iron levels up to 70% (0.05 μM) after 100 kJ/m^2 UVA, compared to the non-irradiated control. The 200 μM ALA treatment showed an increase of only approximately 8% (0.00485 μM) after 50 kJ/m^2 UVA, and a decrease of around 12% (0.00697 μM) after 100 kJ/m^2. The lowest absolute level of chelatable iron measured was after 4h, 200 μM ALA treatment, which resulted in a level of 0.04454 μM.

Fig 4.3. The concentration of chelatable iron in the FEK4 primary human fibroblasts after ALA treatment and UVA. Measurements were performed immediately after treatment. Data represent the mean of 3-5 independent experiments (± S.D.).

ALA Treatment	Chelatable Iron (μM)
Non ALA-treated, non-irradiated	0.08024 ± 0.01747
4 h 100 μM non-irradiated	0.07736 ± 0.01077
4 h 100 μM 50 kJ/m^2 UVA	0.13938 ± 0.01061*
4 h 100 μM 100 kJ/m^2 UVA	0.1786 ± 0.02746*
4 h 200 μM non-irradiated	0.07109 ± 0.00806
4 h 200 μM 50 kJ/m^2 UVA	0.08432 ± 0.0115
4 h 200 μM 100 kJ/m^2 UVA	0.04454 ± 0.009*
18 h 100 μM non-irradiated	0.07388 ± 0.00958
18 h 100 μM 50 kJ/m^2 UVA	0.103432 ± 0.02396*
18 h 100 μM 100 kJ/m^2 UVA	0.12389 ± 0.00743*
18 h 200 μM non-irradiated	0.05924 ± 0.00457
18 h 200 μM 50 kJ/m^2 UVA	0.06409 ± 0.00778
18 h 200 μM 100 kJ/m^2 UVA	0.05227 ± 0.00682

Statistical analyses were made using an unpaired *t* test. *, Significantly different from the corresponding non-irradiated control ($p < 0.05$ level).

4.4 Discussion

The purpose of the study presented in this chapter was to provide an assay that could measure simultaneously two important parameters that appear to be affected by UVA. These parameters are a reduction in the viability of a cell population as reflected by damage to the plasma membrane, and changes in intracellular 'free' iron levels. We initially expected to use a combination of two totally different assays, which use entirely different approaches. However, we are able to combine two assay systems that were developed independently to provide both pieces of data in a single procedure based on the measurement of calcein fluorescence by flow cytometry.

Campbell and co-workers (1996) used an assay involving two fluorescent probes, calcein (CA) and ethidium homodimer-1 (EthD-1), that they claimed could measure and determine cell survival after treatment with ALA and graded doses of 600-700 nm light (i.e. an in vitro method to study the effects of ALA-PDT). These two fluorescent probes were part of a kit known as the Live/Dead Eukolite Viability/Cytotoxicity Kit (Molecular Probes, USA). The principle behind this kit was that it could provide reciprocal (fluorescent) staining of treated cells that could be measured by flow cytometry to indicate viability of those cells, i.e. high CA fluorescence and low EthD-1 fluorescence indicated a viable (or healthy population), and vice versa. Changes in chelatable iron have been performed previously using an assay developed and optimised by Cabantchik and co-workers (Epsztejn et al., 1997). This assay, also known as the calcein assay, monitored changes in calcein fluorescence in response to changes in chelatable iron as measured by spectrofluorimetry.

By combining various aspects of these two assays and using one fluorescent probe, calcein, we have developed an assay that can provide an indication of viability, such as membrane damage (following a specified treatment), and concomitantly measure changes in the intracellular chelatable iron pool of that population. In showing the development stages of this assay (in the results section), the conditions shown in each example are varied (i.e. cell line and treatment). This was done mainly to emphasise a point more clearly, but all the information, including size (forward scatter, granularity (side scatter) and acquired calcein fluorescence is obtained and recorded for each sample measured using flow cytometry.

Fig. 4.3 shows the size and granularity of the two cell lines (FEK4 primary human fibroblasts, and HaCaT immortalised human keratinocytes) as measured by flow cytometry. Consistent with observations made using a light microscope (mentioned in the results), HaCaT are approximately 10% smaller than FEK4 (indicated by forward scatter), as determined by flow cytometry. The apparent lower granularity of HaCaT cells (indicated by side scatter) may also be, to some extent, related to HaCaT being smaller a cell. However, side scatter is an indication of specific structures within a cell (i.e. granularity), such as organelles, large proteins or anything within the cell that can cause the target laser to scatter light perpendicularly to its trajectory. The greater side scatter exhibited by FEK4 would suggest that it contains a greater quantity of such structures. As an example, FEK4 contains approximately a 4-fold higher level of the iron storage protein ferritin (see Chapter 5), which may contribute to side scatter because of the iron stored within it.

An example of the effect of UVA radiation (500 kJ/m^2) on cell size (FSC) and granularity (SSC) is shown in Fig. 4.4. It was observed by light microscopy that cells appear to shrink after UVA treatment. This is also clear when comparing the FSC frequency histograms of sham-irradiated cells and those irradiated with 500 kJ/m^2 UVA. Presumably damage to the plasma membrane as a result of UVA irradiation may cause leakage of intracellular contents. From the comparison of the SSC frequency histograms, it would appear that intracellular components are also either leaking out of the irradiated cells, or are degraded, as reflected by the reduction in SSC. UVA can cause membrane damage (reviewed by Tyrrell, 1991). For example, and in a study using human skin fibroblasts and lactate dehydrogenase (LDH) release as the marker (Gabroriau et al., 1993), it was shown that plasma membranes were damaged by UVA irradiation.

It has been mentioned previously in this chapter that injury to cells can reduce the amount of fluorescent CA produced by a cell population by either, inactivation of intracellular esterases, or by rupturing the cell membrane and thereby allowing the leakage of intracellular CA. Fig. 4.5 shows the most extreme treatment used in this study, 200 μM ALA treatment for 18 h followed by 100 kJ/m^2 UVA irradiation. Also shown is the sham-irradiated control. CA fluorescence intensity is denoted FL-1 Height on the frequency histogram. It is quite clear in this example that the population (ALA treated, then) irradiated have a marked reduction in mean intracellular CA fluorescence. For the presentation of our results using intracellular CA levels as an indicator of viability, we have not represented decreases in CA fluorescence in terms of percentage survival, as has

been the case previously (Campbell et al., 1996). The results herein are presented in terms of CA fluorescence of treated cells as a percentage CA fluorescence of non-treated controls. This represents inactivation of intracellular esterases and membrane damage and this can be interpreted as a measure of viability following treatment.

Fig.4.6 shows the effect of UVA alone on the reduction of intracellular CA content in both FEK4 fibroblasts and HaCaT keratinocytes. CA content is effectively reduced in a UVA dose-dependent manner in both cell lines, but FEK4 appeared to be more sensitive to the UVA treatment as compared with the HaCaT keratinocytes. In previous experiments with keratinocytes and fibroblasts (Applegate et al., 1995: Leccia et al., 1998), keratinocytes have been shown to be more resistant to UVA-induced cell membrane damage. This has been attributed to higher antioxidant content in these cells as compared with fibroblasts (Leccia et al., 1998). In our study, an additional factor that may play a role in the HaCaT's resistance to UVA, is its low iron content. The low chelatable iron concentration and also the lower UVA-induced levels of iron release observed in the HaCaT cells may limit the damaging affects observed in this cell line after UVA irradiation, such as iron-catalysed hydroxyl radical formation and lipid peroxidation (Halliwell and Gutteridge, 1999).

Comparison of the CA fluorescence levels as measured after 4 and 18 hours ALA incubation, followed by UVA irradiation, reveals that there is not a significant difference between the damaging affects observed after the two incubations (Fig. 4.7). This is in contrast to the survival studies performed in Chapter 2 (Figs. 2.14 and 2.15) and which

was consistent with the possibility that suggest that the 4 h incubation results is a greater rate of cytotoxicity after UVA irradiation than 18 h ALA incubation.

It has been previously reported that UVA irradiation of FEK4 fibroblasts results in an increase in the chelatable free iron pool as measured by the calcein assay and spectrofluorimetry (Pourzand et al., 1999). In our study we tested the hypothesis that UVA-induced iron release could not only be detected and measured through monitoring CA fluorescence by flow cytometry, but that viability measurements could be undertaken in the same assay system. This was effectively achieved by adding the cell permeant iron chelator (SIH) which had two consequences. Firstly, it removed any iron from CA (which quenches its fluorescence), thus removing any artifactual quenching of fluorescence for the viability studies. Cells that had high intracellular iron levels after a specified treatment would appear to be less healthy then they actually were, if the iron is not removed from CA. Secondly, removal of this iron that caused artifactual quenching of CA fluorescence, in turn, provides a measure of intracellular chelatable iron in terms of a fluorescence increase (Fig. 4.8). The fluorescence increase observed could be translated to an estimate of intracellular chelatable iron by calibrating CA-loaded cells with FAS (section 4.3.7 and Fig. 4.9). Tables 4.1 and 4.2 show the affects of UVA irradiation on the intracellular chelatable iron pool in FEK4 fibroblasts and HaCaT keratinocytes respectively. Both cell lines show a dose dependent increase in chelatable iron levels as a function of UVA irradition, with FEK4 releasing a greater amount of iron compared to the HaCaT at the same dose. FEK4, on the other hand, has a chelatable iron pool around 3 times larger than the HaCaT cells. This difference, including a greater iron

release after UVA, observed in FEK4 compared to HaCaT, was also evident in aconitase measurements (see Chapter 3). FEK4 cells also possess a much higher ferritin content (see Chapter 5). In a previous study (Pourzand et al., 1999), the author postulated that ferritin is a major source of this chelatable iron increase. In Chapter 5, the results are consistent with the conclusion that UVA leads to ferritin degradation, particularly in the FEK4 cells and this provides an explanation as to why there is a greater increase in chelatable iron observed in FEK4 as compared with HaCaT.

Incubation of FEK4 fibroblasts with ALA appears to have a modest effect on the reduction of the level of chelatable iron (Table 4.3). Stimulating the biosynthesis of PPIX may cause ALA to exert a chelative effect because the penultimate step in the production of haem is the insertion of iron into the tetrapyrrole ring of PPIX. This, in turn, could contribute to the lowering of the chelatable iron pool. Addition of the iron chelator desferal (100 μM, 18 h) effectively abolished the chelatabe iron pool in FEK4 (Table 4.1), suggesting that the effect exerted by ALA as an iron chelator is minor compared to that of desferal. A decrease in aconitase activity was also observed after an identical ALA incubation (Chapter 3), as was a concomitant reduction in ferritin levels.

PPIX has been shown to locate within the ferritin molecule (Precigoux et al., 1994; Michaux et al., 1996) and it is also known to localise in hydophobic environments, particularly cell membranes (Ricchelli, 1995). Therefore, it is conceivable that UVA irradiation of PPIX in either of these locations could induce photosensitisation and aggravate damage to ferritin, resulting in concomitant iron release. PPIX located in

ferritin could cause direct damage to the protein shell upon photosensitisation, or it could damage lysosomal membranes causing hydrolytic enzymes to spill out into the cytosol, which in turn, could degrade ferritin (Pourzand et al., 1999). We intended to show in this study whether or not ALA-induced PPIX could induce, or exacerbate the release of chelatable iron after UVA irradiation.

ALA treatment of cells followed by UVA irradiation appeared to result in two different phenomena depending on the concentration of ALA administered. UVA dose-dependent increases in the chelatable iron levels were observed with 100 μM ALA after both 4 and 18 hours incubation. The absolute increases were higher after 4 h incubation, suggesting that the longer incubation had diminished the source of chelatable iron increase to some degree. In contrast, the 200 μM ALA incubation after both incubations showed a slight increase in the chelatable iron pool after 50 kJ/m^2 UVA, but a decrease (below non-irradiated controls) after 100 kJ/m^2 UVA irradiation. This would suggest that iron bound to CA is able to leak from cells with damaged plasma membranes, and that PPIX produced after incubation with ALA may contribute to this effect. The level of reduction of intracellular CA fluorescence after the higher ALA dose and irradiation with UVA (Fig. 4.8) would appear to support this hypothesis. In order to confirm this, extracellular CA levels would need to be determined, along with the bound iron. This could be done by performing similar spectrofluorimetric measurements on the supernatants of these cells after CA-AM incubation.

We report here that the flow cytometer can be used to detect changes in the chelatable iron pool of a population of cells, and concomitantly provide an indication of viability (as

assessed by membrane damage) using the fluorescent probe calcein. This assay has an added advantage over the calcein assay because it can measure changes in intracellular 'free' iron levels (similar to the calcein assay) and viability in the same procedure. The flow cytometer determines intracellular fluorescence, so loss of CA from cells provides part of the basis of determining membrane damage. The reduction in CA fluorescence, through inactivation of esterases, is also another indication of cell damage. With the calcein assay, this method of determining 'viability' is not possible as it measures both intracellular and extracellular fluorescence (i.e. total fluorescence). CA loss from cells with damaged membranes would therefore not be detected. To combat this, an anti-calcein fluorescence quenching antibody has been used with this method (Breuer et al., 1995), which is intended to quench the fluorescence of any CA leaking from cells. However, in the same study it was shown that addition of this antibody to cells with permeabilised membranes resulted in 90% quenching in total CA fluorescence. The disadvantage of flow cytometry in only being able to detect intracellular fluorescence is manifested when chelatable iron measurements are made with cells that have damaged membranes. If iron bound to calcein leaks from these cells (which does appear to happen under certain conditions, see Table 4.3), then quantification of the total increase in chelatable iron by this method is not possible. However, this problem may be overcome using spectrofluorimetry, by either measuring extracellular CA loss and the iron bound to it, or by performing the iron measurements using the calcein assay.

5. Study of the effects of ALA incubation and UVA irradiation on ferritin in human cells

5.1 Introduction

Iron is an essential nutritional element for most organisms and it plays a critical role in cellular processes such as electron transport and respiration, cell proliferation and differentiation, DNA synthesis and the regulation of gene expression. These major functions of iron rely on its ability to catalyse oxidation and reduction reactions by virtue of its ability to change valence states. Most iron present in organisms is complexed in proteins although some may also be present in a soluble pool of low molecular weight complexes such as ferric citrate and Fe^{3+} ATP (Weaver and Pollock, 1989). Despite iron being an essential element, excess 'free' iron can be toxic as in the presence of superoxide and hydrogen peroxide it can catalyse the formation of the highly reactive hydroxyl radical through the Fenton and Haber-Weiss reactions (Halliwell and Gutteridge, 1999). In turn, the hydroxyl radical can cause damage to a variety of biomolecules, and in particular, cause lipid peroxidation (see Chapter 1). Thus it is crucial for organisms to be able to protect against the toxic effects of iron and this is achieved be the sequestration of iron by two highly specialised iron-binding proteins, the extracellular transferrin and the intracellular ferritin (both binding iron in a relatively safe Fe^{3+} form). Potentially, iron can have a very damaging effect intracellularly, so the regulation of iron trafficking and iron storage is of major importance (discussed in Chapter 3).

5.1.1 *Ferritin*

The ferritin molecule is a cytosolic hollow protein shell made up of 24 polypeptide chains (subunits) of two types, H (heavy) and L (light), with slightly different molecular weights of 21,000 and 19,000 respectively (for most animal species). The ferritin molecule is capable of storing up to 4500 Fe^{3+} atoms in a cavity as an inorganic complex where its weight can vary from approximately 450,000 (depending on H- and L- subunit composition) to approximately 900,000 depending on iron content. All ferritin molecules contain approximately an 8 nm iron-storage cavity within which an iron-core structure composed of an insoluble structure known as hydrated ferric oxide or ferrihydrite $5Fe_2O_3 \cdot 9H_2O$ is formed (Towe, 1981). Normally, ferritin is only about 20% iron-saturated (Reif, 1992). There is a wide variation of the number of ferritin genes found between different species. The human genome, for example, contains 15 H-copies and 5-L-copies of the ferritin genes. The rat genome, in contrast, contains more than 20 L-copies and only 5 H-copies. Most copies are processed pseudogenes and it has been concluded that there is probably only one expressed copy of each type in both genomes (Munro, 1993). Various vertebrate ferritin amino acid sequences have been extensively characterised including those from human, horse, sheep, pig, rabbit, rat, mouse, chicken, and tadpole. The mammalian H- and L-ferritin polypeptide chain sequences show about 54% identity and approximately 90% of H-chain residues, and 85% of L-chains, are identical amongst mammals (Harrison and Arosio, 1996). Ferritins isolated from mammalian tissues consist of a mixture of isoferritins that range in iron content and subunit composition (Arosio et al, 1978). Twenty-five possible isoferritin compositions have been defined, made up of variations in subunit rations of H- and L-polypeptide chains. Generally,

organs that store iron (liver and spleen) tend to be rich in L-rich ferritins that usually have a relatively high average iron content of 1500 Fe atoms/molecule or more (Harrison and Arosio, 1996). H-rich ferritins have a relatively low iron content of less than 100 Fe atoms/molecule and are more characteristic of organs such as the brain and heart.

The ferritin three-dimensional structures are more highly conserved than their primary structures. Each of the 24 subunits consists of a bundle of 4 long helical segments and one short helical segment that confer rigidity, with the remainder of the subunit consisting of non-helical segments connecting the helices. Apoferritin (ferritin devoid of iron) is assembled from 24 structurally equivalent subunits. In heteropolymers (mixed subunit molecules), H- and L-subunits have the same conformations enabling the formation of heteropolymers with a complete range of subunit compositions because there are many similar or identical residues in the subunits. It has been proposed that like chains cluster preferentially within the polymer (Luzzago et al., 1986). The large number of intra- and inter-subunit bonds (salt bridges and H-bonds) contributes to the apparent stability of apoferritin to heat. In the assembled apoferritin molecule, the 24 subunits are related by a 4-, 3-, and 2-fold symmetry axes. Subunits pack tightly together except, at the 3-fold axes where there are narrow channels traversing the shell. It has been proposed that these 3-fold channels are the main entry route of iron and are also Fe^{2+} oxidation sites (Wardwska et al., 1986; Stefanini et al.,1989;Yablonski et al., 1992; Teffry et al, 1993).

5.1.2 *Iron Storage Processes*

When a dose of ^{59}Fe (as labelled ferric ammonium citrate or iron dextran) is injected into a rat, part of the dose will be found in the liver as soluble cytosolic ferritin (Drysdale and Munro, 1966; Kohgo et al., 1980; Bomford et al., 1981; Treffry et al., 1984). The steps by which this occurs have not been fully elucidated though it is known that transferrin delivers much of this iron by receptor mediated endocytosis (reviewed by Richardson and Ponka, 1997). After iron is liberated from transferrin into in the cytosol, the fate of iron is less clear. It is not known what the intracellular donor is in vivo, or the chemical form in which iron is delivered to ferritin. It is however known, that storage involves gradual accumulation by binding of iron to ferritin iron-core particles (Treffry and Harrison, 1984). Ferric citrate is probably one of the low molecular weight iron complexes of the cytosol. However, attempts to load apoferritin with this compound (or other Fe^{3+} compounds) in vitro have been unsuccessful (Treffry and Harrision, 1979) unless a reductant such as ascorbate is present (Lauhere and Briat, 1993).

Though not fully understood, there appears to be a generally accepted mechanism by which Fe^{2+} becomes oxidised and deposited within ferritin (reviewed by Harrison and Arosio, 1996 and refs. cited therein). It would appear that Fe^{2+} is first bound and oxidised at catalytic centres on the protein. Fe^{3+} then migrates to form clusters in the cavity of ferritin yielding stable nuclei (or iron-cores) of crystalline structure (ferrihydrite). Finally, the nuclei that are formed provide a secondary growing surface onto which Fe^{2+} can be deposited and oxidised, nucleated molecules are able to deposit iron faster than those devoid of nuclei. When adding Fe^{2+} to apoferritin, most of the iron

is found on the protein and little in iron-core clusters. However, as more iron is added and becomes oxidised by ferritin, the Fe^{3+} greatly favours attachment to the iron-core compared to the protein. After the early production of Fe^{3+} clusters the rate of Fe^{3+} deposition greatly increases.

Much attention was paid to the oxidation of Fe^{2+} by apoferritin and some of the work undertaken used recombinant ferritins composed of only one subunit type. This led to the discovery that the catalytic ferroxidase activity of ferritin (i.e. oxidation of Fe^{2+} to Fe^{3+}) was associated with H-chains and not L-chains. Additionally, a metal centre was identified in human H-chain homopolymers that was not found in L-ferritin. Mutational studies indicated that removal of these metal centres could remove ferroxidase activity in H-chains. This opens the question as to what function do L-chains have in ferritin and iron storage, and why have heteropolymers at all? Horse spleen ferritin has a high average percentage of L-chain (85%), it also has a relatively high iron (average 2700 Fe atoms/molecule), yet the L-chain fraction extracted from horse spleen ferritin was found to be devoid of iron (Ishitani and Listowsky, 1975). Despite L-chains being unable to take up a significant amount of iron in vivo themselves as subunits, there is clearly an important function of the L-chain when in heteropolymers.

Human L-chain homopolymers are able to produce iron-cores using Fe^{2+} and this led to the suggestion that L-chains may possess an alternative Fe^{2+} oxidation site (Levi et al., 1992). However, this does not happen as quickly or efficiently as the H-chain homopolymer. H-ferritins, on the other hand, are comparatively poor iron-core-formers

(Levi et al., 1992; Levi et al., 1994). The L-chain iron-cores of homopolymers and native heteropolymers have been found to be more regular and slightly larger than those of the H-chain homopolymers, which has led to the view that L-chains may be more efficient at ferrihydrite nucleation (Wade et al., 1991; Levi et al., 1992). It would thus seem that H-chains are essential for rapid Fe^{2+} oxidation and thus removal of potentially toxic iron. L-chains appear to be efficient in nucleation and iron-core formation, hence provide the iron storage capacity of ferritin. This would explain why tissues that store iron tend to be rich in L-ferritin. It is therefore advantageous for ferritin molecules to be composed of both H and L-subunits because of functional and complimentary differences.

5.1.3 *Liberation of Iron from Ferritin*

Mechanisms by which iron is liberated from ferritin for intracellular use are also poorly understood. Experimentally, iron stored within ferritin can be mobilised by the use of iron chelators such as desferal. This has been demonstrated in perfused rat liver (Baker et al., 1980) and in cultured rat hepatocytes (Laub et al., 1985). In vitro, iron can be readily mobilised from ferritin by small reductants such as ascorbate, cysteine and glutathione, assisted by an Fe^{2+} chelator such as ferrozine (Boyer et al., 1988). A variety of physiological reducing agents have been found to be effective, or at least partially effective in releasing iron from ferritin. Reduced flavins such as riboflavin, $FMNH_2$ and $FADH_2$ were found to be very effective (Sirivech et al., 1974), with superoxide found to be partially effective (see below). Dognin and Crichton (1975) tested in vitro a wide variety of biological reductants for possible mobilisation of iron from ferritin. Some of the more effective reductants included cysteine, ascorbate and glutathione, however all

were very slow compared to reduced flavins and none of these agents has been clearly implicated in iron mobilisation from ferritin in vivo. From experiments performed using liver homogenates (Topham et al., 1989), it was proposed that xanthine and NAD(P)H-dependent ferriductase activity promotes the mobilisation of ferritin iron (and transferrin iron within the endosome) using a reduced flavin nucleotide (FAD or FMN) to apparently shuttle electrons from reduced enzymes to the iron contained within the ferritin molecule (Topham et al, 1989). In rat hepatocytes, iron has been shown to be mobilised as a consequence of the uptake of extracellular ferritin and subsequent degradation by lysosomes (Sibille et al., 1989). Ferritin is known to be degraded in secondary lysosomes and this is usually preceeded by ferritin aggregation and auotphagic engulfment by vacuoles. These vacuoles fuse with secondary lysosomes where ferritin is slowly degraded to a non-specific complex containing iron, partially degraded protein, and lipid (Bridges, 1990; Harrison and Arosio, 1996)). This material is known a haemosiderin and is very prominent in cells heavily loaded with iron. Iron is released by controlled interactions with enzyme generated reducing agents, where presumably it is available to enter the cytosol for intracellular use. However, little is known about the mechanisms by which this occurs (Bridges, 1990).

5.1.4 *Ferritin and Oxidative Iron Mobilisation*

In addition to the iron storage role of ferritin, it has long been considered that ferritins are also able to detoxify iron. This toxicity is mainly related to ability of 'free' iron to induce the formation of ROS, which in turn, causes oxidative damage (Halliwell and Gutteridge, 1999). Whilst stored in ferritin, iron is relatively inert as a promoter of ROS formation,

however it becomes active as a catalyst when it is released by reducing agents. Superoxide, a physiological reductant, is produced intracellularly from a number of different sources including enzymes like peroxidases and xanthine oxidase and by haem proteins as well as through auto-oxidation of various biomolecules (Halliwell and Gutteridge, 1999). UVA radiation of NADH and NADPH also produces superoxide (Czochralska et al., 1984;Cunningham et al., 1985). In 1974, Williams and co-workers reported that superoxide (generated by xanthine/xanthine oxidase) in vitro was capable of mobilising iron from ferritin. Since that report, the list of free radicals and toxicants also capable of releasing iron from ferritin has increased (reviewed by Reif, 1992) and will be briefly discussed. The efficiency of superoxide-dependent iron mobilisation that has been reported has been variable. In general, the release of iron by the xanthine oxidase is around a range of 5%. The amount released has been shown to decrease after repeated cycles of the xanthine/xanthine oxidase reaction (Bolann and Ulvik, 1990). In contrast to the xanthine oxidase method used to induce iron release from ferritin, Reif and colleagues (1988) showed that repeated bursts of superoxide generated radiolytically (using ^{137}Cs γ radiation) could release up to approximately 70% of iron from ferritin. It is not known why the two systems of producing superoxide vary so greatly in the relative efficiency of releasing iron from ferritin, although factors such as size and age of the ferritin iron cores used in these experiments seem to have some bearing on the amount that is released (Bolann and Ulvik, 1990). Despite the small amount of iron release from ferritin using the xanthine oxidase method of producing superoxide, the amount has been shown to be sufficient to promote lipid peroxidation of phospholipid liposomes (Thomas et al., 1985).

The reduction potential of a compound appears to be the primary indicator of the ability of that compound to reductively mobilise iron from ferritin. Toxicant xenobiotics with redox cycling capacities such as paraquat (lung toxicant), adriamycin (heart toxicant) and alloxan (pancreatic toxicant), have high reduction potentials and have been shown to mobilise ferritin iron which, in turn, stimulates lipid peroxidation (Thomas and Aust, 1986; Vile and Winterbourn, 1988; Reif et al., 1989). Iron is mobilised by these xenobiotics either indirectly by the production of superoxide, or directly by the free radical form of these agents. Other mechanisms of iron release from ferritin have also been documented, particularly that of photoreduction. It is well known that some Fe^{3+} complexes can be photoreduced by UV light. Aubailly and colleagues (1991) demonstrated that in vitro UVA (and visible) radiation could photoreduce (thus release) approximately 4% of the ferric ions stored in ferritin. Laulhere and colleagues (1990) also demonstrated iron release from pea seed ferritin using UVA and visible wavelengths. They showed that it was the iron-core that was the site of photoreduction. It has also been demonstrated in vitro that ALA can cause the release of iron from ferritin and concomitantly initiate liposome lipid peroxidation (Oteiza et al, 1995).

5.1.5 *The Objectives of this Study*

Recently, it was demonstrated in this laboratory (Pourzand et al., 1999) that UVA irradiation of cultured primary fibroblasts could result in an increase in the intracellular 'free' iron pool as determined by assays based on IRP/IRE binding, cytoplasmic aconitase activity, and calcein fluorescence. It was proposed that the release of

proteolytic enzymes from UVA-damaged lysosomes resulted in ferritin degradation (measured by immunoprecipitation) and the concomitant immediate release of 'free' iron. Previously, Cairo and colleagues (1995) had also shown intracellular iron release by adding the glutathione-depleting drug Phorone. This was similarly attributed to ferritin degradation.

The objective of our study was to quantitatively determine the level of ferritin after specified treatments using a polyclonal (anti-ferritin) enzyme-linked immunosorbent assay kit known as the Enzymun-Test® Ferritin kit (Roche, UK). The basic principles of this method are depicted in Fig. 5.1. In brief, a cytosolic extract is prepared which is added to a streptavidin tube along with biotinylated anti-ferritin antibodies and peroxidase (POD)-labelled anti-ferritin antibodies (the incubation solution). The antibodies bind to specific ferritin epitopes present on ferritin and the biotin part of the biotinylated antibody binds to streptavidin, thus anchoring the ferritin/antibody complexes to the tube. Excess antibodies are removed by washing them with the substrate-chromogen solution, ABTS® (di-ammonium 2, 2'-azino bis (3-ethylbenzothiazoline-6-sulphonate), is added. ABTS® is a peroxidase substrate and is cleaved by the peroxidase to produce a characteristic green coloured product, which is measured spectrophotometrically. This is intended to provide a quantitative determination of ferritin present in the sample extract.

Fig. 5.1. Enzyme-immunoassay for the quantitative determination of ferritin in vitro (Source: Enzymun-Test® Ferritin fact sheet provided with the kit)

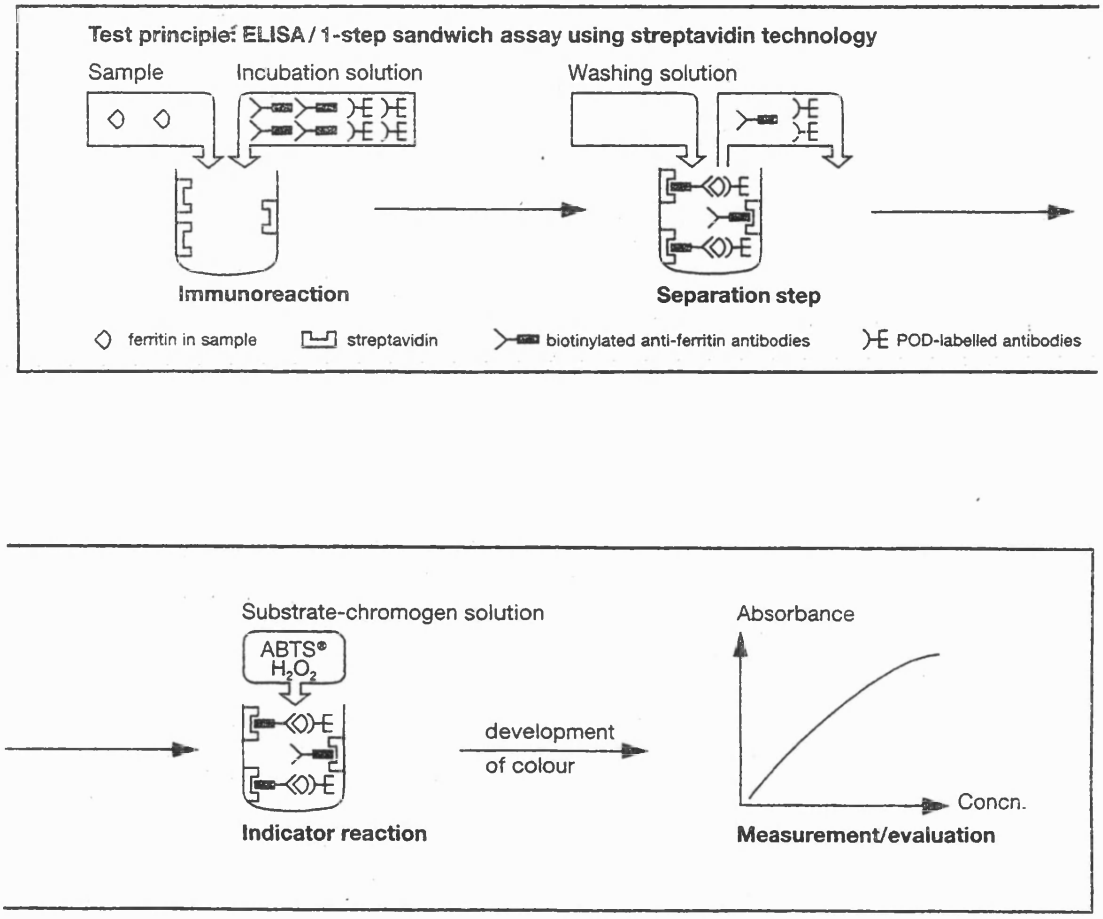

It was the intention of our study to determine ferritin content in FEK4 primary human skin fibroblasts and HaCaT human immortalised epidermal keratinocytes after UVA irradiation. Previous unpublished data, using the cytoplasmic aconitase assay (see Chapter 3), suggests that there is a large increase in detectable iron levels after ALA treatment followed by UVA irradiation. It has been previously reported that PPIX can localise within lysosomal membranes (Morliere et al., 1987) and also within horse ferritin

(Precigoux et al., 1994; Michaux et al., 1996; Crichton et al., 1997). PPIX is known to be a potent photosensitiser (see Chapter 2). Using the enzyme-immunoassay kit, the hypothesis that ALA treatment followed by UVA irradiation could cause ferritin degradation in FEK4 cells was tested. In turn, ferritin degradation would result in the concomitant release of iron release in these cells. This may occur by either rupturing lysosomal membranes allowing proteolytic enzymes to spill into the cytosol, in turn degrading ferritin, or by PPIX causing direct damage to the ferritin shell itself.

5.2 Methods

5.2.1 *Cell Culture*

The primary human fibroblast cell line, FEK4, and the immortalised human keratinocyte cell line, HaCaT, were cultured as described in sections 2.2.2 and 3.2.1 respectively.

5.2.2 *Chemical Treatment and Irradiation Conditions*

FEK4 cells were treated ALA as described in section 2.2.3. Positive controls for the modulation of ferritin levels were prepared for both FEK4 and HaCaT cells. Solutions of 50 μM haemin or 100 μM desferal (Ciba Geigy, Switzerland) were prepared using the appropriate conditioned cell culture media. These solutions were added back to the cells, which were incubated for 18 h at 37°C. Preparation and irradiation conditions of both FEK4 and HaCaT cells are described in section 2.2.6.

5.2.3 *Preparation of Cytoplasmic Extracts for Ferritin Analysis*

Immediately after treatment, plates were placed on ice. Media was removed and cells were washed with ice-cold PBS. Ice-cold PBS containing 1 mM EDTA (Merck, UK) and the protease inhibitors Pefabloc® at a concentration of 50 μg/ml (Roche, UK), chymostatin at a concentration of 50 μg/ml (Roche, UK), and leupeptin at a concentration of 20 μg/ml(Roche, UK), was added and cells were scraped using a rubber policeman. Cells were collected and centrifuged at 4°C for 5 min at 1500 rpm. The supernatant was removed and cells re-suspended in 1 ml of the fresh ice-cold buffer containing the protease inhibitors. Cells were counted and centrifuged as before. The supernatent was aspirated and the cells were re-suspended in ice-cold (1x) Munroe lysis buffer containing

10 mM Hepes (pH 7.5), 3 mM $MgCl_2$, 40 mM KCl and 5% glycerol. The buffer also contained 50 μg/ml Pefabloc®, 50 μg/ml chymostatin, 20 μg/ml leupeptin, 0.3% Nonidet P-40 (Merck, UK), and 1 mM phenylmethlsulphonylfluoride (PMSF) (Sigma, UK). These were added to the lysis buffer just before use. Cell pellets were re-suspended and lysed on ice, using 250 μl per 1 x 10^7 cells of the buffer. Lysates were centrifuged at 4°C for 7 min at 2500 rpm. The cell extract (supernatent) was removed and placed in a 1.5 ml tube then flash frozen in a dry ice/95% ethanol mixture. Extracts were stored at -70°C.

5.2.4 *Determination of Ferritin Content in Cell Extracts*

Cell extracts were prepared for the measurement of ferritin content using a polyclonal enzyme-linked immunosorbent assay (ELISA) known as the Enzymun-Test® Ferritin Kit (Roche, UK). All components of this kit were brought to room temperature before use. The extracts were thawed and protein concentration was determined using the method described by Bradford (1976) with the BioRad reagent kit (UK). Bovine serum albumin (BSA) was used for calibration and absorption measurements were obtained using a microplate reader at 595 nm. Ferritin standards and cell extracts, to be measured, were added to separate streptavidin-coated tubes. Incubation buffer (containing the anti-ferritin antibodies) was added to each tube and incubated at room temperature for 30 min. The tube contents were aspirated, washing solution was added, then the tubes were incubated for a further 30 min. The washing solution was aspirated then the chromogen-substrate solution was added to each tube. The tubes were incubated for 15 min at room temperature and the absorbance was determined immediately at 420 nm using a spectrophotometer. The concentration of ferritin protein in each extract was determined

against the ferritin standards. This value was then normalised using total protein content obtained from the Bradford assay and expressed as nanograms (ng) of ferritin per milligrams (mg) of protein.

5.2.5 *Statistical Analysis*

Results are expressed as the mean ± one standard deviation. Significant differences ($p<0.05$) were determined by an unpaired *t* test.

5.3 Results

5.3.1 *Effects of either UVA Irradiation, Haemin, or Desferal Treatment on the Ferritin Content of the HaCaT Immortalised Human Keratinocytes*

The ferritin content of HaCaT keratinocytes, in response to graded doses of UVA radiation, is shown in Table 5.1. Immediately after irradiation, cell extracts were prepared for the measurement of cytosolic ferritin content using a polyclonal enzyme linked immunosorbent assay (ELISA) kit (see section 5.2.3). After 100 kJ/m^2 UVA there was approximately a 1.25-fold increase in the ferritin content. Increasing the dose of UVA led to a drop in the ferritin content. After 250 kJ/m^2 UVA the ferritin level was not significantly different to that of the control. After 500 kJ/m^2 UVA the ferritin level appeared to drop slightly below that of the control (5-10%), though this was, again, not significant. Positive controls, desferal and haemin, were used to test the efficacy of the ELISA kit (Table 5.1). Incubation of HaCaT cells with the iron chelator desferal (18 h, 100 μM) resulted in a 5–6-fold decrease in ferritin compared to control levels. Incubation with haemin (18 h, 50 μM), on the other hand, resulted in a 10–11-fold-increase in ferritin.

Fig.5.1. Effect of various treatments on the ferritin content of HaCaT cells. Ferritin levels were measured using an enzyme-linked polyclonal immunosorbent assay kit. Data represent the mean of 4-6 independent experiments (± S.D.).

Treatment	Ferritin Content (ng mg protein^{-1})
Non-irradiated	26.45 ± 2.082
100 kJ/m^2 UVA	32.96 ± 1.357*
250 kJ/m^2 UVA	27.2 ± 0.989
500 kJ/m^2 UVA	24.715 ± 1.414
18 h Desferal (100 μM)	4.682 ± 0.350*
18 h Haemin (50 μM)	278.8 ± 7.636*

Statistical analyses were made using an unpaired *t* test. *, Significantly different from non-irradiated control (p , 0.05 level).

5.3.2 *Effects of either UVA Irradiation, Haemin, or Desferal Treatment on the Ferritin Content of the FEK4 Primary Human Fibroblasts*

Table 5.2 shows the effect of graded doses of UVA radiation on the ferritin content of the FEK4 fibroblasts. After irradiation with a UVA dose of 100 kJ/m^2, the level of ferritin appears to rise to almost 1.2-fold above that of the control level. The ferritin level appears to peak around 250 kJ/m^2, approximately 1.4-fold above the control. After a UVA dose of 500 kJ/m^2, the ferritin content had dropped to approximately 1.5-fold below that of the control level. The significance of this result, and how it compares with data from immunoprecipitation studies of ferritin after the same treatment (Pourzand et al., 1999), is detailed in the discussion of this chapter. Positive controls, desferal and haemin, were also used for FEK4 (Table 5.2). Incubation with desferal for 18 h (100 μM) resulted in approximately a 5-fold decrease in ferritin compared to control levels. Haemin treatment (50 μM, 18 h) resulted in approximately a 6-fold increase in ferritin levels. Compared to the HaCaT cells (Table 5.1), FEK4 possess a 3.5–4-fold higher basal content of ferritin.

Fig.5.2. Ferritin content in FEK4 cells after various treatments measured using an enzyme-linked polyclonal immunosorbent assay kit. Data represent the mean of 4-6 independent experiments (± S.D.).

Treatment	Ferritin Content (ng mg protein^{-1})
Non-irradiated	99.828 ± 7.63
100 kJ/m^2 UVA	117.95 ± 7.141*
250 kJ/m^2 UVA	140.69 ± 22.641*
500 kJ/m^2 UVA	65.646 ± 1.578*
18 h Desferal (100 μM)	19.605 ± 2.623*
18 h Haemin (50 μM)	572.43 ± 13.534*

Statistical analyses were made using an unpaired *t* test. *, Significantly different from non-irradiated control (p , 0.05 level).

5.3.3 *Effects of ALA Incubation and UVA Irradiation on the Ferritin Content of the FEK4 Primary Human Fibroblasts*

Table 5.3 shows the effects of ALA treatment (4 and 18 hours) and UVA irradiation on the ferritin content of the FEK4 fibroblasts. Treatment of cells with 100 or 200 μM ALA for 4 h resulted in a decrease in intracellular ferritin content of 1.035- and 1.25-fold respectively, compared to the non-treated control. When these ALA-treated cells were irradiated with UVA, increases of 3 – 3.5-fold in ferritin content were detected compared to the non-irradiated controls (Table 5.3). After irradiation, ferritin levels were higher in the 100 μM ALA treated sample compared to those of the 200 μM treatment (Table 5.3).

Treatment of cells with ALA for 18 h resulted in a decrease in ferritin content of approximately 2.5 – 3-fold, with both 100 and 200 μM concentrations (the effect was not significantly different comparing the two concentrations). Irradiation of these ALA-treated cells led to increases in ferritin levels compared to the non-irradiated controls. The irradiated 100 μM and 200 μM ALA treated populations showed approximate increases in detectable ferritin over the non-irradiated controls of 1.2 – 1.4-fold and 1.6 – 1.7-fold respectively. Comparison of the 50 kJ/m^2 and 100 kJ/m^2 UVA doses, shows there is no significant difference between the two, after incubation with either 100 or 200 μM ALA.

Fig.5.3. Ferritin content in FEK4 cells treatments with ALA then exposed to UVA radiation. Ferritin content was measured using an enzyme-linked polyclonal immunosorbent assay kit. Data represent the mean of 4-6 independent experiments (± S.D.).

ALA Treatment	Ferritin Content (ng mg protein^{-1})
Non ALA-treated/non-irradiated	99.828 ± 7.63
4 h 100 μM non-irradiated	96.475 ± 8.308
4 h 100 μM 50 kJ/m^2 UVA	313 ± 18.129*
4 h 100 μM 100 kJ/m^2 UVA	307.2 ± 14.119*
4 h 200 μM non-irradiated	78.685 ± 4.546
4 h 200 μM 50 kJ/m^2 UVA	274.1 ± 24.748*
4 h 200 μM 100 kJ/m^2 UVA	232.75 ± 19.771*
18 h 100 μM non-irradiated	36.355 ± 5.154
18 h 100 μM 50 kJ/m^2 UVA	46.11 ± 1.569*
18 h 100 μM 100 kJ/m^2 UVA	48.91 ± 3.493*
18 h 200 μM non-irradiated	33.68 ± 1.244
18 h 200 μM 50 kJ/m^2 UVA	55.49 ± 2.135*
18 h 200 μM 100 kJ/m^2 UVA	54.1 ± 3.818*

Statistical analyses were made using an unpaired *t* test. *, Significantly different from non-irradiated control (p , 0.05 level).

5.4 Discussion

The basis of this study was the data produced in this laboratory by Pourzand and colleagues (1999) who demonstrated that UVA treatment of FEK4 fibroblasts resulted in an increase in the intracellular 'free' iron pool. One of the possible sources of this iron was postulated to be ferritin. In the Pourzand et al. study it was shown using immunoprecipitation that ferritin degradation occurred and that the level of degradation was a function of UVA dose. At least some of this degradation appeared to be a result of the release of proteolytic enzymes from lysosomes whose membranes had been damaged by UVA radiation. Quantification of ferritin degradation is difficult using immunoprecipitation, so the purpose of this study was to quantify this apparent ferritin degradation in FEK4 fibroblasts using a polyclonal enzyme–linked immunosorbent assay kit (Roche, UK). This method was also used to assess ferritin content in FEK4 fibroblasts treated with ALA and UVA radiation, and in HaCaT immortalised human keratinocytes exposed to UVA radiation.

Analysis of the basal ferritin content of FEK4 fibroblasts and HaCaT keratinocytes (Tables 5.1 and 5.2) reveals that the basal content of ferritin in FEK4 cells is approximately 3.5 – 4-fold that of HaCaT cells. This is in contrast to previous results with primary fibroblasts and primary keratinocytes. Applegate and co-workers (1995) showed that ferritin levels were 2 – 3-fold higher in keratinocytes compared with matching fibroblasts (i.e. from the same biopsy). The difference between these two studies was that our study involved a comparison of a primary fibroblast cell line, FEK4, with the fast growing immortalised keratinocyte cell line, HaCaT. Primary keratinocytes

grow slower than primary fibroblast cell lines. Recently it has been observed (C. Pourzand, unpublished data, this laboratory) that HaCaT cells possess little or no detectable L-ferritin as measured by immunoprecipitation. Detection of the ferritin that was present (i.e. H-ferritin) was difficult to detect because of the low levels.

In previous chapters, it has been reported that irradiation of FEK4, and to a lesser extent HaCaT cells, results in an increase in the intracellular 'free' iron pool. Quantification of ferritin content in HaCaT cells, in response to UVA radiation (Table 5.1), suggests that UVA has little or no effect on the ferritin content of these cells. With a dose of 100 kJ/m^2 UVA, there appears to be an increase in ferritin levels of approximately 1.25-fold. Doses above 100 kJ/m^2 result in a decrease in ferritin levels to just below the control level (after 500 kJ/m^2 UVA), but this is not significant. In HaCaT cells, the response observed in ferritin levels as a result of UVA-irradiation is not significant.

When FEK4 cells were irradiated with graded doses of UVA, an apparent increase in the level of ferritin (Table 5.2) was observed up to a dose of 250 kJ/m^2, where it peaks at approximately 1.4-fold above that of the control level. Between 250 and 500 kJ/m^2 UVA the level of ferritin decreases. After 500 kJ/m^2 UVA the ferritin level is approximately 1.5-fold below that of the control. This would appear to contradict the result seen with the UVA-mediated degradation of ferritin as measured using immunoprecipitation (Pourzand et al., 1999). In the study by Pourzand et al. (1999) it was shown that UVA irradiation resulted in degradation of ferritin in a dose-dependent manner. However, ferritin levels measured in both our study and the study by Pourzand et al. (1999)

employed cell extracts that were prepared immediately after irradiation (and both used a mouse polyclonal antibody to detect ferritin). This means that it is unlikely that the cell is capable of synthesising new ferritin. The reason and the significance of the different responses observed using the two methods may be explained. For analysis of ferritin using immunoprecipitation, cell extracts are subjected to a number of freeze-thaw cycles to dissociate (radioactively labelled) ferritin into its H and L subunits. The purpose of this procedure is so that H- and L-ferritin subunits are seen as discrete bands (21,000 and 19,000 Da respectively) when run on a Western gel, as revealed by autoradiography. UVA-induced degradation of these subunits results in the disappearance of these distinct bands, presumably because the degradation products are random and varied so that discrete bands are not formed when run on a gel. The ferritin assay (ELISA kit method), on the other hand, does not employ the deliberate dissociation of ferritin into its subunits. This, in part, may explain why an increase in the apparent level of ferritin (in FEK4 cells) is observed after UVA irradiation using the ferritin assay. Allen and colleagues (1997 and 1999) have documented, using an anti-ferritin mouse polyclonal antibody and atomic force microscopy, that ferritin possesses many antibody-antigen binding sites, i.e. it is polyepitopic. We believe that the some of the apparent increases observed in ferritin levels after UVA irradiation, measured using the ferritin assay, may occur as a result of fragmentation of the ferritin molecule into its subunits. Some of the increases may also be due to degradation of subunits, which in turn, might liberate more detectable epitopes. After a dose of 500 kJ/m^2 UVA, the level of ferritin that can be measured by the ferritin assay drops to below that of the control (Table 5.2). This presumably occurs because so

much damage has occurred to the protein that, either fragments are produced that contain one epitope or less, or the epitopes are no longer recognisable by the antibody.

To directly compare data from immunoprecipitation and the ferritin assay, the extracts prepared for the ferritin assay would have to be subjected to freeze thaw cycles to dissociate the subunits before analysis. This would remove any apparent increases in ferritin levels measured due to the ferritin molecule breaking up into its subunits as function of UVA radiation. Any changes in ferritin levels detected after this procedure must be due to changes other than subunit dissociation. Changes in ferritin levels that are then observed after UVA irradiation, as measured using the ferritin assay, could be interpreted in one of two ways. If the levels of ferritin decrease after UVA treatment, this might be interpreted as degradation of the ferritin subunits. This would be convenient as quantitative measurements of ferritin subunits could be made, which could be compared with the immunoprecipitation data. The results would have to be expressed as ng of ferritin subunits per mg of protein rather then ng of ferritin per mg protein (as the ferritin kit specifies). On the other hand, if the apparent level of ferritin increases after UVA treatment, it is possible that degradation of ferritin subunits is occurring, but is liberating more detectable epitopes in the process (or more fragments that contain two or more epitopes). The quantitative measurement under this scenario would have to be defined as number of ferritin epitopes recognised per mg of protein. One very important point does need to be addressed however, and that is certain experimental treatments might cause ferritin damage that results in subunits to dissociate from the ferritin molecule. This would probably induce iron release, as iron-cores may be exposed to the cytosol (and

thus a reducing environment), but may not necessarily require significant damage to the subunits, just breaking of intermolecular bonds. Therefore, iron release from ferritin could occur, but a method that involves dissociating subunits in order to analyse them (i.e. immunoprecipitation) would not detect this form of damage, which in turn could prevent the identification of ferritin as the source of iron release. Under such circumstances, dissociating ferritin into its subunits for analysis would be inappropriate and exemplifies one advantage the ferritin assay may have over immunoprecipitation (if freeze-thaw cycles are not used).

One option may be to perform both assays as originally described i.e. dissociation of subunits with immunoprecipitation, but not with the ferritin assay. If a reduction in ferritin subunits is observed after immunoprecipitation, then an increase observed in the ferritin assay would indicate that subunits are being degraded, but are exposing more epitopes in the process (or more fragments with two or more epitopes). Under this circumstance, a quantitative measurement could be made with the ferritin assay, but would have to be expressed in arbitrary units as the number of epitopes recognised by the anti-ferritin antibody per mg of protein, which otherwise, may not reflect the true level of ferritin. This emphasises the importance of using both techniques, as without the knowledge of the degradation of ferritin, as observed with immunoprecipitation, an incorrect interpretation may be made of results obtained using the ferritin kit. Alternatively, the ferritin assay may measure increases in ferritin levels that occur through the production of more protein e.g. by haemin treatment (Table 5.2). Again, this could be confirmed by performing immunoprecipitation ferritin. The hypothesis that

treatment causes fragmentation of ferritin and the increased recognition of epitopes, could be an explanation for the increased ferritin levels observed in HaCaT cells after UVA irradiation. Because there is a much lower basal level of ferritin in the HaCaT cells, the response to UVA was less than that with the FEK4 cells.

Desferal (an iron chelator), and haemin (ferric haem) treatments were used in this study as controls to show modulation of ferritin levels. HaCaT and FEK4 cells showed a 5 – 6- and 5-fold reduction in the ferritin level respectively in response to desferal treatment (100μM, 18 h), and 10-11- and 5 – 6-fold increase respectively in response to haemin treatment (50 μM, 18 h). The desferal treatment and resultant ferritin down-regulation indicates iron starvation within the cell and the apparent lack of need for iron storage, as expected. After the haemin treatment, on the other hand, the large up-regulation of ferritin protein suggests a protective response by the cell that enables the cell to sequester and store the potentially hazardous influx of iron absorbed in the form of haemin.

Treatment of FEK4 cells with ALA for 4 and 18 hours resulted in a decrease in ferritin levels, as measured using the ferritin assay (Table 5.3). The effect observed was much greater for the longer incubation time (see below). This decrease in ferritin levels would appear to occur as a result of the iron chelator properties ALA-induced PPIX. The penultimate step of haem biosynthesis is catalysed by the enzyme ferrochelatase. This event involves insertion of iron into the tetrapyrrole ring of PPIX producing haem and effectively chelating iron at the same time. The reduction in ferritin content by ALA would suggest that iron could be mobilised from ferritin to produce haem. Cells treated

with ALA show reductions in the 'free' iron pool and aconitase activity, supporting the hypothesis that ALA-induced PPIX can function as an iron chelator (see Chapters 4 and 2 respectively).

Irradiation of ALA-treated cells with UVA resulted in an increase in the detectable number of ferritin epitopes (Table 5.3). Irradiation of cells after 4 h ALA incubation caused a huge increase in the detectable number of ferritin epitopes (between 3 – 3.5-fold above that of the non-irradiated control). This increase far exceeded that observed by UVA alone, suggesting that ALA treatment, followed by UVA irradiation may be more effective in damaging ferritin and act by a different mechanism. The fold increase in the number of ferritin epitopes measured after 4 h, 100 and 200 μM ALA treatment, are comparable after UVA irradiation. However, the number of epitopes detected after the 200 μM treatment, followed by irradiation, is lower compared with that of the 100 μM ALA treatment. This is consistent with the observation that the higher ALA concentration results in greater ferritin depletion. The number of epitopes detected after 4 h ALA treatment appeared to go down after the larger dose of 100 kJ/m^2 UVA compared to the $50kJ/m^2$ dose. This would suggest that the degree of damage caused to the ferritin is more severe.

After incubation of cells with ALA for 18 h (100 and 200 μM), the ferritin content of FEK4 cells had decreased by 2.5 – 3-fold below that of the control level (Table 5.3). This was a much greater decrease than that observed after treatment with ALA for 4 h. Cells that were treated with ALA for 18 h followed by irradiation showed an apparent

increase in ferritin levels as observed for the 4 h treatment, but the fold increases in the number of ferritin epitopes detected were much lower. The fold increases after irradiation, compared to non-irradiated controls, ranged from 1.2 – 1.7-fold depending on the concentration of ALA treatment and the dose of UVA administered (Table 5.3). This low level of ferritin modulation is consistent with the level of ferritin originally present.

The results presented in this study that involved treatment of cells with ALA and UVA would appear to support the hypothesis that ALA-induced PPIX can exacerbate degradation of ferritin by virtue of a photosensitisation mechanism. Whether this degradation process occurs as a result of proteolytic enzymes from damage to lysosomes, as proposed by Pourzand and colleagues (1999), or whether it is due to direct photosensitisation of the ferritin molecule by PPIX, is not clear from this study. As mentioned in the introduction, PPIX has been shown to locate within ferritin (Precigoux et al., 1994; Michaux et al., 1996). If PPIX located within the ferritin molecule is exposed to UVA during irradiation, this could result in direct photosensitised damage to the ferritin protein shell. Clarifying the precise mechanisms involved may be difficult. PPIX added to cells and then irradiated has been shown to damage lysosomes and result in the spillage of proteolytic enzymes into the cytosol (Morliere et al, 1987). Thus, it would seem reasonable to expect proteolytic enzyme spillage from lysosomes (as a result of ALA treatment and UVA irradiation) to be responsible for at least some ferritin degradation. However, if PPIX is located within the ferritin molecule and is able to cause direct photosensitised damage, then this would probably occur before any protease could

reach the ferritin molecule. The action of proteases may be a secondary event, but would still be important.

In conclusion, this study supports the hypothesis that UVA irradiation of human cells results in damage to the ferritin protein. This, in turn, causes an increase in the 'free' iron pool. Treatment of cells with ALA reduces the basal level of ferritin. UVA irradiation of these ALA-treated cells would appear, under the appropriate conditions, to exacerbate damage caused to ferritin.

6. Conclusions and Future Work

This project was divided into two areas. One was to determine the importance of PPIX as an intracellular chromophore in UVA-mediated damage and a second to establish a clearer understanding of the fate of intracellular iron after UVA irradiation. The latter part of the project was investigated using three techniques. These included the direct measurement of intracellular iron by the flow cytometry-based iron assay, indirect measurement of intracellular iron by the cytoplasmic aconitase assay, and measurement of the iron storage protein ferritin as measured by the ferritin assay.

One of the main purposes of this project was to test the hypothesis that the basal content of PPIX may be critical in the UVA-mediated inactivation of human cells. To examine this, PPIX levels were modulated in the human lymphoblastoid cell line, TK6, and the primary human fibroblast cell line, FEK4, by incubation with ALA for 4 and 18 hours. At known intracellular PPIX concentrations (measured by spectrofluorimetry), cells were irradiated with graded doses of UVA radiation to produce dose response curves. The slope of each dose response curve provides the rate of inactivation of a cell population at each particular intracellular PPIX concentration. By examining the relationship between inactivation rate constants at different intracellular PPIX concentrations, an estimate of the basal content of PPIX necessary to lead to significant cell death following UVA irradiation was made (see Chapter 2). From this study it was deduced that the basal content of PPIX in TK6 cells was insufficient to make a significant contribution to UVA-mediated inactivation. In contrast, the basal content of FEK4 cells appears to be critical in the UVA-mediated inactivation of these cells. PPIX therefore, may be an important

UVA absorbing chromophore responsible for inactivation of certain cell types, but not others. This theory would have to be tested further by performing similar studies on other cell lines such as keratinocytes. Other information derived from this study was that the MTS reagent-based assay is an unsuitable method for determining viability after treatment with ALA as we have documented a reaction between the MTS tetrazolium salt with ALA producing a coloured formazan product (Fig. 2.10)

The results measuring the different parameters of intracellular iron including aconitase activity, free iron levels and ferritin levels, all showed that FEK4 cells possess greater intracellular iron levels and ferritin levels than HaCaT cells. It has been observed that HaCaT cells only possess H-ferritin (C. Pourzand, unpublished observation, this laboratory). A recent publication showed that the level of H-ferritin, which possesses ferroxidase activity, appears to have an inverse relationship with the level of intracellular free iron (Beaumont et al., 1999). This may suggest why low free iron levels are observed in HaCaT cells. The lower levels of as membrane damage measured by flow cytometry and calcein fluorescence could be a reflection of the fact that, after UVA irradiation, as lower basal 'free' iron concentration and iron release in HaCaT cells could limit the degree of lipid peroxidation and membrane damage observed in these cells (Fig.4.6). A future study in this area would be to determine whether a correlation exists between intracellular 'free' iron levels of different cell types, and UVA-induced membrane damage. Other factors also need to be considered such as intracellular antioxidant concentration, as this can vary and may affect the results obtained in such a study (Leccia et al., 1998).

UVA irradiation of the two cell lines FEK4 and HaCaT generally resulted in similar trends in the responses measured by the cytoplasmic aconitase assay, the iron assay, and the ferritin assay. The difference between the two cell lines was mainly that the response observed by the FEK4 cells was much greater, in all respects, compared to the HaCaT cells. The results did not provide conclusive evidence that there was a change in ferritin levels of HaCaT cells after UVA irradiation, as measured by ferritin assay.

Treatment of FEK4 cells with ALA reduced the 'free' iron pool as measured by aconitase activity, the iron assay and the ferritin assay. Irradiation of ALA-treated cells produced some very significant results using these three assays. There was a huge increase measured by aconitase activity, much larger than UVA alone (see Chapter 3). Using the ferritin assay, as described herein, there appeared to be fragmentation of ferritin (see below and Chapter 5), but on a considerably greater scale than UVA irradiation alone. The iron assay showed increases in chelatable iron after less severe treatments with ALA and UVA. Treatment of cells with higher ALA concentrations and UVA doses resulted in comparatively lower levels of measurable chelatable 'free' of iron (accompanied by greater increases in membrane damage) and in some cases these levels were below control levels (Chapter 4 and see below). Taking the results together, we speculate that ALA treatment of cells followed by UVA irradiation results in severe damage to ferritin and other cellular targets. This, in turn, results in a huge release of intracellular iron, which is detected by the decrease in binding activity of the IRP and concomitant increase in cytoplasmic aconitase activity. However, the level of damage can be so severe (with the more detrimental experimental conditions) that the cell membrane is damaged

allowing the leakage of cytosolic components including iron and iron bound to CA. This is evident by the damage to the plasma membrane and the drop in iron levels, as measured by the flow cytometry-based iron assay (Chapter 4). The reason why the aconitase activity does not also drop after the more severe treatments that result in loss of iron from the cell is not clear. It is possible that the way the assay is designed does not allow enough time for the IRP to respond to the loss of iron from the cells. Alternatively, there may an additional source of iron such as 'free' haem or another form of iron that is released into the cytosol after treatment that might be recognised by the IRP but not bound by calcein. It is possible that the IRP is responding to forms of iron in the cell that the iron assay cannot detect and that this causes this large change in response in aconitase activity after treatment of cells with ALA followed by UVA irradiation. Future work in this area may lead to the identification of a form of iron that is liberated after oxidative stress and is recognised by the IRP, but not detected by the iron assay.

Concerning the effects of UVA irradiation on the modulation of cytoplasmic aconitase activity of the two cell lines, FEK4 fibroblasts, and HaCaT keratinocytes (Chapter 3), it was observed that these results sharply contrast with those documented in another study that measured the effect of UVA irradiation on the cytoplasmic aconitase activity of NCTC 2544 cultured human keratinocytes (Giordani et al., 1998). The cytoplasmic aconitase activity in the study by Giordani et al. (1998) showed a dose-dependent decrease after UVA irradiation. In contrast to this, both of the cell lines used in our study showed an increase in cytoplasmic aconitase activity up to 250 kJ/m^2 UVA irradiation. Between 250 and 500 kJ/m^2 UVA the aconitase activity decreased. The UVA source

used in our experiments doe not emit the UVA II (320-340 nm) part of the UV spectrum (fig. 2.3), which could be crucial in explaining the differences between the results obtained in our study and the results obtained by Giordani et al. (1998) as the UVA source used by Giordani et al. (1998) emitted the more powerful UVA II wavelengths. Future studies in this area should focus on more discrete wavelength bands of UV radiation and their application to cultured cells to determine if the affect of UV on aconitase activity is wavelength dependent. Similar studies using the flow cytometry-based iron assay should also be run in parallel to confirm if iron release is induced.

The polyclonal (anti-ferritin) enzyme-linked immunosorbent assay (the ferritin assay) was originally employed to quantify ferritin levels after UVA irradiation because quantification of ferritin using immunoprecipitation is difficult. Using immunoprecipitation Pourzand et al. (1999) showed that ferritin was degraded by UVA irradiation in a dose-dependent manner. We have shown using the ferritin assay that an apparent increase in the level of ferritin occurs after UVA irradiation. The significance and explanation for this (see Chapter 5 for detailed discussion) is that the ferritin protein is polyepitopic and when exposed to UVA radiation degradation occurs resulting in the exposure of more epitopes. This appears as an increase in ferritin protein as measured by the ferritin assay.

It is clear that both immunoprecipitation and the ferritin assay need to be employed to assess ferritin status. The ferritin assay can provide a quantifiable method of determining ferritin levels, however, the method of expressing the result may need to be modified

depending on the treatment applied to the cells. For example, the kit specifies that measurements made using this method should be expressed as ng of ferritin per mg protein, which is acceptable if treatments that induce the production of ferritin (such as haemin treatment) are used. However, treatments that result in the degradation of ferritin (which should be initially investigated using immunoprecipitation) should be expressed as number of epitopes recognised per mg of protein. This may go up initially as the protein is degraded (and more epitopes are exposed), but may also decrease if treatment results in the destruction of epitopes or the degradation and production of fragments containing one or no epitopes. Future studies in this area, using the ferritin assay, should ideally concentrate on the initial elucidation of what increase in epitopes measured is contributed by dissociation of ferritin into its subunits, and what increase in epitopes measured is contributed by the degradation of subunits into smaller fragments. This can be done by freeze-thawing extracts, which dissociates ferritin into its subunits. The purpose of this step would be to determine what level of dissociation of subunits is induced by a particular treatment before subunits are themselves degraded. This may provide information on the release of iron from ferritin that is induced by subunit dissociation, but that is not detected by immunoprecipitation.

The mechanisms that result in such large increases in ferritin epitopes as measured by the ferritin assay after treatment of cells with ALA followed by UVA irradiation should be investigated. It would appear that damage caused to ferritin by UVA irradiation of cells with altered PPIX levels does not occur in an identical way to that in cells that are treated with UVA alone. Release of proteolytic enzymes into the cytosol from cells with UVA-

damaged lysosomes has been demonstrated by Pourzand et al. (1999) which were proposed to be responsible for the degradation of ferritin. Release of these proteolytic enzymes should be investigated after treatment of cells with ALA and UVA irradiation in order to determine if there is any difference after this treatment, compared with treatment of cells with UVA alone. If a large increase in the release of these enzymes was observed, this may be correlated with the damage observed to ferritin after such a treatment. If, however, such an increase was not observed after ALA treatment and UVA irradiation, then it would appear that the increase in epitopes observed using the ferritin assay would be attributable to an alternative mechanism, possibly by direct photosensitised damage of the ferritin molecule by PPIX.

The iron assay, detailed in Chapter 4, represents the development of a method that can measure both intracellular chelatable iron and membrane damage in the same assay system based on the fluorescence measurements of calcein by flow cytometry. The method is not complete, as a procedure of evaluating CA bound iron loss through damaged membranes needs to be established because the flow cytometer is only capable of measuring intracellular fluorescence. This procedure would probably involve the use of a technique such as the calcein assay (Epsztejn et al., 1997), which uses spectrofluorimetry to obtain fluorescence measurements. As described in Chapter 4, the iron assay has been used to estimate values of the chelatable iron pool. There is however, a more accurate process of obtaining the intracellular 'free' iron concentration that could be employed in this system. This more accurate method also includes the determination of chelatable iron that is not bound to CA. Previously Epsztejn et al. (1997) have

described this method for the calcein assay. To obtain the total chelatable 'free' iron concentration using our system, some additional measurements are required. The total intracellular CA concentration needs to be determined by calibrating the cell system with known concentrations of CA. The concentration of iron bound to calcein, [CA-Fe], is also needed. This is obtained by the measuring the change in fluorescence evoked by adding the fast permeating iron chelator, SIH, which is then translated into a CA concentration using the CA calibration. CA binds Fe stoichiometrically (1:1) so this reveals the concentration of Fe bound to CA. The 'free' cell iron concentration [Fe^{2+}] that is not bound to CA, but is chelatable, can be derived from experimentally determined values of CA-Fe^{2+} dissociation constant (K_d) in the particular cell lines used. The K_d is obtained by titrating CA-loaded cells with Fe^{2+} (i.e. FAS) and measuring the concomitant fluorescence changes. The [Fe] value is calculated from application of the mass law equation using the experimentally derived K_d value of [CA-Fe], the [CA-Fe] value and the intracellular CA concentration:

$$K_d = [CA]\cdot[Fe]/[CA\text{-}Fe]$$

The total intracellular chelatable 'free' iron is defined as the sum of [CA- Fe] and [Fe]. Derivation of this value is the next step in the development and refinement of the iron assay.

In conclusion, we provide evidence in this study to implicate PPIX as an important UVA absorbing chromophore that may be crucial in the UVA-mediated inactivation of certain cell types. We also document the development of a flow-cytometry-based fluorescence

assay system that is capable of determining membrane damage and intracellular 'free' iron levels. Using this system and also measuring cytoplasmic aconitase activity, we show that UVA radiation induces an increase in intracellular 'free' iron levels which is augmented by ALA treatment prior to irradiation. We also show using the ferritin assay that UVA irradiation results in the degradation of the iron storage protein ferritin (which is also augmented by ALA pre-treatment), providing evidence that ferritin is a major source of iron release after such treatment.

7. References

Allen, S., Xinyong, C., Davies, J., Davies, M.C., Dawkes, A.C., Edwards, J.C., Roberts, C.J., Sefton, J., Tendler, S.J.B., Williams, P.M. (1997) Detection of antigen-antibody binding events with the atomic force microscope. Biochemistry, 36, 7457-7463.

Allen, S, Davies, J, Davies, M.C., Dawkes, A.C., Roberts, C.J., Tendler, S.J.B., Williams, P.M. (1999) The influence of epitope availability on atomic-force microscopy studies of antigen-antibody interactions. Biochem. J., 341, 173-178.

Amstad, P., Peskin, A., Shah, G., Mirault, M.E., Moret, R., Zbinden, I., Cerutti, P. (1991) The balance between Cu,Zn-superoxide dismutase and catalase affects the sensitivity of mouse epidermal cells to oxidative stress. Biochemistry, 30(38), 9305-13.

Andley, U.P., Clark, B.A. (1989) The effects of near-UV radiation on human lens β-crystallins: protein structural changes and the production of O_2^- and H_2O_2. Photochem. Photobiol., 50(1), 97-105.

Applegate, L.A., Luscher, P., Tyrrell, R.M. (1991) Induction of heme oxygenase: a general response to oxidant stress in cultured mammalian cells. Cancer Res., 51, 974-978.

Applegate, L.A., Frenk, E., Gibbs, N., Johnson, B., Ferguson, J., Tyrrell, R.M. (1994) Cellular sensitivity to oxidative stress in the photosensitivity dermatitis/actinic reticuloid syndrome. J. Invest. Dermatol., 102(5), 762-767.

Applegate, L.A., Noel, A., Vile, G., Frenk, E., Tyrrell, R.M. (1995) Two genes contribute to different extents to the heme oxygenase activity measured in cultured human skin fibroblasts and keratinocytes: Implications for protection against oxidant stress. Photochem. Photobiol., 61(3), 285-291.

Arosio, P., Adelman, T.G., Drysdale, J.W. (1978) On ferritin heterogeneity. Further evidence for heteropolymers. J. Biol. Chem., 253(12), 4451-8.

Baker, E., Morton, A.G., Tavill, A.S. (1980) The regulation of iron release from the perfused rat liver. Br. J. Haematol., 45(4), 607-620.

Bando, Y., Aki, H. (1990) Superoxide-mediated release of iron from ferritin by some flavoenzymes. Biochem. Biophys. Res. Comm., 168(2), 389-395.

Beaumont, C., Cabantchik, Z.I. (1999) H-ferritin subunit overexpression in erythroid cells reduces the oxidative stress response and induces multidrug resistance properties. Blood, 94(10), 3593-3603.

Bech-Thomsen, N., Wulf, H.C. (1995) Carcinogenic and melanogenic effects of filtered metal halide UVA source and a tubular fluorescent UVA tanning source with or without additional solar-simulated UV radiation in hairless mice. Photochem. Photobiol., 62(4), 773-779.

Beitner, H. (1986) The effect of high dose long-wave ultraviolet radiation (UVA) on epidermal melanocytes in human human skin: a transmission electron microscopic study. Photodermatol., 3(3), 133-139.

Bestak, R., Halliday, G.M. (1996) Chronic low-dose UVA irradiation induces local suppression of contact hypersensitivity, Langerhans cell depletion and suppressor cell activation in C3H/HeJ mice. Photochem. Photobiol., 64(6), 969-974.

Bezdetnaya. L., Zeghari, N., Belitchenko, I., Barberi-Heyob, M., Merlin, J.-L., Potapenko, A., Guillemin, F. (1996) Spectroscopic and biological testing of photobleaching of porphyrins in solutions. Photochem. Photobiol., 64(2), 382-386.

Bissett, D.L., Chatterjee, R, Hannon, D.P. (1991) Chronic ultraviolet radiation-induced increase in skin iron and the photoprotective effect of topically applied iron chelators. Photochem. Photobiol., 54(2), 215-23.

Bolann, B.J., Ulvik, R.J. (1990) On the limited ability of superoxide to release iron from ferritin. Eur. J. Biochem, 193, 899-904.

Bomford, A., Conlon-Hollingshead, C., Munro, H.N. (1981) Adaptive responses of rat tissue isoferritins to iron administration. Changes in subunit synthesis, isoferritin abundance, and capacity for iron storage. J Biol Chem, 256(2), 948-55.

Boukamp, P., Petrussevska, R.T., Breitkreutz, D., Hornung, J., Markham, A., Fusenig, N.E. (1988) Normal keratinization in a spontaneously immortilzed aneuploid human keratinocyte cell line. J. Cell. Biol., 106, 761-771.

Bouton, C., Hirling, H., Drapier, J.C. (1997) Redox modulation of iron regulatory proteins by peroxynitrite. J. Biol. Chem., 272, 19969-19975.

Boyer, R.F., Grabill, T.W., Petrovich, R.M. (1988) Reductive release of ferritin iron: a kinetic assay. Anal. Biochem., 174, 17-22.

Bradford, M.M. (1976) A rapid and sensitive method for the quantitation of microgram quantities of protein utilizing the principle of protein-dye binding . Anal. Biochem., 72, 248-254.

Brash, D.E.,Rudolph, J.A., Simon, J.A., Lin, A., McKenna, G.J., Baden, H.P., Halperin, A.J., Ponten, J. (1991) A role for sunlight in skin cancer: UV-induced p53 mutations in squamous cell carcinoma. Proc. Natl. Acad. Sci. USA, 88(22), 10124-10128.

Breuer, W., Epsztejn, S., Millgram, P., Cabantchik, I.Z. (1995) Transport of iron and other transition metals into cells as revealed by a fluorescent probe. Am. J. Physiol., 268, C1354-C1361.

Breuer, W., Epsztejn, Cabantchik, I.Z. (1995a) Iron acquired from transferrin by K562 cells is delivered to a cytoplasmic pool of chelatable iron (II). J. Biol. Chem., 270(41), 24209-24215.

Breuer, W., Epsztejn, Cabantchik, I.Z. (1996) Dynamics of the cytosolic chelatable iron pool of K562 cells. FEBS Lett., 382, 304-308.

Breuer, W., Greenberg, E., Cabantchik, Z.I. (1997) Newly delivered transferrin iron and oxidative cell injury. FEBS Lett., 403, 213-219.

Bridges, K.R. (1990) Modulation of the availability of intracellular iron. In Ponka, P., Sculman, H.M., Woodworth, R.C. (eds): Iron transport and storage. CRC Press, Inc., Florida, USA, pp. 297-314.

Bucala, R. (1996) Lipid and lipoprotein oxidation: basic mechanisms and unresolved questions in vivo. Redox Report, 2(5), 291-307.

Cabantchik, Z.I., Glickstein, H., Milgram, P., Breuer, W. (1996) A fluorescence assay for assessing chelation of intracellular iron in a membrane model system and mammalian cells. Anal. Biochem., 233, 221-227.

Cairo, G., Tacchini, L., Pogliaghi, G., Anzon, E., Tomasi, A., Bernelli-Zazzera, A. (1995) Induction of ferritin synthesis by oxidative stress. J. Biol. Chem., 270(2), 700-703.

Cammack, R., Wrigglesworth, J.M., Baum, H. (1991) Iron-dependent enzymes in mammalian sytems. In Ponka, P., Schulman, H.M., Woodworth, R.C. (eds): Iron transport and storage. CRC Press Inc., Florida, USA, pp. 17-39

Campbell, D.L., Fisher, M.E., Johnson, J.G., Rossi, F.M., Campling, B.G., Pottier, R.H.,Kennedy, J.C. (1996) Flow Cytometric Technique for Quantitating Cytotoxic Response to Photodynamic Therapy. Photochem. Photobiol., 63(1), 111-116.

Carbonare, M.D., Pathak, M.A. (1992) Skin photosensitizing and the role of reactive oxygen species in photoaging. J. Photochem. Photobiol. B: Biol., 14, 105-124.

Carvalho, H., Bechara, E.J.H., Meneghini, R., Demasi, M. (1997) Haem precursor δ-aminolevulinic acid induces activation of the cytosolic iron regulatory protein 1. Biochem. J., 328, 827-832.

Casey, J.L., Koeller, D.M., Ramin, V.C., Klausner, R.D., Harford, J.B. (1989) Iron regulation of transferrin receptor mRNA levels requires iron-responsive elements and a rapid turnover determinant in the 3' untranslated region of the mRNA. EMBO J., 8, 3693-3699.

Castro, L., Rodriguez, M., Radi, R. (1994) Aconitase is readily inactivated by peroxynitrite, but not by its precursor, nitric oxide. J. Biol. Chem., 269(47), 29409-29415.

Chedekel, M.R., Ziese, L. (1997) Melanins. In Lowe, N.J., Shaath, N.A., Pathak, M.A. (eds): Sunscreens development, evaluation, and regulatory aspects. Marcel Dekker, Inc., N.Y., USA, pp.117-137.

Cooper, K.D., Oberhelman, L., Hamilton, T.A., Baadsgaard, O., Terhune, M., LeVee, G., Anderson, T. (1992) UV exposure reduces immunization rates and promotes tolerance to epicutaneous antigens in humans: relatioship to dose, CD1a-DR+ epidermal macrophage induction, and Langerhans cell depletion. Proc. Natl. Acad. Sci. USA, 89(18), 8497-8501.

Crichton, R.R., Ward, R.J. (1992) Structure and molecular biology of iron binding proteins and the regulation of 'free' iron pools. In Lauffer, R.B. (ed): Iron and human disease. CRC Press Inc., Florida, USA, pp. 23-75.

Crichton, R.R., Soruco, J.A., Roland, F., Michaux, M.A., Gallois, B., Precigoux, G., Mahy, J.P., Mansuy, B. (1997) Remarkable ability of horse spleen apoferritin to demetallate hemain and to metallate protoporphyrin IX as a function of pH. Biochemistry, 36, 15049-15054.

Cunningham, M.L., Johnson, J.S., Giovanazzi, S.M., Peak, M.J. (1985) Photosensitized production of superoxide anion by monochromatic (290-405 nm) ultraviolet radiation of NADH and NADPH coenzymes. Photochem. Photobiol., 42(2), 125-128.

Czochralska, B., Kawczynski, W., Bartosz, G., Shugar, D. (1984) Oxidation of excited-state NADH and NAD dimer in aqueous medium involvement of O_2^- as a mediator in the presence of oxygen. Biochim. Biophys. Acta, 801, 403-409.

Darr, D., Combs, S., Dunston, S., Manning, T., Pinnell, S. (1992) Topical vitamin C protects porcine skin from ultraviolet readiation-induced damage. Br. J. Dermatol., 127(3), 247-253.

Daynes, R.A., Bernhard, E.J., Gurish, M.F., Lynch, D.H. (1981) Experimental photoimmunology: immunological ramifications of UV-induced carcinogenesis. J. Invest. Dermatol., 77(1), 77-85.

de Laat, A., van deLeun, J.C., de Gruijl, F.R. (1997) Carcinogenesis induced by UVA (365-nm) radiation: the dose-time dependence of tumor formation in hairless mice. Carcinogenesis, 18(5), 1013-20.

Desai, I.D., Sawant, P.L., Tappel, A.L. (1964) Peroxidative and radiation damage to isolated lysosomes. Biochim. Biophys. Acta, 86, 277-285.

Djavaheri-Mergny, M., Mergny, J.L., Bertrand, F., Santus, R., Maziere, C., Dubertret, L., Maziere, J.C. (1996) Ultraviolet-A induces activation of AP-1 in cultured human kertinocytes. FEBS Lett., 384, 92-96.

Dognin, J., Crichton, R.R. (1975) Mobilisation of iron from ferritin fractions of defined iron content by biological reductants. FEBS Lett., 54(2), 234-236.

Drapier, J.C., Hibbs, Jr., J.B. (1986) Murine cytotoxic activated macrophages inhibit aconitase in tumor cells. J. Clin. Invest., 78, 790-797.

Drysdale, J.W., Munro, H.N. (1966) Regulation of synthesis and turnover of ferritin in rat liver. J. Biol. Chem., 241(15), 3630-3637.

Epsztejn, S., Kakhlon, O., Glickstein, H., Breuer, W., Cabantchik, I. (1997) Fluorescence analysis of the labile iron pool of mammalian cells. Anal. Biochem., 248, 31-40.

Fahmy, M., Young, S.P. (1993) Modulation of iron metabolism in monocyte cell line U937 by inflammatory cytokines: changes in transferrin uptake, iron handling and ferritin mRNA. Biochem. J., 296, 175-181.

Ferris, C.D., Jaffrey, S.R., Sawa, A., Takahashi, M., Brady, S.D., Barrow, R.K., Tysoe, S.A., Wolosker, H., Baranano, D.E., Dpre, S., Poss, K.D., Snyder, S.H. (1999) Haem oxygenase-1 prevents cell death by regulating cellular iron. Nature, 1, 152-157.

Fisher, M.S., Kripke, M.L. (1982) Suppressor T lymphocytes control the development of primary skin cancers in ultraviolet-irradiated mice. Science, 216(4550), 1133-1134.

Fischer-Neilsen, A., Poulsen, H.E., Loft, S. (1992) 8-Hydroxydeoxyguanosine in vitro: effects of glutathione, ascorbate, and 5-aminosalicylic acid. Free Radic. Biol. Med., 12(2), 121-6.

Fischer-Neilsen, A., Loft, S., Jensen, K.G. (1993) Effect of ascorbate and 5-aminosalicylic acid on light-induced 8-hydroxydeoxyguanonosine formation in V79 Chinese hamster cells. Carcinogenesis, 14(11), 2431-2433.

Fraga, C.G., Onuki, J., Lucesoli, F., Bechara, E.J.H., Di Mascio, P. (1994) 5-Aminolevulinic acid mediates the in vivo and in vitro formation of 8-hydroxy-2'-deoxyguanosine in DNA. Carcinogenesis, 15(10), 2241-2244.

Frausto da Silva, J.J.R. (1991) The inorganic chemistry of life. In: The biological chemistry of the elements, Oxford, Clarendon Press.

Freeman, S.E., Gange, R.W., Matzinger, E.A., Sutherland, J.C. (1986) Higher pyrimidine dimer yields in skin of normal humans with higher UVB sensitivity. J. Invest. Dermatol., 86(1), 34-36.

Freeman, S.E., Hachan, H., Gange, R.W., Maytum, D.J., Sutherland, J.C., Sutherland, B.M. (1989) Wavelength dependence of pyrimidine dimer formation in DNA of human skin irradiated in situ with ultraviolet light. Proc. Natl. Acad. Sci. USA, 86(14), 5605-5609.

Fryer, M.J. (1993) Evidence for the photoprotective effects of vitamin E. Photochem. Photobiol., 58(2), 304-312.

Fukuda, H., Battle, A.M.C., Riley, P.A. (1993) Kinetics of porphyrin accumulation in cultured epithelial cells exposed to ALA. Int. J. Biochem., 25 (10), 1407-1410.

Gabroriau, F., Morliere, P., Marquis, I., Moysan, A., Geze, M., Dubertret, L. (1993) Membrane damage induced in cultured human skin fibroblasts by UVA irradiation. Photochem. Photobiol., 58(4), 515-520.

Gantt, R., Jones, G.M., Stephens, E.V., Baeck, A.E., Sanford, K.K. (1979) Visible light-induced DNA crosslinks in cultured mouse and human cells. Biochim. Biophys. Acta, 565(2), 231-240.

Gaullier, J.M., Geze, M, Santus, R., Melo, T.S., Maziere, J.C., Bazin, M., Morliere, P., Dubertret, L. (1995) Subcellular localization of and photosensitzation by protoporphyrin IX in human keratinocytes and fibroblasts cultivated with 5-aminolevulinic acid. Photochem. Photobiol. 62(1), 114-122.

Geze, M, Morliere, P., Maziere, J.C., Smith, K.M., Santus, R. (1993) Lysosomes, a key target of hydrophobic photosensitizers proposed for photochemotheraputic applications. J. Photochem. Photobiol. B: Biol., 20, 22-35.

Gibson, S.L., Havens, J.J., Foster, T.H., Hilf, R. (1997) Time-dependent intracellular accumulation of δ-aminolevulinic acid, induction of porphyrin synthesis and subsequent phototoxicity. Photochem. Photobiol., 65 (3), 416-421.

Giordani, A., Morliere, P., Djavaheri-Mergny, M., Santus, R. (1998) Ultaviolet-A-dependent inhibition of cytoplasmic aconitase activity of iron regulatory protein-1 in NCTC 2544 keratinocytes. Photochem. Photobiol. 68(3), 309-313.

Girotti, A.W. (1990) Photodynamic lipid peroxidation in biological systems. Photochem. Photobiol, 51(4), 497-509.

Gray, N.K., Quick, S., Goosen, B., Constable, A., Hirling, H., Kuhn, L.C. (1993) Recombinant iron-regulatory factor functions as an iron-responsive-element-binding protein, a translational repressor and an aconitase. Eur. J. Biochem., 218, 657-667.

Gray, N.K., Hentze, M.W. (1994) Iron regulatory protein prevents binding of the 43S translation pre-initiation complex to ferritin and eALAS mRNAs. EMBO J., 13, 3882-3891.

Greene, M.I., Sy, M.S., Kripke, M., Benacerraf, B. (1979) Impairment of antigen-presenting cell function by ultraviolet radiation. Proc. Natl. Acad. Sci. USA, 76(12), 6591-6595.

Guyton, K.Z., Kensler, T.W. (1993) Oxidative mechanisms in carcinogenesis. Br. Med. Bull., 49(3), 523-544.

Guzzo, A., Karatzios, C., Diorio, C., DuBow, M.S. (1994) Metallothionein-II and ferritin H mRNA levels are increased in arsenite-exposed HeLa cells. Biochem. Biophys. Res. Comm., 205(1), 590-595.

Haile, D.J. (1999) Regulation of genes of iron metabolism by the Iron-response proteins. Am. J. Med. Sci., 318(4), 230-240.

Halliwell, B., Gutteridge, J.M.C. (1999) Free radicals in biology and medicine. 3rd ed., Oxford University Press, Oxford, UK.

Harrison P.M., Arosio, P. (1996) The ferritins: molecular properties, iron storage function and cellular regulation. Biochim. Biophys. Acta, 1275, 161-203.

Hattori-Nakakuki, Y., Nishigori, C., Okamoto, K., Imamura, S., Hiai, H., Toyokuni, S. (1994) Formation of 8-hydroxy-2'-deoxyguanosine in epidermis of hairless mice exposed to near-UV. Biochem. Biophys. Res. Comm., 201(3), 1132-1139.

Hausladen, A., Fridovich, I. (1994) Superoxide and peroxynitrite inactivate aconitases, but nitric oxide does not. J. Biol. Chem., 269(47), 29405-29408.

He, D., Behar, S., Nomura, N., Sassa, S., Lim, H.W. (1995) The effect of ALA and radtion on porphyrin/heme biosynthesis in endothelial cells. Photochem. Photobiol. 61(6) 656-661.

Henderson, B.R., Kuhn, L.C. (1995) Differential modulation of the RNA-binding proteins IRP-1 and IRP-2 inresponse to iron. J. Biol. Chem. 270, 20509-20515.

Hentze, M.W., Argos, P. (1991) Homology between IRE-BP, a regulatory RNA-binding protein, aconitse, and isopropylmalate isomerase. Nucl. Acids Res., 19, 1739-1740.

Hentze, M.W., Kuhn, L.C. (1996) Molecular control of vertebrate iron metabolism: mRNA-based regulatory circuits operated by iron, nitric oxide, and oxidative stress. Proc. Natl. Acad. Sci. U.S.A., 93, 8175-8182.

Iinuma, S., Farshi, S.S., Ortel, B., Hasan, T. (1994) A mechanistic study of cellular photodestruction with 5-aminolevulinic acid-induced porphyrin. Int. J. Cancer, 70, 21-28.

Ishitani, K., Listowsky, I. (1975) Differences in subunit composition and iron content of isoferritins. J. Biol. Chem., 250(14), 5446-5449.

Ito, A., Ito, T. (1983) Visible involement of membrane damage in the inactivation by broad-band near-UV radiation in *Saccharomyces cerevisiae* cells. Photochem. Photobiol., 37(4), 395-401.

Kelfkens, G., de Guijl, F.R., vander Leun, J.C. (1991) Tumorigenesis by short-wave ultraviolet A: papilloma verses squamous cell carcinomas. Carcinogenesis, 12(8), 1377-1382.

Kelfkens, G., de Guijl, F.R., vander Leun, J.C. (1992) The influence of ventral UVA exposure on subsequent tumorigenesis in mice by UVA or UVB irradiation. Carcinogenesis, 13(11), 2169-2174.

Kennedy, J.C., Pottier, R.H. (1992) Endogenous protoporphyrin IX, a clinically useful photosensitizer for photodynamic therapy. J. Photochem. Photobiol. B: Biol., 14, 275-292.

Kennedy, M.C., Mende-Mueller, L., Blondin, G.A., Beinhert, H. (1992) Purification and characterization of cytosolic aconitase from beef liver and its relationship to the iron-responsive element binding protein. Proc. Natl. Acad. Sci. USA., 89, 11730-11734.

Keyse, S. M., Tyrrell, R.M. (1987) Both near ultraviolet radiation and the oxidizing agent hydrogen peroxide induce a 32-kDa stress protein in normal human skin fibroblasts. J. Biol. Chem., 262(30), 14821-14825.

Keyes, S.M., Tyrrell, R.M. (1989) Heme oxygenase is the major 32-kDa stress protein induced in human skin fibroblasts by UVA radiation, hydrogen peroxide, and sodium arsenite. Proc. Natl. Acad. Sci. USA, 86, 99-103.

Kim, H.Y., LaVaute, T., Iwai, K., Klausner, R.D., Rouault, T.A. (1996) Identification of a conserved and functional iron-responsive element in the 5'-untranslated region of mammalian mitochondrial aconitase. J. Biol. Chem., 271(39), 24226-24230.

Klausner, R.D., Rouault, T.A., Harford, J.B. (1993) Regulating the fate of mRNA: The control of cellular iron metabolism. Cell, 72, 19-28.

Kligman, L.H., Kligman, A.M. (1997) Ultraviolet radiation-induced skin aging. In Lowe, N.J., Shaath, N.A., Pathak, M.A. (eds): Sunscreens development, evaluation, and regulatory aspects. Marcel Dekker, Inc., N.Y., USA, pp.117-137.

Kligman, L.H., Sayre, R.M. (1991) An action spectrum for ultraviolet induced elastosis in hairless mice: quantification of elastosis by image analysis. Photochem. Photbiol., 53(2), 237-242.

Kohgo, Y., Yokota, M., Drysdale, J.W. (1980) Differential turnover of rat liver isoferritins. J. Biol. Chem., 255(11), 5195-5200.

Konijn, A.M., Carmel, N., Levy, R., Hershko, C. (1981) Ferritin synthesis in inflammation. II. Mechanism of incresed ferritin synthesis. Br. J. Haematol., 49(3), 361-370.

Korytowski, W., Bachowski, G.J., Girrotti, A.W. (1992) Photoperoxidation of cholesterol in homogenous solution, isolated membranes, and cells: comparison of the 5α- and 6β-hydroperoxides as indicators of singlet oxygen intermediacy. Photochem. Photobiol., 56, 1-8.

Kozlov, A.V., Yegorov, D.Y., Vladimirov, Y.A., Azizova, O.A. (1992) Intracellular free iron in liver tissue and liver homogenate: studies with electron paramagnetic resonance on the formation of paramagnetic complexes with desferal and nitric oxide. Free Radic. Biol. Med.;13(1), 9-16.

Krinsky, N.I., Deneke, S.M. (1982) Interaction of oxygen and oxy-radicals with carotenoids. J. Natl. Cancer. Inst., 69(1), 205-210.

Kripke, M.L. (1974) Antigenicity of murine skin tumors induced by ultraviolet light. J. Natl. Cancer Inst., 53(5), 1333-1336.

Kuchino, Y., Mori, F., Kasai, H., Inoue, H., Iwai, S., Muira, K., Ohtsuka, E., Nishimura, S. (1987) Misreading of DNA templates containing 8-hydroxydeoxyguanosine at the modified base and at adjacent residues. Nature, 327, 77-79.

Kumakiri, M., Hashimoto, K., Willis, I. (1977) Biologic changes due to long-wave ultraviolet irradiation on human skin: ultrastructural study. J. Invest. Dermatol., 69(4), 392-400.

Kvam, E., Tyrrell, R.M. (1997) Induction of oxidative DNA damage in human skin cells by UV and near visible radiation. Carcinogenesis, 18(12), 2379-2384.

Kvam, E., Noel, A., Basu-Modak, S., Tyrrell, R.M. (1999) Cyclooxygenase dependent release of heme from microsomal hemeproteins correlates with induction of heme oxygenase 1 transcription in human fibroblasts. Free. Radic. Biol. Med., 26(5-6), 511-7.

Laub, R., Schneider, Y.J., Octave, J.N., Trouet, A., Crichton, R.R. (1985) Cellular pharmacology of desferrioxamine B and derivatives in cultured rat hepatocytes in relation to iron mobilization. Biochem. Pharmacol., 34(8), 1175-1183.

Laulhere, J.P., Briat, J.F. (1993) Iron release and uptake by plant ferritin: effects of pH, reduction and chelation. Biochem. J., 290(3), 693-699.

Lavker, R.M., Gerberick, G.F., Veres, D., Irwin, C.J., Kaidbey. K.H. (1995) Cumulative effects from repeated exposures to suberythemal doses of UVB and UVA in human skin. J. Am. Acad. Dermatol., 32(1), 53-62.

Lautier. D., Luscher, P., Tyrrell, R.M. (1992) Endogenous glutathione levels modulate both constitutive and UVA radiation/hydrogen peroxide inducible expression of the human heme oxygenase gene. Carcinogenesis, 13(2), 227-232.

Leccia, M.T., Richard, M.J., Beani, J.C., Faure, H., Monjo, A.M., Cadet, J., Amblard, P., Favier, A. (1993) Protective effect of selenium and zinc on UV-A damage in human skin fibroblasts. Photochem. Photobiol., 58(4), 548-53.

Leccia, M.T., Richard, M.J., Joanny-Crisci, F., Beani, J.C. (1998) UV-A1 cytotoxicity and antioxidant defence in keratinocytes and fibroblasts. Eur. J. Dermatol., 8(7), 478-482.

Leung, H.W., Vang, M.J., Mavis, R.D. (1981) The co-operative interaction between vitamin E and vitamin C in suppression of peroxidation of membrane phospholipids. 664(22), 266-272.

Levi, S., Yewdall, S.J., Harrison, P.M., Santambrogio, P., Cozzi, A., Rovida, E., Albertini, A., Arosio, P. (1992) Evidence that H- and L-chains have co-operative roles in the iron-uptake mechansim of human ferritin. Biochem. J., 288, 591-596.

Levi, S., Santambrogio, P., Cozzi, A., Rovida, E., Corsi, B., Tamborini, E., Spada, S., Albertini, A., Arosio, P. (1994) The role of the L-chain in ferritin iron incorporation. J. Mol. Biol., 238, 649-654.

Lowe, N.J., Meyers, D.P., Weider, J.M., Luftman, D., Borget, T., Lehman, M.D., Johson, A.W., Scott, I.R. (1995) Low doses of repetitive ultraviolet A induce morphological changes in human skin. J. Invest. Dermatol., 105(6), 739-743.

Luzzago, A., Arosio, P., Iacobella, C., Ruggeri, G., Capucci, L., Brochi, E., De Simone, F., Gamba, D., Gabri, E., Levi, S., Albertini, A. (1986) Immunochemical characterization of human liver and heart ferritins with monoclonal antibodies. (Biochim. Biophys. Acta, 872, 61-71.

Lytton, S.D., Mester, B., Libman, J., Shanzer, A., Cabantchik, Z.I. (1992) Monitoring of iron(III) removal from biological sources using a fluorescent siderophore. Anal. Biochem., 205(2), 326-33.

McCormick, J.P., Fischer, J.R., Pachlatko, J.P., Eisenstark, A. (1976) Characterization of a cell-lethal product from the photooxidation of tryptophan: hydrogen peroxide. Science, 191(4226), 468-469.

Malik, Z., Dishi, M., Garini, Y. (1996) Fourier transform multipixel spectroscopy and spectral imaging of protoporphyrin in single melanoma cells. Photochem. Photobiol., 63(5), 608-614.

Menter, J.M., Sayre, R.M., Etemadi, A.A., Agin, P.P., Willis, I. (1996) Chronic exposure of Sk-1 hairless mice to narrow-band ultraviolet A (320-355 nm). Photodermatol. Photoimmunol. Photomed., 12(1), 7-11.

Michaux, M.A., Dautant, A., Gallois, B., Granier, T., Langois d'Estaintot, B., Precigoux, G. (1996) Structural investigation of the complexation properties between horse spleen apoferritin and metalloporphyrins. Proteins, 24, 314-321.

Miller L.L., Miller, S.C., Torti, S.V., Tsuji, Y., Torti, F.M. (1991) Iron-independent induction of ferritin H chain by tumor receptor necrosis factor. Proc. Natl. Acad. Sci., 88, 4946-4950.

Minami, H., Sato, K., Maeda, T., Taguchi, H., Yoshikawa, K., Kosaka, H., Shiga, T., Tsuji, T. (1999) Hypoxia potentiates ultraviolet A-induced riboflavin cytotoxicity. J. Invest. Dermatol., 113, 77-81.

Moan, J., Berg, B. (1991) The photodegradation of porphyrins in cells can be used to estimate the lifetime of singlet oxygen. Photochem. Photobiol., 53, 549-553.

Moan, J., Dahlback, A., Setlow, R.B. (1999) Epidemiological support for a hypothesis for melanoma induction indicating a role for UVA radiation. Photochem. Photobiol., 70(2), 243-247.

Monteiro, H.P., Abdalla, D.S.P., Augusto, O., Bechara, E.J.H. (1989) Free radical generation during δ-aminolevulinic acid autooxidation: Induction by hemoglobin and connections with porphyrinpathies. Arch. Biochem. Biophys., 271(1), 206-216.

Morliere, P., Kohen, E, Reyftmann, J.P., Santus, R., Kohen, C., Maziere J.C., Goldstein, S., Mangel, W.F., Dubertret, L. (1987) Photosensitization by porphyrins delivered to L cell fibroblasts by human serum low density lipoproteins. A microfluorimetric study. Photochem. Photobiol., 46(2), 183-191.

Morliere, P., Moysan, A., Santus, R., Huppe, G., Maziere, J.C., Dubertret, L. (1991) UVA-induced lipid peroxidation in cultured human fibroblasts. Biochim. Biophys. Acta, 1084 (261-268).

Moysan, A., Marquis, I., Gaboriau, F., Santus, R., Dubertret, L., Morliere, P. (1993) Ultraviolet A-induced lipid peroxidation and antioxidant defense systems in cultured human fibroblasts. J. Invest. Dermatol., 100, 692-698.

Moysan, A., Morliere, P., Marquis, I., Richard, A., Dubertret, L. (1995) Effects of selenium on UVA-induced lipid peroxidation in cultured human skin fibroblasts. Skin Pharmacol., 8(3), 139-48.

Munro, H. (1993) The ferritin genes: their response to iron status. Nut. Rev., 51(3), 65-73.

Njus, D., Kelley, P.M. (1991) Vitamins C and E donate single hydrogen atoms in vivo. FEBS Lett., 284(2), 147-151.

Noodt, B.B., Berg, K., Stokke, T., Peng, Q., Nesland, J.M. (1996) Apoptosis and necrosis induced with light and 5-aminolevulinic acid-derived protoporphyrin IX. Br. J. Cancer. 74, 103-112.

Noonan, F.P., Kripke, M.L., Pedersen, G.M., Greene, M.I. (1981) Suppression of contact hypersensitivity in mice by ultraviolet irradiation is associated with defective antigen presentation. Immunology, 43(3), 527-533.

Noonan, F.P., De Fabo, E.D., Morrison, H. (1988) Cis-urocanic acid, a product formed by ultraviolet B irradiation of the skin, initiates an antigen presentation defect in splenic dendritic cells in vivo. J. Invest. Dermatol., 90(2), 92-99.

Norval, M., Gibbs, N.K., Gilmour, J. (1995) The role of urocanic acid in UV-induced immunosuppresion: recent advances (1992-1994). Photochem. Photobiol., 62(2), 209-217.

Ochsner, M. (1997) Photophysical and photobiological processes in the photodynamic therapy of tumours. J. Photochem. Photobiol. B: Biol., 39, 1-18.

O'Connell, M.J., Ward, R.J., Baum, H., Peters, T.J. (1989) Iron release from haemosiderin and ferritin by therapeutic and physiological chelators. Biochem. J., 260, 903-907.

Olsen, W.M., Huitfeldt, H.S., Eggset, G. (1989) UVB-induced (6-4) photoproducts in hairless mouse epidermis studied by quantitative immunohistochemistry. Carcinogenesis, 10(9), 1669-1673.

Ortel, B., Tanew, A., Honigsmann, H. (1993) Lethal photosensitization by endogenous porphyrins of PAM cells – modification by desferrioxamine. J. Photochem. Photobiol. B: Biol., 17, 273-278

Oteiza, P.I., Bechara, E.J.H. (1993) 5-Aminolevulinic acid induces lipid peroxidation in cardiolipin-rich liposomes. Arch. Biochem. Biophys., 305(2), 282-287.

Oteiza, P.I., Kleinman, C.G., Demasi, M., Bechara, E.J.H. (1995) 5-Aminolevulinic acid induces iron release from ferritin. Arch. Biochem. Biophys., 316, 607-611.

Pantopoulos, K., Mueller, S., Atzberger, A., Ansrge, W., Stremmel, W., Hentze, M.W. (1997) Differences in the regulation of iron regulatory protein-1 (IRP-1) by extra- and intracellular oxidative stress. J. Biol. Chem., 272(15) 9802-9808.

Paraskeva, E., Hentze, M.W. (1996) Iron-sulphur clusters as genetic regulatory switches: the bifunctional iron regulatory protein-1. FEBS Lett., 389, 40-43.

Parat, M.O., Richard, M.J., Leccia, M.T., Amblard, P., Favier, A., Beani, J.C. (1995) Does manganese protect cultured human skin fibroblasts against oxidative injury by UVA, dithranol and hydrogen peroxide? Free. Radic. Res.,23(4),339-51.

Pathak, M.A. (1997) Photoprotection against harmful effects of solar UVB and UVA radiation: an update. In Lowe, N.J., Shaath, N.A., Pathak, M.A. (eds): Sunscreens development, evaluation, and regulatory aspects. Marcel Dekker, Inc., N.Y., USA, pp.117-137.

Peak, M.J., Peak, J.G., Jones, C.A. (1985) Different (direct and indirect) mechanisms for the induction of DNA-protein crosslinks in human cells by far- and near-ultraviolet radiations (290 and 405 nm). Photochem. Photobiol., 42(2), 381-387.

Peak, M.J., Peak, J.G., Carnes, B.A. (1987a) Induction of direct and indirect single-strand breaks in human cell DNA by far- and near-ultraviolet radiations: action spectrum and mechanisms. Photochem. Photobiol., 45(3), 381-387.

Peak, M.J., Johnson, J.S., Tuveson, R.W., Peak, J.G. (1987b) Inactivation by monochromatic near-UV radiation on an *Escherichia coli hemA8* mutant grown with and without δ-aminolevulinic acid: the role of DNA vs membrane damage. Photochem. Photobiol., 45(4), 473-478.

Peak, M.J., Peak, J.G. (1990) Hydroxyl radical quenching agents protect against DNA breakage caused by both 365-nm UVA and by gamma radiation. Photochem. Photobiol., 51(6), 649-652.

Peng, Q., Berg, K., Moan, J., Kongshaug, M., Nesland, J.M. (1997) 5-Aminolevulinic acid-based photodynamic therapy: principles and experimental research. Photochem. Photobiol., 65(2), 235-251.

Petersen, M.J., Hansen, C., Craig, S. (1992) Ultraviolet A irradiation stimulates collagenase production in cultured human fibroblasts. J. Invest. Dermatol, 99(4), 440-444.

Pflaum, M., Kielbassa, C., Garmyn, M., Epe, B. (1998) Oxidative DNA damage induced by visible light in mammalian cells: extent, inhibition by antioxidants and genotoxic effects. Mutat. Res., 408, 137-146.

Philpott, C.C., Klausner, R.D., Rouault, T.A. (1994) The bifunctional iron-responsive element binding protein/cytosolic aconitase: The role of active-site residues in ligand binding and regulation. Proc. Natl. Acad. Sci. USA, 91, 7321-7325.

Ponka, P. (1997) Tissue-specific regulation of iron metabolism and heme synthesis: distinct control mechanisms in erythroid cells. Blood, 89(1), 1-25.

Poswig, A., Wenk, J., Brenneisen, P., Wlaschek, M., Hommel, C., Quel, G., Faisst, K., Dissemond, J., Briviba, K., Krieg, T., Scharffetter-Kochanek, K. (1999) Adaptive antioxidant response of manganese-superoxide dismutase following repetitive UVA irradiation. J. Invest. Dermatol., 112(1), 13-18.

Pourzand, C., Watkin, R.D., Brown, J.E., Tyrrell, R.M. (1999) Ultraviolet A radiation induces immediate release of iron in human primary skin fibroblasts: The role of ferritin. Proc. Natl. Acad. Sci. USA, 96(12) 6751-6756.

Precigoux, G., Yariv, J., Gallois, B., Dautant, A., Courseille, C., Langlois d'Estaintot, B. (1994) A crystallographic study of haem binding to ferritin. Acta Cryst., D50, 739-743.

Promega Corporation. (1996) CellTiter 96® AQ_{ueous} one solution cell proliferation assay technical bulletin #TB169.

Punnonen, K., Jansen, C.T., Puntala, A., Ahotupa, M. (1991) Effects of in vitro UVA irradiation and PUVA treatment on membrane fatty acids and activities of antioxidant enzymes in human keratinocytes. J. Invest. Dermatol., 96(2), 255-9.

Reeve, V.E., Tyrrell, R.M. (1999) Heme oxygenase induction mediates the photoimmunoprotective activity of UVA radiation in the mouse. Proc. Natl. Acad. Sci. USA, 96(16), 9317-9321.

Reif, D.W., Schubert, J., Aust, .S.D. (1988) Iron release from ferritin and lipid peroxidation by radiolytically generated reducing radicals. Arch. Biochem. Biophys., 264(1), 238-243.

Reif, D.W., Samokyszyn, V.M., Miller, D.M., Aust, S.D. (1989) Alloxan- and glutathione-dependent ferritin iron release and lipid peroxidation. Arch. Biochem. Biophys., 269(2), 407-414.

Reif, D.W. (1992) Ferritin as a source of iron for oxidative damage. Free Radic. Biol. Med., 12, 417-427.

Richardson, D.R., Ponka, P. (1997) The molecular mechanisms of the metabolism and transport of iron in normal and neoplastic cells. Biochim. Biophys. Acta, 1997, 1331, 1-40.

Ricchelli, F. (1995) Photophysical properties of porphyrins in biological membranes. J. Photochem. Photobiol. B: Biol., 29, 109-118.

Rogers, J.T., Bridges, K.R., Durmowicz, G.P., Glass, J., Auron, P.E., Munro, H.N. (1990) Translational control during acute phase response. J. Biol. Chem., 265(24), 14572-14578.

Rogers, J.T., Andriotakis, J.L., Lacroix, L., Durmowicz, G.P., Kasschau, K.D., Bridges, K.R. (1994) Translational enhancement of H-ferritin mRNA by interleukin-1β acts through 5' leader sequences distinct from the iron response element. Nucleic Acids Res., 22(13), 2678-2686.

Rouault, T.A., Klausner, R.D. (1996) Iron-sulfer clusters as biosensors of oxidants and iron. Trends Biochem. Sci., 21, 174-177.

Rouault, T.A., Stout, C.D., Kaptain, S., Harford, J.B., Klausner, R.D. (1991) Structural relationship between an iron-regulated RNA-binding protein (IRE-BP) and aconitase: Functional implications. Cell, 64, 881-883

Roza, L., van der Schans, G.P., Lohman, P.H. (1985) The induction and repair of DNA damage and its influence on cell death in primary human fibroblasts exposed to UV-A or UV-C irradiation. Mutat. Res., 146(1), 89-98.

Ryter, S.W., Tyrrell, R.M. (1998) Singlet molecular oxygen ($^1O_2$): A possible effector of eukaryotic gene expression. Free Radic. Biol. Med., 24 (9), 1520-1534.

Salet, C., Moreno, G. (1990) New trends in photobiology (invited review) photosensitization of mitochondria. Molecular and cellular aspects. J. Photochem. Photobiol. B: Biol., 5, 133-150.

Sandberg, S., Glette, J., Hopen, G., Solberg, C.O., Romslo, I. (1981) Porphyrin-induced photodamage to isolated human neutrophils. Photochem. Photobiol., 34, 471-475.

Sato, H., Yamaguchi, M., Bannai, S. (1994) Regulation of ferritin synthesis in macrophages by oxygen and a sulphydryl-reactive agent. Biochem. Biophys. Res. Comm., 201(1), 38-44.

Sato, K., Taguchi, H., Maeda, T., Yoshikawa, K. (1993) Pyridoxine toxicity to cultured fibroblasts caused by near-ultraviolet light. J. Invest. Dermatol., 100, 266-270.

Sato, K., Taguchi, H., Maeda, T., Minami, H., Asada, Y., Wantanabe, Y., Yoshikawa, K. (1995) The primary cytotoxicity in ultraviolet-A-irradiated riboflavin solution is derived from hydrogen peroxide. J. Invest. Dermatol., 105, 608-612.

Schevchuk, I., Chekulayev, V., Moan, J., Berg, K. (1996) Effects of Iodinamine and levamisole on 5-aminolevulinic acid-induced photochemotherapy. Int. J. Cancer, 67, 791-799.

Schiaffonati, L., Rappocciolo, E., Tacchini, L., Bardella, L., Arosio, P., Cozzi, A., Cantu, G.B., Cairo, G. (1988) Mechanisms of regulation of ferritin synthesis in rat liver during experimental inflammation. Exp. Mol. Pathol., 48(2), 174-181.

Segel, I.H. (1976) Biochemical calculations: How to solve mathematical problems in general biochemistry. 2rd ed., John Wiley & Sons, Inc., Canada.

Setlow, R.B., Woodhead, A.D. (1994) Temporal changes in the incidence of malignant melanoma: explanation from action spectra. Mutat. Res., 307(1), 365-374.

Shevchuk, I., Chekulayev, V., Moan, J., Berg, K. (1996) Effects of the inhibitors of energy metabolism, lonidamine and levamisole, on 5-aminolevulinic-acid-induced photochemotherapy. Int. J. Cancer, 67(6), 791-9.

Shibutani, S., Takeshita, M., Grollman, A.P. (1991) Insertion of specific bases during DNA synthesis past the oxidation-damaged base 8-oxodG. Nature, 349, 431-434

Schoenfeld, N., Mamet, R., Nordenberg, Y., Shafran, M., Babushkin, T., Malik, Z. (1994) Protoporphyrin biosynthesis in melanoma B16 cells stimulated by 5-aminolevulinic acid and chemical inducers: characterization of photodynamic inactivation. Int. J. Cancer, 56, 106-112.

Shindo, Y., Witt, E., Han, D., Packer, L. (1994) Dose-response effects of acute ultraviolet irradiation on antioxidants and molecular markers of oxidation in murine epidermis and dermis. J. Invest. Dermatol., 102(4), 470-475.

Sibille, J.C., Kondo, H., Aisen, P. (1989) Uptake of ferritin and iron bound to ferritin by rat hepatocytes: modulation by apotransferrin, iron chelators and chloroquine. Biochim. Biophys. Acta, 1010, 204-209.

Sirivech, S., Frieden, E., Osaki, S. (1974) The release of iron from horse spleen ferritin by reduced flavins. Biochem. J., 143, 311-315.

Smith, G.J. (1985) The effects of aggregation on the fluorescence and triplet state yield of hematoporphyrin. Photochem. Photobiol., 42(2), 123-126.

Steinbach, P., Weingandt, H., Baumgartner, R., Kriegmair, M., Hofstadter, F., Knuchel, R. (1995) Cellular fluorescence of the endogenous photosensitizer protoporphyrin IX following exposure to 5-aminolevulinic acid. Photochem. Photobiol., 62(5), 887-895.

Stefanini, S., Desideri, A., Vecchini, P., Drakenberg, T., Chiancone, E. (1989) Identification of iron entry channels in apoferritin. Chemical modification and spectroscopic studies. Biochemistry, 28(1), 378-82.

Sterenborg, H.J., van der Leun, J.C. (1990) Tumorigenesis by a long wavelength UV-A source. Photochem. Photobiol., 51(3), 325-30.

Stewart, M.S., Cameron, G.S., Pence, B.C. (1996) Antioxidant nutrients protect against UVB-induced oxidative damage to DNA of mouse keratinocytes in culture. J. Invest. Dermatol., 106(5), 1086-1089.

Stocker, R., Yamamoto, Y., McDonagh, A.F., Glazer, A.N., Ames, B.N. (1987) Bilirubin is an antioxidant of possible physiological importance. Science, 235(4792),1043-6.

St. Pierre, T.G., Richardson, D.R., Baker, E., Webb, J. (1992) A low-spin iron complex in human melanoma and rat hepatoma cells and a high-spin iron(II) complex in rat hepatoma cells. Biochim. Biophys. Acta;1135(2), 154-8.

Strauss, W.S.L., Sailer, R., Gschwend, M.H., Emmert, H., Steiner, R., Schneckenburger, H. (1998) Selective examination of plasma membrane-associated photosensitizers using total internal reflection fluorescence spectroscopy: Correlation between photobleaching and photodynamic efficacy of protoporphyrin IX. Photochem. Photobiol., 67 (3), 363-369.

Tanelian, C., Heinrich, G. (1995) Effect of aggregation on hematoporphyrin-sensitized production of singlet molecular oxygen. Photochem. Photobiol., 61, 131-133.

Thilly, W.G. (1979) Study of mutagenesis in diploid human fibroblasts. In Hsie, A.W., O'Neill, J.P., and McElheny, Y.K., (eds), Banbury Report 2, Mammalian Cell Mutagenesis: The Maturation of Test Systems. Cold Spring Harbor Laboratory Press, Cold Spring Harbor, pp. 341-350.

Toma, S., Losardo, P.P., Vincent, M., Palumbo, R. (1995) Effectiveness of beta-carotene in cancer prevention. Eur. J. Cancer Prev., 4(3), 213-224.

Thomas, C.E., Morehouse, L.A., Aust, S.D. (1985) Ferritin and superoxide-dependent lipid peroxidation. J. Biol. Chem., 260(6), 3275-3280.

Thomas, C.E., Aust, S.D. (1986) Release of iron from ferritin by cardiotoxic antibiotics. Arch. Biochem. Biophys., 248(2), 684-689.

Topham, R., Goger, M., Pearce, K., Schultz, P. (1989) The mobilization of ferritin iron by liver cytosol. Biochem. J., 261, 137-143.

Towe, K.M. (1981) Structural distinction between ferritin and iron-dextran (imferon). An electron diffraction comparison. J. Biol. Chem., 256(18), 9377-9378.

Treffrey, A., Harrison, P.M. (1979) The binding of ferric iron by ferritin. Biochem. J., 181(3), 709-716.

Treffrey, A., Harrison, P.M. (1984) Non-random distribution of iron entering rat liver ferritin in vivo. Biochem. J., 220(3), 857-859.

Treffry, A., Lee, P.J., Harrison, P.M. (1984) Functional studies on rat-liver isoferritins. Biochim. Biophys. Acta, 785(1-2), 22-29.

Treffry, A., Bauminger, E.R., Hechel, D., Hodson, N.W., Nowik, I., Yewdall, S.J., Harrison, P.M. (1993) Defining the roles of the threefold channels in iron uptake, iron oxidation and iron-core formation in ferritin: a study aided by site-directed mutagenesis. Biochem. J., 296(3), 721-728.

Tsfack, A., Loyevsky, M., Ponka, P., Cabantichik, I.Z. (1996) Mode of action of iron (III) chelators as antimalarials. J. Lab. Clin. Med., 127, 574-582.

Tyrrell, R.M., Werfelli, P., Moraes, E.C. (1984) Lethal action of ultraviolet and visible (blue-violet) radiations at defined wavelengths on human lymphoblastoid cells: Action spectra and interaction sites. Photochem. Photobiol., 39, 183-189.

Tyrrell, R. M., Pidoux, M. (1986) Quantitative differences in host cell reactivation of ultraviolet damaged virus in human skin fibroblasts and epidermal keratinocytes cultured from the same foreskin biopsy. Cancer Res., 46, 2665-2669.

Tyrrell, R.M., Pidoux, M. (1989) Singlet oxygen involvement in the inactivation of cultured human fibroblasts by UVA (334 nm, 365 nm) and near-visible (405 nm) radiations. Photochem. Photobiol., 49(4), 407-412.

Tyrrell, R.M. (1991) UVA (320-380 nm) radiation as an oxidative stress. In: Sies, H. (ed): Oxidative stress: Oxidants and antioxidants. Academic Press, London, pp. 57-83.

Tyrrell, R.M. (1994) Oxidant regulation of genes with emphasis on the influence of UVA radiation on expression of the human heme oxygenase-1 gene. In Paoletti et al. (eds): Oxidative processes and antioxidants. Raven Press, Ltd., NewYork, pp. 1-12.

Tyrrell, R.M. (1996) Activation of mammalian gene expression by the UV component of sunlight – from models to reality. BioEssays, 18(2), 139-148.

Ullrich, S.E. (1995) Modulation of immunity by ultraviolet radiation: key effects on antigen presentation. J. Invest. Dermatol., 105(1 Suppl.), 30S-36S.

Uberriegler, K.P., Banieghbal, E., Krammer, B. (1995) Subcellular damage kinetics within co-cultivated WI38 and VA13-transformed WI38 human fibroblasts following 5-aminolevulinic acid-induced protoporphyrin IX formation. Photochem. Photobiol., 62(6), 1052-1057.

Valenzeno, D.P. (1987) Photomodification of biological membranes with emphasis on singlet oxygen mechanisms. Photochem. Photobiol. 46(1), 147-60.

Vile, G.F., Winterbourn, C.C. (1988) Microsomal reduction of low-molecular-weight Fe^{3+} chelates and ferritin enhancement by adriamycin, paraquat, menadione, and anthraquinone 2-sulfonate and inhibition by oxygen. Arch. Biochem. Biophys., 267(2), 606-613.

Vile, G.F., Tyrrell, R.M. (1993) Oxidative stress resulting from ultraviolet A irradiation of human skin fibroblasts leads to a heme oxygenase-dependent increase in ferritin. J. Biol. Chem., 268 (20), 14678-14681.

Vile, G.F., Basu-Modak, S., Waltner, C., Tyrrell, R.M. (1994) Heme oxygenase 1 mediates an adaptive response to oxidative stress in human skin fibroblasts. Proc. Natl. Acad. Sci. USA, 91, 2607-2610.

Vile, G.F., Tyrrell, R.M. (1995) UVA radiation-induced oxidative damage to lipids and proteins in vitro and in human skin fibroblasts is dependent on iron and singlet oxygen. Free Radic. Biol. Med., 18(4), 721-730.

Wade, V.J., Levi, S., Arosio, P., Treffry, A., Harrison, P.M., Mann, S. (1991) Influence of site-directed modifications on the formation of iron cores in ferritin. J. Mol. Biol., 221(4), 1443-1452.

Wardeska, J.G., Viglione, B., Chasteen N.D. (1986) Metal ion complexes of apoferritin. Evidence for initial binding in the hydrophilic channels. J. Biol. Chem., 261(15), 6677-6683.

Washbrook, R., Fukuda, H., Battle, A., Riley, P. (1997) Stimulation of tetrapyrrole synthesis in mammalian epithelial cells in culture by exposure to aminolevulinic acid. Brit. J. Cancer, 75(3), 381-387

Weaver, J., Pollack, S. (1989) Low-M_r iron isolated from guinea pig reticulocytes as AMP-Fe and ATP-Fe complexes. Biochem. J., 261, 787-792.

Webber, J., Luo, Crilly, R., Fromm, D., Kessel. (1996) An apoptotic response to photodynamic therapy with endogenous protoporphyrin IX in vivo. J. Photochem. Photobiol. B: Biol., 35, 209-211.

Williams, D.M., Lee, G.R., Cartwright, G.E. (1974) The role of superoxide anion radical in the reduction of ferritin iron by xanthine oxidase. J. Clin. Invest., 53, 665-667.

Yablonski, M.J., Theil, E.C. (1992) A possible role for the conserved trimer interface of ferritin in iron incorporation. Biochemistry, 31(40), 9680-9684.

Yegorov, D.Y., Kozlov, A.V., Azizova, O.A., Vladimirov, Y.A. (1993) Simultaneous determination of Fe(III) and Fe(II) in water solutions and tissue homogenates using desferal and 1,10-phenanthroline. Free Radic. Biol. Med.;15(6), 565-74.

Yohn, J.J., Norris, D.A., Yrastorza, D.G., Buno, I.J., Leff, J.A., Hake, S.S., Repine, J.E. (1991) Disparate antioxidant enzyme activities in cultured human cutaneous fibroblasts, keratinocytes, and melanocytes. J. Invest. Dermatol., 97(3),405-9.

Zuurendonk, P.F., Tager, J.M. (1974) Rapid separation of particulate components and soluble cytoplasm of isolated rat-liver cells. Biochim. Biophys. Acta, 333, 393-399.